MAR 26 1957

Journal of Research

of the

National Bureau of Standards

UNIVERSITY OF MICHIGAN
MAR 22 1957
PHYSICS LIBRARY

MARCH 1957

VOLUME 58 NUMBER 3

U. S. DEPARTMENT OF COMMERCE
Sinclair Weeks, Secretary
NATIONAL BUREAU OF STANDARDS
A. V. Astin, Director

MARCH • 1957
VOLUME • 58
NUMBER • 3

JOURNAL OF RESEARCH
of the
NATIONAL BUREAU OF STANDARDS

PERIODICALS OF THE NATIONAL BUREAU OF STANDARDS
(Published monthly)

The National Bureau of Standards is engaged in fundamental and applied research in physics, chemistry, mathematics, and engineering. Projects are conducted in fifteen fields: electricity and electronics, optics and metrology, heat and power, atomic and radiation physics, chemistry, mechanics, organic and fibrous materials, metallurgy, mineral products, building technology, applied mathematics, data processing systems, cryogenic engineering, radio propagation, and radio standards. The Bureau has custody of the national standards of measurement and conducts research leading to the improvement of scientific and engineering standards and of techniques and methods of measurement. Testing methods and instruments are developed, physical constants and properties of materials are determined, and technical processes are investigated.

JOURNAL OF RESEARCH

The Journal presents research papers by authorities in the specialized fields of physics, mathematics, chemistry, and engineering. Complete details of the work are presented, including laboratory data, experimental procedures, and theoretical and mathematical analyses. Annual subscription: domestic, $4.00; $1.25 additional for foreign mailing.

TECHNICAL NEWS BULLETIN

Summaries of current research at the National Bureau of Standards are published each month in the Technical News Bulletin. The articles are brief, with emphasis on the results of research, chosen on the basis of their scientific or technologic importance. Lists of all Bureau publications during the preceding month are given, including Research Papers, Handbooks, Applied Mathematics Series, Building Materials and Structures Reports, Miscellaneous Publications, and Circulars. Each issue contains 12 or more two-column pages; illustrated. Annual subscription: domestic, $1.00; 35 cents additional for foreign mailing.

BASIC RADIO PROPAGATION PREDICTIONS

The Predictions provide the information necessary for calculating the best frequencies for communication between any two points in the world at any time during the given month. The data are important to all users of long-range radio communications and navigation, including broadcasting, airline, steamship, and wireless services, as well as to investigators of radio propagation and ionosphere. Each issue, covering a period of one month, is released three months in advance and contains 16 large pages, including pertinent charts, drawings, and tables. Annual subscription: domestic, $1.00; 25 cents additional for foreign mailing.

Order all publications from the Superintendent of Documents
U. S. Government Printing Office, Washington 25, D. C.

Use of funds for printing this publication approved by the Director of the Bureau of the Budget (May 14, 1956).

Journal of Research of the National Bureau of Standards Vol. 58, No. 3, March 1957 Research Paper 2742

Relative Dimensional Stabilities of a Selected Series of Stainless-Steel Decimeter Bars

Benjamin L. Page

The results of intercomparisons of the lengths of a series of stainless-steel decimeter bars for the past twenty-five years are reported. Data on the degree of dimensional stability of these bars were obtained and the results were analyzed. Some of the bars were found suitable for use as line standards of length.

1. Introduction

It is known that the length of most linear standards at any specified temperature cannot be assumed to remain the same over a period of years, nor can it be assumed that the secular changes in the bars are uniform over any definite period of time. It is, therefore, essential that a stable material be obtained for use as a line standard of length so that frequent calibrations are not required. Other requirements are that the surface to be graduated must take a good polish, be free from pits and inclusions, have graduations that are straight, and have clean sharp edges in order that the standards can be fully relied upon to give the requisite degree of accuracy in their use.

Several of the National Bureau of Standards decimeter standards that have been frequently calibrated in terms of the International Prototype Meter were used in conjunction with the 13 stainless-steel decimeter bars selected for the present investigation. To calibrate these bars intercomparisons by pairs were made using different combinations in order to obtain the most probable corrections to their lengths.

Because the intercomparison of 15 bars (2 NBS standards and the 13 bars in this group) consumed a great deal of time in the earlier measurements, a method[1] that substantially diminished the time without significant loss of accuracy was used in the 1955 intercomparisons.

This group of 13 decimeter bars was first intercompared in 1930 and in subsequent years up to 1955. The trends in length changes of the bars over the 25-year period are discussed.

In making the present measurements on the decimeter bars, every reasonable precaution was taken to have the results reflect the accuracy and precision that is obtainable with the present NBS equipment.

The investigation was initiated by C. G. Peters, formerly of the Bureau. He prepared the decimeter blanks, determined some properties of the bars, and graduated them by the use of wavelengths of light.

[1] W. J. Youden and W. S. Connor, New experimental design for paired observations, J. Research NBS **53**, 191 (1954) RP2532; Willard H. Chatworthy, Partially balanced incomplete block designs with two associate classes and two treatments per block, J. Research NBS **54**, 177 (1955) RP2579.

2. Description of the Decimeter Bars

The 13 decimeter bars are made of stainless steel (Fe-Cr) 130 mm in length and have a cross section of 15 by 15 mm. The upper rectangular surface of each bar has a 3-mm bevel in order to facilitate the optical polishing of the surface to be graduated, and in each case is remarkably free from any pits, inclusions and scratches, and closely approximates a true plane.

Each decimeter bar has only a single 1-dm interval, which, as is the custom, is defined as the distance from the center of the central line of a group of three lines near one end to the center of the central line of a similar group of lines near the other end. The lines have a width of approximately 3 μ.

On each bar two parallel lines approximately 0.2 mm apart are ruled at right angles to the graduations. Only that portion of a graduation lying between these two lines is considered when measurements are made.

The coefficients of linear thermal expansion of the decimeter bars was determined as 10.25×10^{-6}/deg C at room temperature.

Table 1 gives available data on the chemical composition, heat treatment, and scleroscope hardness of the bars.

3. Description of Longitudinal Comparator

The longitudinal comparator described by Page[2] was used for the intercomparisons of the decimeter bars during the investigation of their dimensional stabilities. In this comparator there is a beam carrying two microscopes, which moves in a longitudinal direction. The axes of the scales being compared were collinear.

4. Calibration of the Decimeter Bars

The latest intercomparisons of the decimeter bars were made in 1955. The results of the previous measurements of the total lengths of these bars

[2] Benjamin L. Page, Calibration of meter line standards of length at the National Bureau of Standards, J. Research NBS **54**, 1 (1955) RP2559.

TABLE 1. *Chemical composition, heat treatment, and hardness of the stainless-steel bars*

Bar [a]	Chemical composition								Treatment		Sclero-scope hardness
	Cr	C	Mn	P	S	Si	Cu	Ni	Quenched from 930° C	Tempered at—	
	%	%	%	%	%	%	%	%		°C	
2	13.9	0.32	0.28	0.02	0.03	0.35	0.03	0.07	In oil	400	66
7	13.9	0.32	0.28	0.02	0.03	0.35	0.03	0.07	do	360	67
8	13.9	0.32	0.28	0.02	0.03	0.35	0.03	0.07	do	340	70
9	13.9	0.32	0.28	0.02	0.03	0.35	0.03	0.07	do	320	67
10	13.9	0.32	0.28	0.02	0.03	0.35	0.03	0.07	do	300	73
11	13.9	0.32	0.28	0.02	0.03	0.35	0.03	0.07	In H_2O	400	70
12	13.9	0.32	0.28	0.02	0.03	0.35	0.03	0.07	do	310	72
13	13.9	0.32	0.28	0.02	0.03	0.35	0.03	0.07	do	Not tempered	67
14 [b]	14.0	0.3 to 0.4	0.4	.....	.....	0.05	.....	.....	do	do	72
15 [b]	14.0	0.03 to 0.4	0.4	.....	.....	0.05	.....	.....	do	do	do
16 [c]	12 to 14	0.10	.....	.....	.....	.....	.....	.....	do	do	48
17 [d]	16.5 to 18	1.05	.....	.....	.....	0.05	.....	.....	(e)	.....	33
20	11.0	0.5 to 1.0	.....	.....	.....	.....	.....	0.9	In oil	480	70

[a] All bars conform to American Iron and Steel Institute specifications, AISI 420, with the exception of bars 16 and 17.
[b] Slight longitudinal crack developed when quenched.
[c] AISI 410.
[d] AISI 440.
[e] Annealed.

made in 1930, 1932, 1938, and 1941, together with the results of the latest measurements, are included here.

4.1. Determination of Total Length

All measurements on the bars were made with the NBS comparator described above, with the temperature of the room controlled at 20° C. The bars were allowed to remain in the comparator for a sufficient length of time to assure thermal equilibrium at a temperature very near 20° C before any measurements were begun. All measured differences between any two bars were corrected to 20° C by using the respective coefficients of linear thermal expansion.

For convenience, the corrections to the bars are given instead of actual lengths. The actual length is equal to the nominal length plus the correction; hence, a plus correction indicates that a bar is longer than the nominal length.

The 13 selected decimeter bars and 2 NBS standard decimeter bars were placed in the comparator in a random manner with respect to their relative positions, either to the right or to the left. Several bars were placed at either end of the comparator at any one time so that more than two bars could be intercompared in any one day without danger of a serious change in thermal equilibrium of the bars caused by their being handled and by the removal of the covers on the comparator tank in which the bars were mounted. All measurements were made with the bars in air while supported on a horizontal flat surface.

To obtain the differences in the length of two bars, two microscopes, separated by any convenient distance, were focused, one on the 0 graduation of the bar on the left and the other on the 0 graduation of the bar at the right. Micrometer observations were then made on the 0 graduation of each bar. The carriage was then moved so that the microscopes were over the 1-dm graduations before the observations were made. For convenience in computing, the bar at the right was always designated as A and the other as B. The comparisons to determine the differences in length between each pair of bars, A and B, were repeated six times, and the temperature of each bar was recorded. The mean of these differences was corrected to 20° C, and the differences in the length of the bars, $L=A-B$, was thus determined.

The results obtained in the 1955 series of comparisons are shown in table 2. The values in brackets were computed from the directly observed differences.

As the work required to observe and determine values for the $N(N-1)/2=105$ differences between 15 bars, consumes an excessive amount of time if all differences are directly determined, it was decided to divide the bars into 4 groups; 3 of 6 bars each, and 1 of 4 bars. The grouping of the 15 bars was as follows:

Group 1: 57, 24,2,7,8, and 9.
Group 2: 57, 24, 10, 11, 12, and 13.
Group 3: 57, 24, 14, 15, 16, and 17.
Group 4: 57, 24, 8, and 20.

This procedure reduces the number of observed and determined values between 15 bars to 51.

In order further, to reduce the number of directly determined differences between the bars, a method (see footnote 1) was used, whereby only 9 of the 15 differences were directly observed in each of the first 3 groups, with the remaining 6 differences computed from the directly observed values. All of the differences in group 4 were observed directly. This plan reduced the number of directly observed differences to a total of 33. As the value for dm 57−dm 24 is used 4 times, and the value for dm 57−dm 8 is used twice in the computations, the number of directly observed differences was finally reduced to 29.

It has been previously determined (see footnotes 1 and 2) that in spite of this reduction in the number of observations, the desired accuracy for the comparisons is obtained.

TABLE 2. *Differences in length of decimeter bars at 20° C*

(1955 series of comparisons)

Observations made at temperature, t, and reduced to 20° C, using the respective values of the coefficients of linear thermal expansion. Directly observed differences ($A-B$) are the values not in brackets. Values in brackets have been computed from the directly observed differences.

Bars compared		Observed difference, L	Observed temperature, t	
			Bar A	Bar B
A minus B		μ	°C	°C
57	24	−3.24	20.00	20.00
2	24	−13.76	19.88	19.86
7	24	−14.15	19.88	19.86
8	24	[−13.76]	.....	.....
9	24	[−14.37]	.....	.....
2	57	[−10.37]	.....	.....
7	57	[−10.72]	.....	.....
8	57	−10.31	19.96	19.95
9	57	−11.00	19.96	19.95
7	2	[−0.35]	.....	.....
8	2	−0.07	20.00	19.96
9	2	−0.66	20.27	20.24
8	7	+0.24	19.99	19.95
9	7	−0.31	19.99	19.95
9	8	[−0.61]	.....	.....
57	24	−3.24	20.00	20.00
10	24	−13.72	19.98	19.94
11	24	−13.44	20.01	19.97
12	24	[−13.61]	.....	.....
13	24	[−16.20]	.....	.....
10	57	[−10.56]	.....	.....
11	57	[−10.20]	.....	.....
12	57	−10.53	20.02	19.98
13	57	−12.88	20.24	20.22
11	10	[+0.36]	.....	.....
12	10	+0.27	20.52	20.50
13	10	−2.48	20.62	20.57
12	11	−0.17	20.58	20.53
13	11	−2.83	20.60	20.55
13	12	[−2.59]	.....	.....
57	24	−3.24	20.00	20.00
14	24	−16.86	20.07	20.03
15	24	−16.16	19.97	19.94
16	24	[−14.11]	.....	.....
17	24	[−13.23]	.....	.....
14	57	[−13.60]	.....	.....
15	57	[−13.05]	.....	.....
16	57	−10.83	19.94	19.91
17	57	−10.14	20.03	20.00
15	14	[+0.54]	.....	.....
16	14	+2.64	20.10	20.06
17	14	+3.56	20.03	20.05
16	15	+2.13	20.06	20.04
17	15	+3.14	20.05	20.03
17	16	[+0.87]	.....	.....
57	24	−3.24	20.00	20.00
8	24	−13.58	20.20	20.17
20	24	−13.65	20.03	20.01
8	57	−10.31	19.96	19.95
20	57	−10.23	20.01	19.99
20	8	+0.22	19.99	19.96
Mean of all observed temperatures			20.08	

In order to select the pairs of bars, in a group of 6, that are to be compared directly and those to be computed, a procedure, called a partially balanced incomplete block design, can be developed for the intercomparison, in which 9 of the comparisons are made directly and 6 are computed from the direct comparisons. To illustrate this design, the bars can be represented by the letters a to f. The direct comparisons will be as follows: a with b, c, and d; and b, c, and d each with e and f. This can be illustrated as follows:

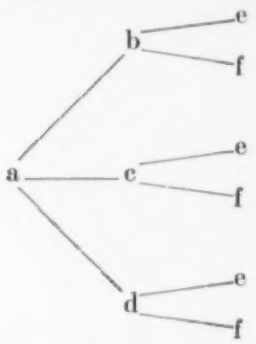

The remaining computed differences will be: a with e; a with f; e with f; b with c; c with d, and b with d. Illustrated graphically this will be

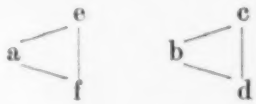

Another way to illustrate this design graphically is:

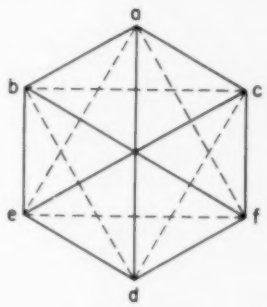

The letters at the ends of the solid lines represent the bars that will be compared directly, and those at the ends of the dotted lines represent the bars whose differences will be computed from the directly observed differences.

To compute these unobserved differences in length between the bars the following method, illustrated by 8–24, was used. First, the mean of the differences between 8 and each of the other bars with which it was directly compared, and for which there is a corresponding directly observed comparison of that other bar with 24, was found. Next, the mean of the differences between 24 and each of the others with which it was compared, and for which there is a corresponding directly observed comparison of that other bar with 8, was found. Finally, the mean values were added algebraically. This is the computed value for the difference, 8—24, or −13.76 μ, as is shown in brackets in table 3. The other bracketed figures in table 3 were computed in a similar manner.

TABLE 3. *Calculations of corrections to decimeter bars (group 1) at 20° C*

Directly observed differences ($A-B$) are taken from table 2, and are the values not in brackets or parentheses. Values in brackets have been computed from the directly observed differences. Calculated ("most probable") differences for $A-B$, given in parentheses, are derived by taking the differences of $\Sigma/6$; e. g., dm 57−dm 24=+6.53−(+9.88)=−3.35 μ, dm 2−dm 57=−3.84−(+6.53)=10.37 μ, and dm 7−dm 2=−4.19−(−3.84)=−0.35 μ. Correction to dm 24=+12.96 μ at 20°C. Correction dm 57=+9.72 μ. Correction to bar equals the mean of the corrections to dm 24+(bar−24) and dm 57+(bar−57). Length of bar equals 1 dm+correction. All values expressed in microns.

B	A						Residuals, r
	24	57	2	7	8	9	
24	0	−3.24	−13.76	−14.15	[−13.76]	[−14.37]	+0.11
		(−3.35)	(−13.72)	(−14.07)	(−13.76)	(−14.37)	−.04
							−.08
							.00
							.00
57	+3.24	0	[−10.37]	[−10.72]	−10.31	−11.00	.00
			(−10.37)	(−10.72)	(−10.41)	(−11.02)	.00
							+.10
							+.02
							.00
2	+13.76	[+10.37]	0	[−0.35]	−0.07	−0.66	−.03
				(−0.35)	(−0.04)	(−0.65)	−.01
							−.07
							−.01
							.00
7	+14.15	[+10.72]	[+0.35]	0	+0.24	−0.31	
					(+0.31)	(−0.39)	Σr^2=0.0365
8	[+13.76]	+10.31	+0.07	−0.24	0	[−0.61]	[a]P. E.=±0.025
						(−0.61)	
9	[+14.37]	+11.00	+0.66	+0.31	[+0.61]	0	
Σ	+59.28	+39.16	−23.05	−25.15	−23.29	−26.95	
Σ/6	+9.88	+6.53	−3.84	−4.19	−3.88	−4.49	
Bar−24	0		−13.72	−14.07	−13.76	−14.37	
Correction to bar	+12.96		−0.76	−1.11	−0.80	−1.41	
Bar−57		0	−10.37	−10.72	−10.41	−11.02	
Correction to bar		+9.72	−0.65	−1.00	−0.69	−1.30	
Mean correction to bar			−0.70	−1.06	−0.74	−1.36	

[a] Probable error of the calculated value of the differences in the corrections between any two bars that were directly compared.

The reduction of these observed and computed differences by the method of least squares was carried out for bars of group 1 by the use of the form [3] shown in table 3. Tables for the bars of groups 2 to 4 are not shown because they are similar in form.

The differences, r, between observed and calculated differences are shown in table 3. These 15 residuals range from 0.00 to 0.11 μ, and the average, neglecting sign, is 0.03 μ. The probable error of the calculated value of the differences in the corrections between any two bars that were directly compared, r, is given by the formula [4]

$$r=0.6745\sqrt{\frac{\Sigma r^2}{\frac{N}{N_t}(N-N_t)}},$$

where Σr^2 is the sum of the squares of the residuals; N, the number of observational equations; N_t, the number of unknowns. In the example considered, N_t is equal to 5 and N equal to 9. For the case given in table 3, r is calculated to be ± 0.025 μ. The probable error of the calculated value of the differences in the corrections between any two bars that were not directly compared is slightly different. The probable errors of the calculated values of the other 3 groups of bars in the 1955 series of comparisons are of the same order of magnitude.

In the comparison of the bars to determine their total corrections for the study of their stabilities, the smallness of the residuals indicates that the bars were in good thermal equilibrium while the observations were being made. It is believed that the corrections determined for the total lengths of the decimeter bars in each of the five series of calibrations are not in error by more than 0.1 μ.

During the period 1930 to 1956, inclusive, 5 series of determinations of the corrections to the group of 13 dm bars were made. The corrections to the total length of the bars at 20° C are given in table 4.

[3] A. Pérard and C. Volet, Les mètres prototypes du Bureau International Travaux et Mémoires du Bureau International des Poids et Mesures, p. 21, (1945).

[4] T. W. Wright and J. F. Hayford, The adjustment of observations, p. 133, 137, 143, (1906).

TABLE 4. *Determination of corrections to decimeter bars at 20° C*

(1930 to 1955 series of comparisons)

Correction to bar=correction to standard used+(bar−standard used). All values expressed in microns.

Bars	Year of correction determination					Differences				
	1930	1932	1938	1941	1955	1932−1930	1938−1932	1941−1938	1955−1941	1955−1930
2	−0.95	−0.85	−1.15	−1.30	−0.70	+0.10	−0.30	−0.15	+0.60	+0.25
7	−0.60	−0.65	−0.80	−0.80	−1.05	−0.05	−0.15	0.00	−0.25	−0.45
8	−0.50	−0.35	−0.35	−0.60	−0.75	+0.15	0.00	−0.25	−0.15	−0.25
9	−0.60	−0.65	−0.75	−0.65	−1.35	−0.05	−0.10	+0.10	−0.70	−0.75
10	−0.55	−0.65	−0.55	−0.70	−0.85	−0.10	+0.10	−0.15	−0.15	−0.30
11	−0.45	−0.30	−0.20	−0.35	−0.45	+0.15	+0.10	−0.15	−0.10	0.00
12	−0.40	−0.35	−0.50	−0.50	−0.65	+0.05	−0.15	0.00	−0.15	−0.25
13	−0.60	−1.45	−2.10	−2.35	−3.25	−0.85	−0.65	−0.25	−0.90	−2.65
14	−0.70	−1.70	−2.80	−3.15	−3.85	−1.00	−1.10	−0.35	−0.70	−3.15
15	−0.40	−1.40	−2.10	−2.70	−3.30	−1.00	−0.70	−0.60	−0.60	−2.90
16	−0.65	−1.20	−1.10	−1.55	−1.15	−0.55	+0.10	−0.45	+0.40	−0.50
17	−0.25	−0.15	−0.35	−0.30	−0.30	+0.10	−0.20	+0.05	0.00	−0.05
20		−0.10	−0.15	−0.30	−0.60		−0.05	−0.15	−0.30	[a] −0.50

[a] 1955−1932.

It will be noted that all of the bars, with the exception of bars 2 and 11 shortened during the 25-year period. Bar 2 lengthened by 0.25 μ; bar 11 remained the same length. The changes in length range from −3.15 μ to +0.25 μ, as shown in figures 1 and 2.

Table 5 shows the average annual changes for each of the decimeter bars over a period of 25 years. These changes in length per decimeter are rather small, with the exception of AISI 420 bars 13, 14, and 15, which were quenched but not tempered. The average annual change in length over a period of 25 years for these three bars was −0.12 μ/dm, or −1.2 μ/m. It is significant that the average annual change in length over the same period for the remaining 8 AISI 420 bars, which were both quenched and tempered, was only −0.01 μ/dm, or −0.1 μ/m. The annealed bar 17 was exceedingly stable, but it did not take a good polish on account of its low hardness and therefore was not suitable for a line standard.

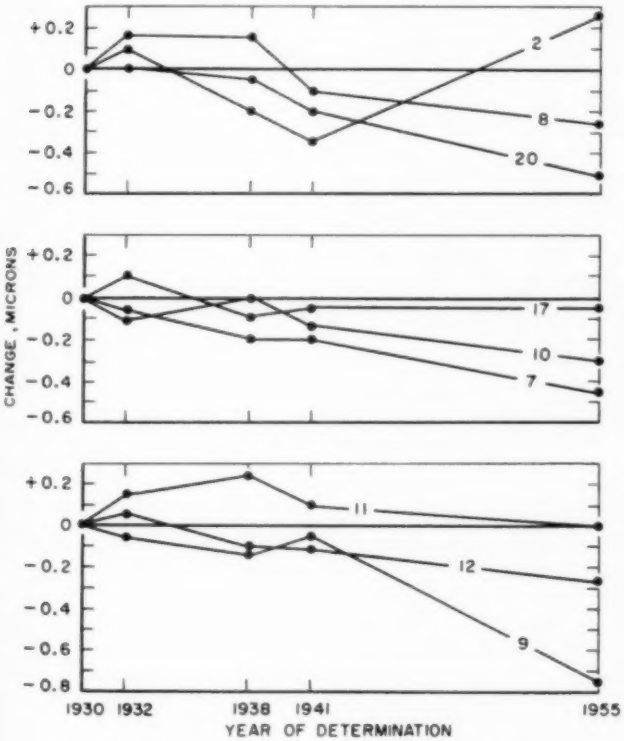

FIGURE 1. *Change in length of decimeter bars.*

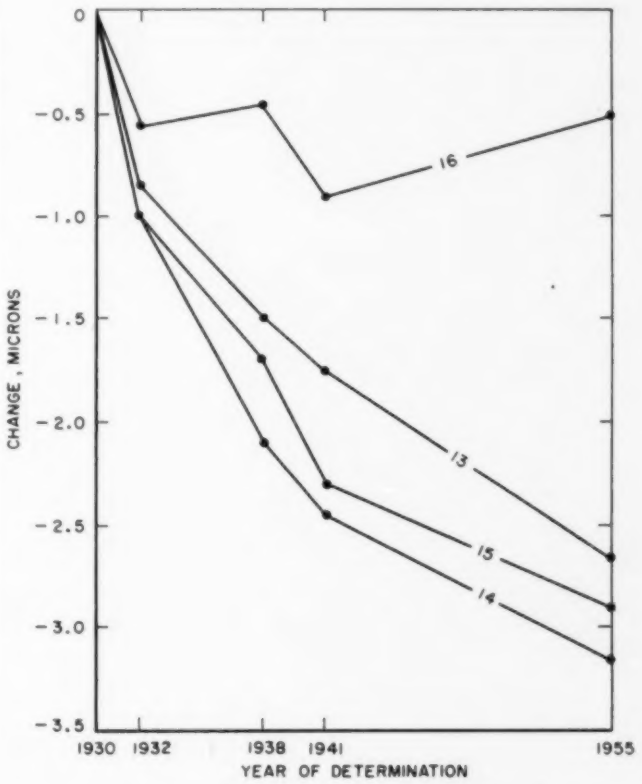

FIGURE 2. *Change in length of decimeter bars.*

TABLE 5. *Length changes of decimeter bars*

Bars	Average changes per year				
	1930 to 1932	1932 to 1938	1938 to 1941	1941 to 1955	1930 to 1955
	μ	μ	μ	μ	μ
2	+0.05	−0.05	−0.05	+0.04	+0.01
7	−0.03	−0.03	0.00	−0.02	−0.02
8	+0.08	0.00	−0.08	−0.01	−0.01
9	−0.03	−0.02	+0.03	−0.05	−0.03
10	−0.05	+0.02	−0.05	−0.01	−0.01
11	+0.08	+0.02	−0.05	−0.01	0.00
12	+0.03	−0.03	0.00	−0.01	−0.01
13	−0.43	−0.11	−0.08	−0.06	−0.11
14	−0.50	−0.18	−0.12	−0.05	−0.13
15	−0.50	−0.12	−0.20	−0.04	−0.12
16	−0.28	+0.02	−0.15	+0.03	−0.02
17	+0.05	−0.03	+0.02	0.00	0.00
20	.....	−0.01	−0.05	−0.02	[a]−0.02

[a] 1932 to 1955.

5. Conclusion

The average annual change in length of 8 dm bars of quenched and tempered AISI 420 stainless steel was −0.1 μ/m during a period of 25 years. This small change was approximately one-half the average annual changes of a group of four meter bars made of invar, 42 percent nickel-steel, and "Fix Invar", over a similar period of time. This degree of stability indicates that AISI 420 stainless steel would be suitable for line standards of length, for which a permanence of 0.1 μ/m over many years is required.

The author expresses his appreciation to W. B. Emerson, P. Hidnert, L. V. Judson, and W. J. Youden for valuable discussions and assistance during the preparation of this paper.

WASHINGTON, October 25, 1956.

Journal of Research of the National Bureau of Standards Vol. 58, No. 3, March 1957 Research Paper 2743

Thermal Quenching in Alpha- and Gamma-Excited Fluorescent Solutions

H. H. Seliger and C. A. Ziegler [1]

The effects of reduction of temperature on the relative light outputs of the gas-free liquid scintillators, DPO, αNPO, and PBD+POPOP, dissolved in xylene, have been investigated. From room temperature down to −35° C the relative light outputs increase markedly under both alpha and gamma excitation. Under the conditions of the present experiments it has been possible to make a gas-free solution of PBD+POPOP in xylene more efficient than crystal anthracene.

1. Introduction

In a previous paper the application of the 4π-crystal-scintillation counter [1] [2] to the standardization of the disintegration rates of medium- and high-energy beta emitters was described. The method, however, possesses no advantages over the $4\pi\beta$-gas-proportional counter [2,3,4] in that the method of source preparation is the same and, therefore, the source self-absorption is not changed. The liquid-scintillation-counting technique offers a means of completely eliminating source self-absorption because the active material can be incorporated into the solution directly. This is especially important for low-energy beta emitters and electron capturers where source self-absorption can be appreciable [4].

As a first step in the application of liquid scintillators to absolute beta counting it was decided to determine the optimum conditions for maximum light-conversion efficiency of the liquid scintillators. It has been well known in the field of fluorescence that molecular oxygen in solution in an organic fluorescent liquid is in many instances a strong quenching agent [5,6,7,8,9]. In 1931 Kautsky [6] showed that the quenching by oxygen of the fluorescence of the dye, trypaflavine, increases as the dye is dissolved in water, alcoholic solutions, and acetonic solutions, corresponding to the increasing solubility of oxygen in these solutions. Seliger, Ziegler, and Jaffe have recently reported [10] that the quenching by oxygen in the cases of DPO and αNPO in xylene solutions is primarily a solute effect, which appears to be in agreement with results tabulated by P. Pringsheim [11] for other fluorescent solutions. The removal of dissolved oxygen is, therefore, of primary concern in the improvement of light-conversion efficiency.

A thermal quenching effect for certain fluorescent dyes was also reported by Pringsheim [11]. It was decided to investigate this phenomenon for several of the most efficient liquid scintillators reported [12,13]. However, in view of the previous work on oxygen quenching, the thermal quenching was investigated for solutions in which all dissolved gases had been removed. These included 2,5-diphenyloxazole (DPO); 2-(1-naphthyl)-5-phenyloxazole (αNPO); phenylbiphenyloxadiazole-1,3,4 (PBD); anthracene; and *p*-bis(2-(5-phenyloxazolyl))-benzene (POPOP).

2. Experiments and Results

In previous experiments on the effects of oxygen quenching [14,15] it was reported that relative oxygen quenching was a function of solute concentration. It was therefore decided to measure any possible effects of temperature at concentrations of solute close to the peak light-output concentrations which have been reported by Hayes and co-workers [12,13] at room temperature. The vacuum system that was used to prepare liquid solutions free of all gases is shown in figure 1. Weighed samples of dry solute were delivered to 5-ml cylindrical Pyrex absorption cells and appropriate volumes of purified *m*-xylene were vacuum distilled into the individual cells, using liquid nitrogen as condensing agent. Each of the cells while still under high vacuum (10^{-5} mm) was flame-sealed from the system. The cells were laid flat on the face of a phototube and were surrounded by an aluminum reflector, the scintillator-phototube combination being inside a light-tight refrigerator. Temperatures were measured by means of a copper-constantan thermocouple in direct contact with the outside of the glass cell.

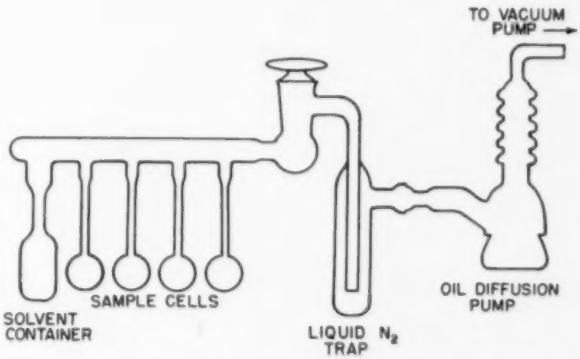

FIGURE 1. *Glass system employed for preparing gas-free solutions.*

[1] Present address: Tracerlab, Inc., Boston, Mass.
[2] Figures in brackets indicate the literature references at the end of this paper.

2.1. Alpha-Particle Measurements

In addition to the dry solute, inside each cell was placed a small gold trident on one spear of which was plated sufficient polonium to give 1,000 to 2,000 counts per second. The pulse-height distribution of the source was observed with a single-channel pulse-height analyzer. The change in the light output with temperature was assumed to be proportional to the displacement of the peak position of the pulse-height distribution.

2.2. Gamma-Ray Measurements

Sample cells, prepared without the polonium-plated tridents, were placed in the collimated beam of a 1-millicurie radium source. This time the change in the light output with temperature was assumed to be proportional to the d-c current measured with a vibrating-reed electrometer.

The experimentally observed data are summarized in figure 2. The solid curves are the results of the gamma-ray-excitation measurements and the dashed curves are the results of the alpha-particle-excitation measurements. The relative increases observed due to lowered temperatures are of the same order for both alpha and gamma excitation. However, the shapes of the curves are decidedly different. The relative increases in the alpha-excitation case are linear with temperature over the range investigated. The gamma-excitation curves, while exhibiting a steeper initial slope, tend to flatten out somewhat below 0° C.

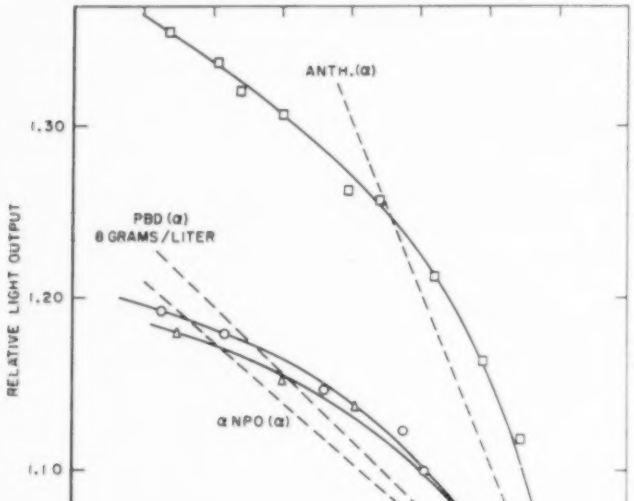

FIGURE 2. *Relative light outputs versus temperature for gas-free liquid scintillators.*

The dashed curves represent previously obtained data for alpha excitation. The solid curves represent the data for gamma excitation. □, Anthracene 1 g/liter; ○, PBD 10 g/liter+POPOP 2 g/liter; △, αNPO 3.2 g/liter.

3. Discussion

The results reported are for the liquid-scintillator-phototube combination. The phototube temperature response has been investigated previously and was found to decrease slightly with decreasing temperature [16], so that the net increase in liquid-scintillator light output would appear to be even greater. However, the phototube effect is small (0.1 to 0.2% per deg C) and seems to vary from one tube to another and with the previous history of the tube.

It is surprising that this effect has not been reported previously, especially as refrigeration is so frequently used in liquid-scintillation counting, to reduce thermal tube noise. However, the increasing solubility of O_2 with decreasing temperature gives rise to additional quenching, tending to mask the increase observed with gas-free solutions. Kallmann has measured the light outputs of air-saturated *p*-terphenyl-xylene solutions at room temperature relative to crystal anthracene and reported a ratio of 0.48 [17]. The results of our own gamma-ray-excitation measurements made at room temperature on gas-free PBD+POPOP in xylene and on air-saturated *p*-terphenyl in xylene give a ratio of light outputs of 2.03:1. From figure 2 a further factor of 1.20 is to be gained by a temperature reduction of the PBD+POPOP solution to −35° C. Thus the maximum efficiency obtained in the present experiments for PBD+POPOP in xylene was 1.17 relative to crystal anthracene, the latter at room temperature.

It is intended to extend the measurements described in reference [1] to the liquid scintillator combination of PBD+POPOP at reduced temperatures and under gas-free conditions.

4. References

[1] C. C. Smith, H. H. Seliger, and J. Steyn, J. Research NBS **57,** 251 (1956) RP2716.
[2] H. H. Seliger and L. M. Cavallo, J. Research NBS **47,** 41 (1951) RP2226.
[3] W. B. Mann and H. H. Seliger, J. Research NBS **50,** 197 (1953) RP2409.
[4] H. H. Seliger and A. Schwebel, Nucleonics (7) **12,** 54 (1954).
[5] S. Boudin, J. chim. phys. **27,** 285 (1930).
[6] H. Kautsky and R. Eberlein, Chem. Ber. **64,** 2677 (1931).
[7] R. W. Pringle, L. D. Black, B. L. Funt, and S. Sobering, Phys. Rev. **92,** 1582 (1953).
[8] F. N. Hayes, Los Alamos Report LA–1837, October 1954 (unpublished).
[9] H. Kallmann, U. S. Army Signal Corps Progress Report, February 1955 (unpublished).
[10] H. H. Seliger, C. A. Ziegler, and I. Jaffe, Phys. Rev. **101,** 998 (1956).
[11] P. Pringsheim, Fluorescence and Phosphorescence, p. 334 (Interscience Publishers, Inc., New York, N. Y., 1949).
[12] F. N. Hayes, D. G. Ott, V. N. Kerr, and B. S. Rogers, Nucleonics (12) **13,** 38 (1955).
[13] F. N. Hayes, D. G. Ott, and V. N. Kerr, Nucleonics [1] **14,** 42 (1956).
[14] C. A. Ziegler, H. H. Seliger, and I. Jaffe, Phys. Rev. **99,** 663 (1955).
[15] C. A. Ziegler, H. H. Seliger, and I. Jaffe, Nucleonics (5) **14,** 84 (1956).
[16] H. H. Seliger and C. A. Ziegler, Nucleonics [4] **14,** 49 (1956).
[17] H. Kallmann, U. S. Army Signal Corps Report, December 1951 (unpublished).

WASHINGTON, October 11, 1956.

Journal of Research of the National Bureau of Standards Vol. 58, No. 3, March 1957 Research Paper 2744

Two-Parameter Gloss Methods

I. Nimeroff

The concept of a parameter of glossiness, that is, measurement under one set of illuminating and viewing conditions, is developed. To describe completely the glossiness of a specimen requires multiparametric measurements on the geometric distribution of reflected light-flux. As one-parameter methods have been found to yield inadequate descriptions of specimen glossiness, two-parameter methods were investigated. For specimens with differing incidence-angle dependency, a two-parameter method using specular gloss measurements at two incidence angles is suggested. For specimens with differing flux-scattering characteristics, a two-parameter method using specular gloss measurements for two receptor apertures is suggested. Several existing standard two-parameter methods are reviewed. Results of a seven-laboratory round-robin test of the two-parameter (receptor aperture) method are reported and analyzed. To establish correlation between measurements obtained with the suggested two-parameter (receptor aperture) method and subjective evaluation of image brightness and image distinctness, a subjective test was formulated. The results of this test, here analyzed and discussed, indicate the usefulness of the two-parameter method.

1. Introduction

For many years American Society for Testing Materials committee deliberations on glossimetry definitions have been concerned with use of terms like "aspects," "criteria," "modes," and "types" of gloss in describing instrumental measurement techniques found to correlate with some glossiness characteristics. Glossiness, or glossy appearance, is a function of how an observer evaluates the geometric distribution of flux reflected by a specimen. To evaluate completely this appearance characteristic, called glossiness, observations under many conditions of illumination and view are required. A measurement under each illuminating and viewing condition may be called a parameter of glossiness.

Techniques involved in methods for evaluating of specimens have ranged from one-parameter to multiparameter observations. The multiparameter technique is complex, time consuming, and too costly to perform for every specimen. While a one-parameter technique can yield data simply, rapidly, and inexpensively, it is an oversimplified solution to the problem of instrumental evaluation of gloss characteristics. One-parameter data often lead to erroneous conclusions about the comparative appearance of specimens. To decrease the number of erroneous conclusions without materially increasing the complexity, time, and cost of the measurement, a compromise between a one-parameter and a multiparameter technique is required.

2. Multiparameter Technique

2.1. Multiplane Goniophotometry

Multiparametric observations can be taken on either multiplane or monoplane instruments, called goniophotometers. A multiplane goniophotometer would have many geometric variables at its disposal. Such an instrument was designed and constructed by McNicholas [1].[1] Figure 1 shows the geometric variables: θ, the angle between the axis of the incident beam and the perpendicular to the specimen plane; ϕ, the azimuth angle (the angle between a reference line in the plane of the specimen and the projection of the incident axis on that plane); ω, the solid angular subtense, or aperture, of the incident beam; θ', ϕ', and ω', the corresponding geometric variables of the reflected beam.

If the goniophotometric readings for a specimen under each set of illuminating and viewing conditions (parameters) are represented by $G_{i,r}$, where i refers to the incident beam, and r refers to the reflected beam, the complete gloss description of the specimen, G_ϕ, would be a function of these parameters. This may be symbolically stated:

$$G_\phi = F(G_{i,r}), \tag{1}$$

where i is dependent on θ, ϕ, and ω, and r is dependent on θ', ϕ', and ω'. This dependence may be stated:

$$\left.\begin{aligned} i &= f\ (\theta,\phi,\omega) \\ r &= g\ (\theta',\phi',\omega'). \end{aligned}\right\} \tag{1a}$$

An analysis of goniophotometric data can be considered as a solution of eq (1) for the functional description, $F(G_{i,r})$. Thaler [2] published a rather complete set of parametric measurements for a series of MgO specimens, using constant ω and ω', but did not develop a functional description of the appearance of the material.

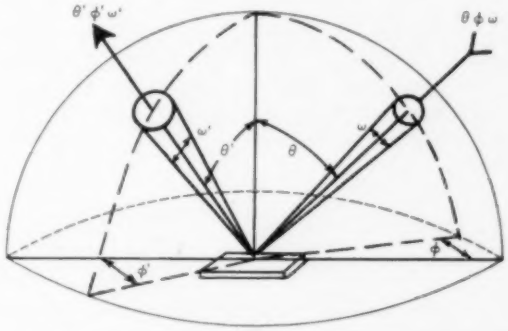

FIGURE 1. *Geometric variables of a multiplane goniophotometer*

[1] Figures in brackets indicate the literature references at the end of this paper.

2.2. Monoplane Goniophotometry

A monoplane instrument has one less variable at its disposal than a multiplane instrument. The variables of a monoplane goniophotometer are those of figure 1, except that $\phi' = \phi$. The variables are θ and ω for the incident beam, θ' and ω' for the reflected beam. If rectangular source and receptor are substituted for the circular ones, the angular sizes ω and ω' become $\alpha\beta$ and $\alpha'\beta'$, respectively. Goniophotometers of this type have been designed and constructed by Wetlaufer and Scott [3], Moon and Laurence [4], Hammond and Nimeroff [5], and Middleton and Mungall [6].

For this type of instrument, the gloss description of the specimen, G, could be symbolically represented by:

$$G = F(G_{i,r}),$$

where i is dependent on θ, α, and β, and r is dependent on θ', α', and β'. This dependence is stated:

$$\left.\begin{aligned} i &= f[\theta,(\alpha\beta)] \\ r &= g[\theta',(\alpha'\beta')]. \end{aligned}\right\} \tag{2a}$$

Analyses of goniophotometric data obtained on this type of instrument have been made. Barkas [7] suggested a method for theoretically separating the specular and diffuse reflection components of a specimen by finding an equivalent theoretical surface that will have the same goniophotometric reflectance as the specimen. Middleton and Mungall [6] suggested a similar analysis for goniophotometric data. These analyses were confined to fairly matte surfaces, such as beaverboard and snow.

ASTM Method, D636–54 [8] recommends use of a Dows-Baumgartner reflectometer [9] and analysis of its goniophotometric data in terms of reflective diffusion indexes:

$$\left.\begin{aligned} D_{ra} &= \frac{\int_{3°}^{90°} R(\theta')d\theta'}{97R(3°)} \\ D_{rb} &= \frac{\int_{15°}^{90°} R(\theta')d\theta'}{75R(15°)}, \end{aligned}\right\} \tag{3}$$

where $R(\theta')$ is the reflectance at viewing angle, θ'. The specimen is illuminated perpendicularly, $\theta = 0°$.

Analysis of goniophotometric data for specimens ranging in gloss from matte to highly specular was made by Nimeroff [10]. The goniophotometric data were analyzed in terms of indexes of dispersion, skewness, and kurtosis (peakedness index), related to the second, third, and fourth moments, respectively.

3. One-Parameter Technique

3.1. Specular Glossmeters

One-parameter instruments that have been developed recently have been monoplanar with fixed source and receptor apertures and fixed incidence and specular reflecting angles. Symbolic representation for the geometry of such a one-parameter instrument is

$$\left.\begin{aligned} i &= f[\theta,(\alpha\beta)] \\ r &= g[-\theta,(\alpha'\beta')]. \end{aligned}\right\} \tag{4}$$

Specular glossmeters have been developed for at least five different incidences angles, 20°, 45°, 60°, 75°, and 85°, and are described in ASTM, PEI, and TAPPI gloss methods. These methods have proven satisfactory except for occasional confusion resulting from inadequacy of a one-parameter technique.

3.2. Inadequacies of the One-Parameter Technique

Specular reflectance of a specimen depends on the angle at which light flux is incident on the specimen. For some specimens the rate of increase of specular reflectance with increasing incidence angles exceeds the rate for other specimens. Thus two specimens can have the same gloss when illuminated at one incidence angle and have much different gloss when illuminated at another incidence angle. A one-parameter technique, specular reflectance measurement at one set of geometric conditions, will not reveal this incidence-angle dependency of the appearance of these specimens.

More frequently than in the above instance, inadequacy of a one-parameter technique is demonstrated when one specimen has a more peaked distribution of reflected flux than the other. Even though two such specimens may differ markedly in appearance, the flux reflected from one specimen and accepted by the receptor may equal the accepted flux reflected from the other specimen. The instrument, therefore, will indicate that both specimens have the same gloss in spite of their difference in appearance.

4. Two-Parameter Techniques

A two-parameter monoplane technique would provide for two variations of geometry. ASTM Method of Test for Mar Resistance of Plastics [11], Designation D673–44T, requires a two-parameter instrument that measures flux reflected on the specular angle, 45°, and at an angle displaced 15° from the specular angle, namely, 30°. The geometry of that instrument can be represented as

$$\left.\begin{aligned} i &= f[45°,(\alpha\beta)] \\ r &= g[45°,30°,(\alpha'\beta')]. \end{aligned}\right\} \tag{5}$$

The data obtained by this method are analyzed in terms of percentage of gloss thus: Gloss, percent $= 100[1-(G_{45,30}/G_{45,45})]$, where G is the instrument reading for the geometry indicated by the subscripts.

Middleton and Mungall [12] described a distinctness-of-image glossmeter designed to use the maximum slope of the goniophotometirc curve as the gloss index of a specimen. This instrument measures flux reflected from a specimen at the specular angle, 45°, and at an angle displaced $\Delta\theta$ from the specular

angle. The geometry of that instrument can be represented as

$$\left.\begin{aligned} i &= f[45°,(\alpha\beta)], \\ r &= g[45°,45+\Delta\theta,(\alpha'\beta')]. \end{aligned}\right\} \quad (6)$$

The instrument analyzes the data thus obtained in terms of a gloss index. Gloss index $=(G_{45,45}-G_{45,45+\Delta\theta})/\Delta\theta$, where G is the instrument reading for the geometry indicated by the subscripts.

For two-parameter glossmeters of the specular type the two variations of geometry would be variation of the specular angle or variation of the size of the receptor aperture. The symbolic representation for the geometry of a two-parameter instrument designed for measurements at two specular angles might be written

$$\left.\begin{aligned} i &= f[\theta_1,\theta_2,(\alpha\beta)], \\ r &= g[\theta_1,\theta_2,(\alpha'\beta')]. \end{aligned}\right\} \quad (7)$$

The geometry for such an instrument is shown in figure 2. The symbolic representation for the geometry of a two-parameter instrument designed for measurements with two receptor apertures might be

$$\left.\begin{aligned} i &= f[\theta,(\alpha_1\beta_1),(\alpha_2\beta_2)], \\ r &= g[\theta,(\alpha'_1\beta'_1),(\alpha'_2\beta'_2)]. \end{aligned}\right\} \quad (8)$$

The geometry for such an instrument is shown in figure 3.

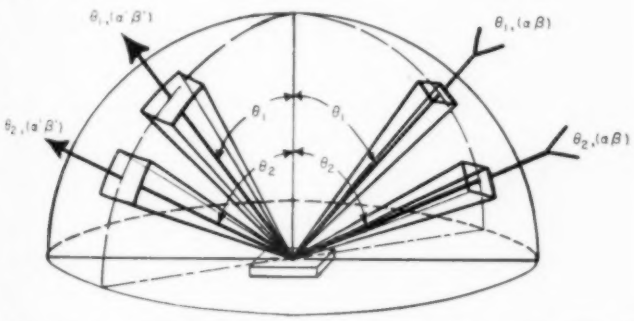

FIGURE 2. *Geometry of an incidence angle two-parameter glossmeter.*

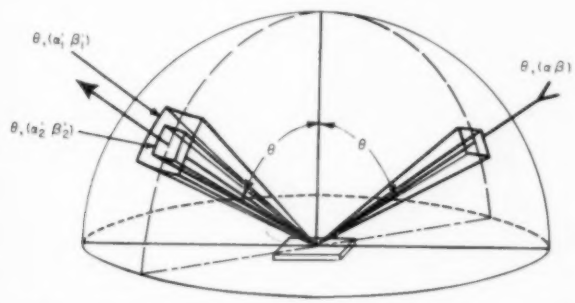

FIGURE 3. *Geometry of a receiver aperture two-parameter glossmeter.*

4.1. Specular Angle

To illustrate how a two-parameter instrument might be used to resolve problems where specular-angle dependence is important, two low-gloss specimens were selected. These specimens appear to have nearly equal gloss when viewed at angles ranging from perpendicular to about 65°. At angles greater than 65° one specimen appears considerably glossier than the other. Figure 4 shows plots of fractional reflectance, the ratio of flux reflected within a 0.6° cone to the incident flux, as a function of angle, d, between the viewing direction and that of mirror reflection as measured on a monoplane goniophotometer. The specimens are designated A and B. At 60° incidence both curves are flat (reflected flux is uniformly distributed) with A having a slightly higher fractional reflectance. At 80° incidence the curve for A remains reasonably flat, whereas that for B becomes quite peaked, having a peakedness index of 182 compared with 1.9 for A. Peakedness index for a unimodal curve was shown by Nimeroff [10] to be an index of the relative peak to shoulder heights.

A goniophotometer, arranged for the 60° geometry of ASTM Method D523–53T, [13] was used to measure the specular gloss of specimens A and B for 60°

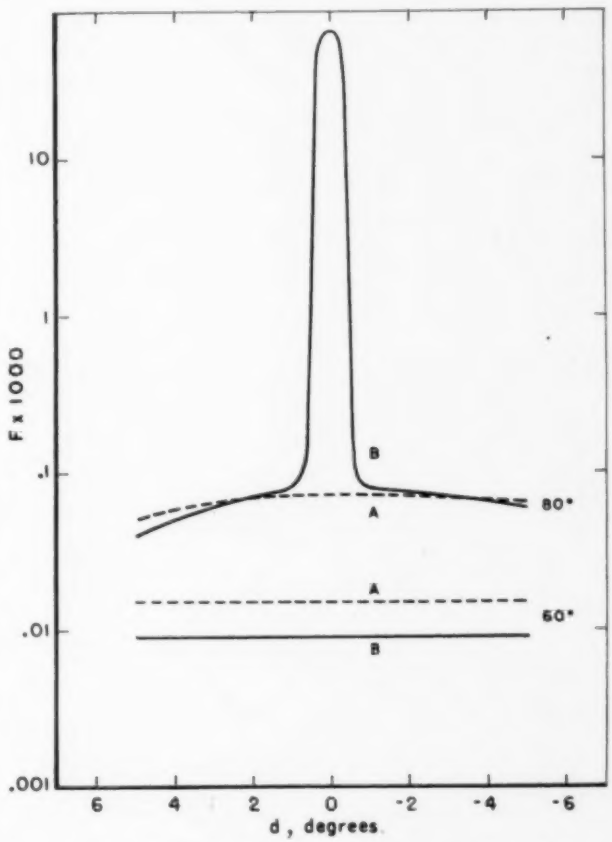

FIGURE 4. *Fractional reflectance curves for two specimens exhibiting incidence-angle dependency at incidence angles of 60° and 80°.*

and 80° incidence. At 60° incidence, the gloss reading for A is 6 and for B is 4, whereas at 80° incidence the gloss reading for A is 24 and for B is 109. These readings show the much stronger incidence-angle dependence for B than for A. This dependence is not suggested in a measurement of specular gloss at 60° incidence alone.

The solution to problems involving incidence-angle dependence is obvious. Measure the specular gloss at two incidence angles and relate the resulting data. The slope of the line joining plotted points of the gloss readings for a specimen obtained with two incidence angles may be used as an index of the dependence of gloss on incidence angle.

4.2. Receptor Aperture

Appearance characteristics ascribable to gloss may be classified into three distinct types, either in accord with appearance or in accord with flux-scattering properties. Appearance wise, the two extreme types are image-forming and nonimage forming; the third type exhibits intermediate characteristics. Goniophotometric distributions for specimens of the image-forming type are shown in figure 5. These curves are characterized by sharp peaks near the specular angle, with scattering at wide angles from the specular. As a considerable amount of scattered flux is found at wide angles, these specimens may be called "wide-angle scatterers." Goniophotometric distributions for specimens of the nonimage-forming type are shown in figure 6. These

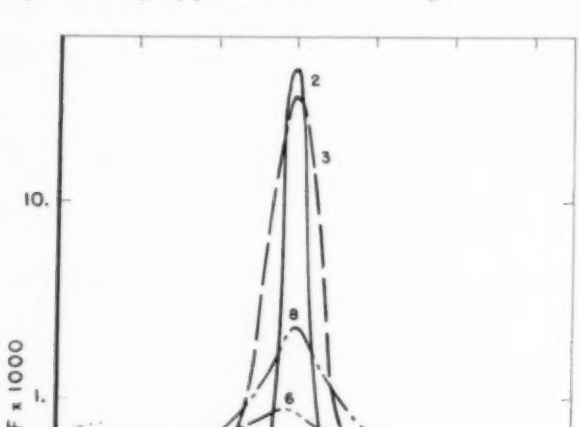

FIGURE 5.—*Fractional reflectance curves for wide-angle scatterers.*

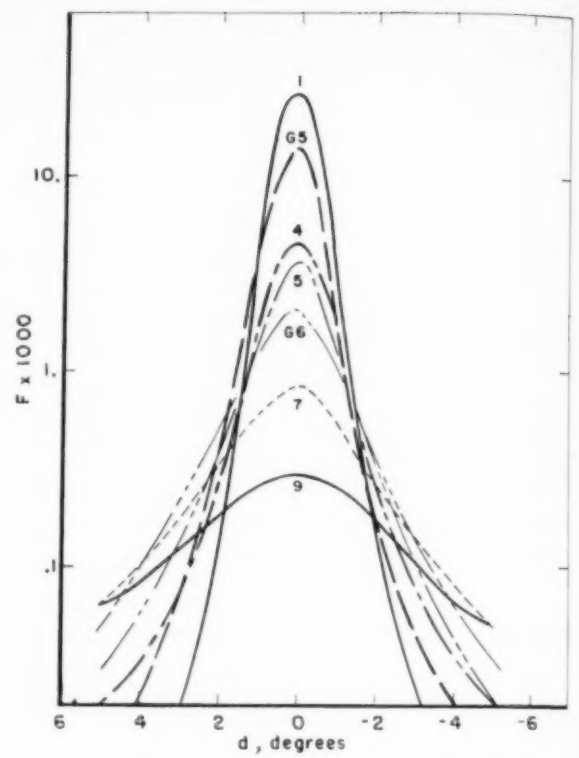

FIGURE 6.—*Fractional reflectance curves for narrow-angle scatterers.*

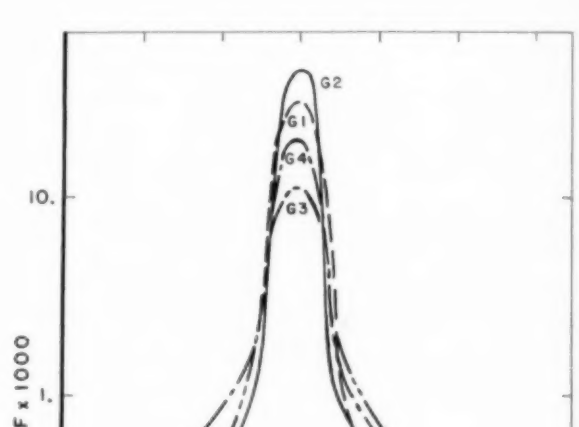

FIGURE 7.—*Fractional reflectance curves for intermediate-angle scatterers.*

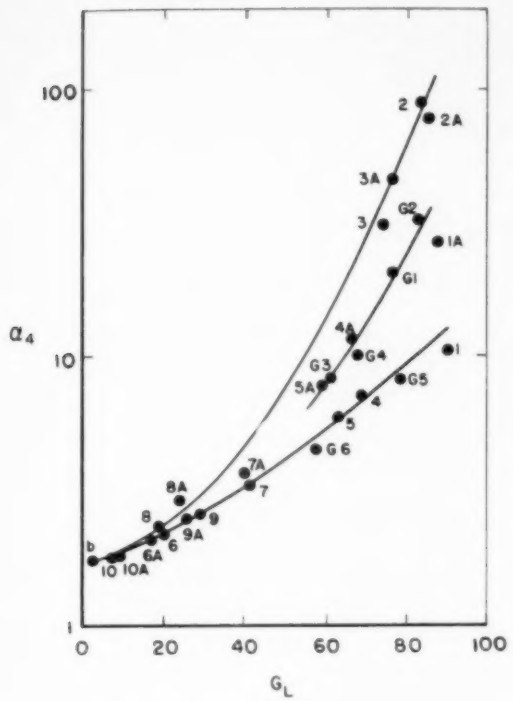

FIGURE 8. *Plot of peakedness index, α_4, against 60° specular glossmeter readings, G_L, showing separation into three groups.*

curves are are characterized by broad peaks with very little wide-angle scattering. As the scattering is confined to angles near the specular angle, these specimens may be called "narrow-angle scatterers," or "near-specular scatterers." Goniophotometric distributions for specimens of the intermediate type are shown in figure 7. These curves are characterized by peaks broader than those for the wide-angle scatterers but narrower than those for the narrow-angle scatterers. Such specimens might be called "intermediate-angle scatterers."

Nimeroff [10] showed that two parameters are required to reveal instrumentally the two extreme types of specimen appearance due to scattering. Figure 8 shows separation of the three types using the ASTM 60° specular gloss readings [7] and the peakedness indexes, α_4, obtained from analysis of goniophotometric curves of the specimens, some of which are shown in figures 5, 6, and 7.

5. Gloss of Transparent Finishes

Recently a problem arose in correlating the measured gloss with the observed appearance of transparent finishes applied to wood substrates. Difficulty was encountered in the measurement of the gloss of these finishes in that one-parameter techniques failed to yield data consistent with visual evaluation of the glossy appearance. In seeking a technique that would correlate with visual evaluations, 26 specimen panels were prepared by the Sherwin-Williams Co. and the Grand Rapids Varnish Co. Goniophotometric curves of representative panels are shown in figures 5, 6, and 7.

As stated above, a two-parameter technique was indicated as a possible solution to this problem. The slope of the monoplanar geometric distribution might be a useful representation of the gloss. An indication of the slope can be obtained from the ratio of a reading at the peak to a reading at the shoulder of a goniophotometric curve. The large receptor aperture used with the 60° geometry of ASTM Method D523 provides a measure of the sum of the peak and shoulders of the reflected flux distribution. A receptor aperture small enough to measure only the flux about the peak of a distribution was needed to supplement the reading with the larger aperture so that the slope of the flux distribution of a specimen can be evaluated:

$$\text{Slope}=\frac{2G_S-G_L}{\alpha'_1\beta'_1-\alpha'_2\beta'_2}, \tag{9}$$

where G_S is the instrument reading for the small receptor aperture, $\alpha'_1\beta'_1$, and G_L is the instrument reading for the large receptor aperture, $\alpha'_2\beta'_2$. The small receptor aperture arbitrarily chosen is $\alpha'_1\beta'_1=2.0°\times4.5°$. The larger aperture already prescribed by Method D523 is $\alpha'_2\beta'_2=4.4°\times11.7°$.

Measurement of the slope by this procedure is useful over regions of a curve where the slope is constant. As the goniophotometric curves of most specimens do not have constant slope, other relationships between G_L and G_S were sought. Several graphical representations of data were considered.

Figure 9 shows specular gloss data taken with the large aperture, G_L, plotted against data taken with the small aperture, G_S, for the specimens whose

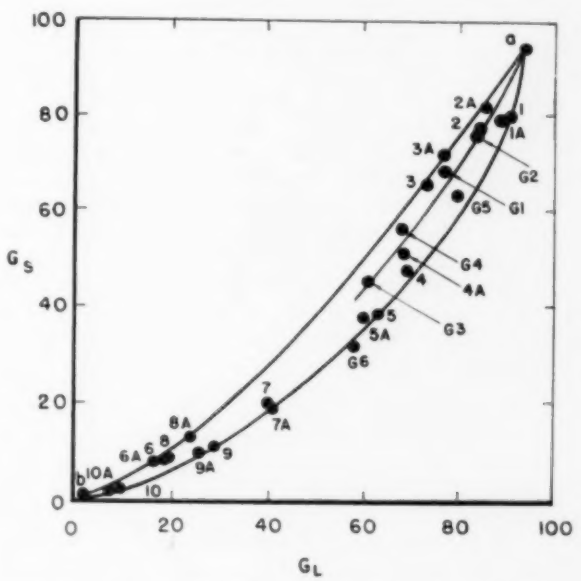

FIGURE 9. *Plot of glossmeter readings with small aperture against those with large.*

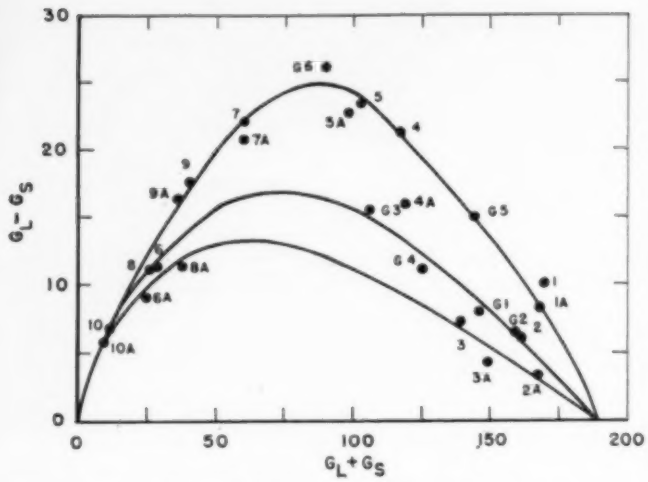

FIGURE 10. *Plot of differences, $D=G_L-G_S$, against sums, $S=G_L+G_S$.*

goniophotometric curves were shown earlier. The three branches that result are consistent with the separation into appearance types, as evidenced by the goniophotometric data. As aperture reduction stops more flux for narrow-angle scatterers than for wide-angle scatterers the data for the former lie in the lower branch. The plotted points in each branch lie in a sequence consistent with the order of the peaks of the goniophotometric curves for the specimens represented. The curve for a group of intermediate scatterers lies between those for the extreme types.

Terminal points *a* and *b* (fig. 10) occur at the indicated locations for the following reasons: If a receiver aperture is reduced to a size just larger than the source image the reading for a perfectly polished specimen is not varied because all the flux reflected from the surface of a polished specimen will enter the receiver if the receiver aperture is larger than the source image. Point *a* represents the specular gloss of a specimen of polished glass of index 1.527 and is plotted at 93.6 on both scales.

When a receiver aperture is reduced in area the glossmeter reading for a perfect diffuser will be reduced by the ratio of the areas. The glossmeter reading of a perfect diffuser for the receiver aperture of the 60° geometry of ASTM Method D523 was reported by Hammond and Nimeroff [5] to be 2.1. As the ratio of large to small receiver entrance window is 5.7, point *b* is plotted at G_L equal to 2.1 and G_S equal to 0.37.

6. Round-Robin Test

A round-robin test was undertaken on 26 specimens to evaluate data reproducibility, data repeatability, and specimen classification by the two-parameter (receptor aperture) method for specular gloss. By these terms are meant the following:

1. Data repeatability (within laboratory precision): Repetition by each laboratory of data obtained at that laboratory to within a reasonably small tolerance.

2. Data reproducibility (between laboratory variability): Reproduction by each laboratory of data obtained by the other laboratories to within a reasonably small tolerance.

3. Specimen Classification: The existence of at least three classes of gloss characteristics that can be distinguished by a two-parameter gloss technique.

6.1. Analysis of Round-Robin Data

The data resulting from the round-robin are shown in table 1.

To test repeatability and reproducibility we select a suitable mathematical model. The model used here for the measurement of the ith specimen in the jth laboratory is

$$y_{ij}=t_i+L_j+\epsilon_{ij}, \tag{10}$$

where y_{ij} is the measurement, t_i is the population, or "true," value of the measurement, L_j is a random variable having an average value of zero and variance σ_L^2, which reflects the variability between laboratories, and ϵ_{ij} is a random variable having an average value of zero and variance σ_j^2, which reflects the precision for laboratory j.

a. Repeatability

A duplicate measurement is denoted by a prime, as y'_{ij}. Then the difference between duplicate measurements is a quantity d_{ij}, thus

$$d_{ij}=y_{ij}-y'_{ij}=\epsilon_{ij}-\epsilon'_{ij} \tag{10a}$$

having an average value of zero and variance $2\sigma^2$. Thus if there is no reason to believe that the within-laboratory error varies with the different specimens, the variance σ_j^2 of each laboratory for the 26 specimens can be estimated by means of the equation.

$$s_j^2=\frac{\sum_i d_{ij}^2}{2n}=\frac{d_{1j}^2+\ldots+d_{26j}^2}{52}. \tag{11}$$

Systematic errors in duplicate measurements of G_L by laboratories 2 and 5 and of G_S by laboratory 2 were detected and eliminated from the estimates of precision for the determinations. Systematic errors in duplicate measurements for a laboratory are those in which d_{ij} is the same sign for all or most specimens. This error is evident when the average value for all specimens differs appreciably from zero. The results for each laboratory are given in table 2.

The variance of the within-laboratory data is of the same order of magnitude for all laboratories when systematic errors are eliminated from the estimates of variance. The average variance, s^2, within laboratories is 0.217 for G_L when s_5^2 is eliminated, and 0.212 for G_S when s_2^2 is eliminated. Thus repeatability for G_L is approximately equal to that and G_S and both variances are reasonably small.

TABLE 1. *Data for round-robin test*

Specimen	G_L for laboratory—							G_S for laboratory—						
	1	2	3	4	5	6	7	1	2	3	4	5	6	7
1	90.7	90.5	89.8	90.0	90.0	89.5	88.4	79.4	77.3	77.0	79.0	81.0	83.3	73.1
	90.4	90.6	90.0	90	92	89.3	89.1	80.2	79.1	79.2	79	....	84.2	72.4
1A	89.5	86.1	87.6	88	91	86.7	86.8	74.3	71.1	83.1	81	77	84.5	81.5
	87.5	88.8	88.8	89	92	85.0	87.5	75.8	79.8	84.5	82	....	86.5	80.9
2	83.8	83.3	82.2	84	86	83.9	80.4	79.1	77.8	76.2	77	78	77.0	73.7
	83.6	84.1	83.0	83	87	84.5	80.9	79.3	79.5	76.1	77	....	78.8	73.1
2A	84.6	84.7	84.4	85	88	85.0	81.9	82.6	82.7	83.2	82	81	78.4	76.5
	85.5	85.7	85.0	85	88	85.1	82.1	82.9	82.3	83.1	82	....	77.6	76.6
3	73.6	73.6	73.1	73	74	76.0	69.8	66.3	65.2	66.2	67	66	60.1	59.5
	74.0	74.1	73.8	73	75	76.2	70.3	66.9	66.5	66.4	66	....	58.9	59.3
3A	75.6	75.8	76.0	76	80	77.8	71.3	73.1	72.9	73.7	74	72	71.4	66.2
	76.0	75.5	76.0	76	82	77.8	71.7	73.4	74.1	72.3	74	....	70.2	64.6
4	70.8	69.6	68.2	68	67	70.5	67.9	49.2	47.0	44.5	45	51	45.2	41.9
	71.4	71.6	68.1	68	67	70.8	68.2	50.2	48.1	44.9	46	....	45.8	41.6
4A	69.5	68.8	65.7	66	64	71.3	66.5	53.4	50.8	50.9	51	52	45.5	46.9
	69.8	69.6	66.3	66	64	70.7	66.9	53.3	54.0	50.1	50	....	46.5	46.7
5	63.7	62.6	61.3	62	62	63.0	59.4	40.6	38.9	37.6	38	42	37.5	33.6
	63.8	63.0	62.4	62	64	62.7	59.5	40.3	40.6	37.6	39	....	37.9	33.2
5A	60.4	60.1	60.1	60	60	59.8	55.6	38.5	35.3	37.2	38	40	35.1	29.8
	60.5	60.0	60.5	60	63	59.4	56.0	38.5	37.8	37.8	38	....	36.2	29.5
6	18.6	19.2	18.1	19	21	21.4	14.6	8.2	9.2	7.8	8.6	8.3	9.6	4.4
	18.6	19.5	18.1	18	23	21.2	14.5	8.3	9.5	7.5	8.3	....	9.7	4.3
6A	16.0	16.2	15.4	15	19	19.7	11.7	7.3	8.0	6.7	7.4	7.2	8.6	3.5
	15.9	16.5	15.8	16	20	18.4	11.9	7.3	8.3	6.5	7.3	....	8.7	3.4
7	41.8	41.5	39.5	41	40	41.6	36.5	19.0	19.3	17.5	19	20	19.0	12.9
	41.8	42.1	40.7	41	41	41.4	36.8	19.0	20.2	17.2	19	....	18.9	12.9
7A	40.3	40.4	39.3	40	41	41.9	35.6	19.9	20.4	19.0	20	21	20.4	14.1
	40.5	40.5	40.3	40	43	42.0	35.7	19.8	21.0	19.0	19	....	20.2	14.0
8	17.1	18.8	17.9	17	22	20.9	13.7	7.5	9.1	7.9	7.6	7.7	8.3	3.9
	17.7	19.3	17.8	18	23	20.0	13.6	7.7	9.1	7.4	8.2	....	9.4	3.8
8A	21.0	24.0	24.1	23	29	24.2	17.6	11.3	14.9	13.2	13	12	13.8	7.9
	22.5	24.8	22.0	23	29	25.1	17.5	12.7	14.6	12.1	13	....	15.0	7.6
9	29.3	29.7	28.2	29	30	29.9	24.4	10.9	11.8	9.9	11	12	11.9	6.3
	29.4	29.8	28.6	29	31	30.0	24.5	11.8	12.2	9.7	11	....	11.9	6.2
9A	26.2	26.4	25.2	26	27	27.0	21.4	9.6	10.4	8.4	9.8	9.7	11.0	5.4
	26.1	26.6	25.2	26	28	27.2	21.5	9.6	10.6	8.5	9.7	....	10.7	5.3
10	8.5	9.4	7.6	8.6	9.0	9.4	5.1	1.8	2.4	1.4	1.9	1.9	2.8	0.0
	8.5	9.4	7.7	8.6	10.0	9.3	5.1	1.8	2.5	1.4	1.9	....	2.8	0.0
10A	7.4	8.0	6.8	7.4	8.0	8.4	4.0	1.6	2.2	1.4	1.9	1.6	2.6	0.0
	7.4	8.2	6.8	7.4	8.0	8.4	4.0	1.6	2.2	1.3	1.8	....	2.6	0.0
G1	79.1	76.7	76.6	75	76	75.6	70.7	70.4	67.2	71.1	67	68	48.0	46.9
	79.1	77.7	78.8	76	76	75.3	70.8	70.7	70.7	70.1	67	....	46.7	48.3
G2	82.7	82.4	83.2	82	80	84.8	77.6	76.3	75.0	78.2	76	75	75.3	68.0
	83.7	83.7	83.3	83	84	85.0	78.3	78.0	77.2	78.2	76	....	77.1	68.1
G3	63.5	60.8	59.3	60	60	61.1	54.4	49.6	43.3	43.2	44	47	45.0	37.6
	62.6	58.7	58.7	60	64	61.6	54.6	48.7	44.4	43.1	45	....	44.4	37.0
G4	67.6	64.0	67.4	67	70	69.8	61.6	57.8	53.6	57.8	54	57	59.0	49.0
	67.6	66.6	68.3	66	74	68.6	62.4	57.7	56.3	57.2	54	....	58.6	47.4
G5	79.8	78.2	79.2	79	80	79.1	73.0	64.1	59.7	64.2	64	67	54.6	52.5
	79.9	78.3	80.9	79	80	78.9	73.7	65.4	63.4	64.5	64	....	55.5	52.3
G6	59.3	57.2	55.8	58	56	58.7	53.2	32.0	32.5	29.3	32	35	30.7	25.0
	59.4	57.6	57.4	58	59	58.4	53.7	32.0	33.5	29.6	31	....	30.8	24.7

TABLE 2. *Variance of laboratories for G_L and G_S determinations*

Laboratory	s_i^2	
	G_L	G_S
1	0.196	0.152
2	.330	.727
3	.360	.179
4	.154	.144
5	.847	.....
6	.152	.396
7	.108	.188

b. Reproducibility

The variance for the average of six laboratories, each laboratory result being made up of two duplicate readings, is

$$[\sigma_L^2+(\sigma^2/2)]/6,$$

where σ_L^2 is the variability between laboratories and σ^2 is the variance within laboratories. The variability between laboratories for G_L is 2.07 and for G_S is 2.21. This analysis may be represented thus:

	$\sigma^2(G_L)$	$\sigma^2(G_S)$
Variance of a laboratory average of two readings	2.18	2.21
Variance of 6 laboratories average	0.36	0.37

This analysis shows that the reproducibility of G_L and G_S is approximately equal and the variance in both is reasonably small for the average of 6 laboratories, but is somewhat large for 1 laboratory average of 2 duplicate readings.

c. Specimen Classification

The data shown in figure 9 are the arithmetic mean values of readings obtained with the small aperture, G_S, plotted against arithmetic mean values of readings obtained with the large aperture, G_L. Because the errors in readings for G_L and G_S are correlated, simple functions of G_L and G_S are desired in which the errors are uncorrelated. These statistically uncorrelated functions would be useful for the final discrimination of gloss characteristics, that are, however, functionally related. Two simple functions, which seem to work well, are the sums, S, and differences, D:

$$S=G_L+G_S$$

$$D=G_L-G_S.$$

If only the determinations G_L and G_S are used for discrimination, the statistical correlations between them may obscure the discrimination between different gloss characteristics. Use of S and D accentuates the ability to discriminate gloss characteristics.

The fact that S and D are statistically uncorrelated can be demonstrated by the following simple argument. The correlation between S and D is given [14] by

$$\rho(S, D)=E[(S-\overline{S})(D-\overline{D})]/\sigma(S)\sigma(D), \qquad (12)$$

where E is read as "the expected value of"; $\overline{S}$ and $\overline{D}$ are the mean values of S and D, respectively. When G_L+G_S is substituted for S and G_L-G_S is substituted for D in eq (12), the following expression for the correlation between S and D results:

$$\rho(S,D)=\frac{\sigma^2(G_L)-\sigma^2(G_S)}{\sigma(S)\sigma(D)}. \qquad (12a)$$

Experimental results, discussed above, indicate that the variances, $\sigma^2(G_L)$ and $\sigma^2(G_S)$ are equal. Thus

$$\rho(S, D)=0.$$

Figure 10 shows a plot of the D versus S values for the data of figure 9.

7. Two-Parameter Method and Subjective Evaluation

The two-parameter (receptor aperture) method was found to correlate with goniophotometric curve evaluation in that three groups are established by both methods, each containing essentially the same specimens in essentially the same order (see figs. 8 and 10). Correlation between subjective and instrumental evaluation is required to esablish firmly the utility of the two-parameter method.

7.1. Image Distinctness and Constant Image Brightness

A test was arranged to determine whether image distinctness could be evaluated as the two-parameter method evaluates it, when variation in brightness is minimized. Twelve sets of three specimens, each set of approximately equal brightness (G_L), were selected from the 26 specimens and presented to the observers.

The source was a bank of fluorescent lamps. The standards were placed on a table so that images of the lamps were reflected at a specular angle of approximately 60°. The observers were asked to arrange the specimens in order of image distinctness, indicating ties where necessary. The selected sets of three specimens are listed in table 3, together with the corresponding G_L values. Image distinctness in each set of triplets increased from left to right and are given numbers 1, 2, and 3, respectively. In set 11, specimens 3 and 3A are from the same family of image distinctness and are both ranked 2.5. Similarly, specimens 4A and G3 of set 12 are ranked 2.5.

TABLE 3. *Sets of three specimens for evaluation of I with constant G_L*

Set	Specimens [a]			Corresponding G_L		
1	1	G2	2A	90	83	86
2	1A	2	2A	88	84	86
3	G5	2	2A	79	84	86
4	G5	G1	3	79	77	74
5	G5	G2	3A	79	83	77
6	G5	G1	3A	79	77	77
7	4	G1	3A	69	77	77
8	4	G1	3	69	77	74
9	4	G4	3	69	68	74
10	9A	6	8A	26	20	24
11	G1	[b] 3	[b] 3A	77	74	77
12	5	[c] 4A	[c] G3	63	67	61

[a] Image distinctness increases from left to right in each set of triplets, and are given numbers 1, 2, 3, respectively.
[b] Same image family.
[c] Same image family.

The results of this test are listed in table 4. As a measure of agreement between ranking given by the m judges and ranking assigned by G_S of the two-parameter method, an average of m rank correlations was determined. The Spearman rank correlation coefficient was used, and the average is indicated by $\overline{R}_S$. If (X_1, X_2, X_3) is the assigned ranking of three objects and (Y_{i1}, Y_{i2}, Y_{i3}), for $i=1$ to m, are the rankings given by the m judges, then,

$$\overline{R}_s=\frac{1}{m}\sum_1^m{}_i\left\{\sum_1^3{}_j(X_jY_{ij}-4)/2\right\}$$

$$=\frac{1}{2m}\sum_1^3{}_j\left\{X_j\left(\sum_1^m{}_iY_{ij}\right)-4m\right\}. \qquad (13)$$

The results of the computation of $\overline{R}_S$ for these specimens show quite good agreement between the assigned and the given rankings.

TABLE 4. *Rankings of triplets by 10 judges*

Set	DBJ	WAH	KLK	MMB	LEB	MAB	HKH	IN	MZ	JRR	Average ranking	$\overline{Rs}$
1	1 2 3	1 2 3	1 2 3	1 2 3	1 2 3	1 2 3	1 2 3	1 2 3	1 3 2	1 2 3	1 2 3	0.95
2	1 2.5 2.5	1 2 3	1.5 1.5 3	1 2 3	1 2 3	1 2.5 2.5	1 2.5 2.5	1 2 3	1 2 3	1 2.5 2.5	1 2 3	.88
3	1 2 3	1 2.5 2.5	1 2 3	1 2 3	1 2 3	1 2 3	1 2.5 2.5	1 2 3	1 2 3	1 2 3	1 2 3	.95
4	1 2 3	1 2 3	1 2 3	1 2 3	1 2 3	1 2 3	1 2 3	1 2 3	1 2 3	1 2 3	1 2 3	1.00
5	1 2 3	1 3 2	1 2 3	1 2 3	1 3 2	1 2 3	1 2 3	1 2 3	1 3 2	1 2 3	1 2 3	0.85
6	1 2 3	1 2 3	1 2 3	1 2 3	1 2 3	1 2 3	1 2 3	1 2 3	1 2 3	1 2 3	1 2 3	1.00
7	2 1 3	1 2 3	1 2 3	1 2 3	1 2 3	1 2 3	1 2 3	1 2 3	1 2 3	1 2 3	1 2 3	0.95
8	1 2 3	1 2 3	1 2 3	1 2 3	1 2 3	1 2 3	1 2 3	1 2 3	1 2 3	1 2 3	1 2 3	1.00
9	1 2 3	1 2 3	1 2 3	1 2 3	1 2 3	1 2 3	1 2 3	1 2 3	1 2 3	1 2 3	1 2 3	1.00
10	1 2 3	2 1 3	2 1 3	1 2 3	2 1 3	1 2 3	1 2 3	1 2 3	2 1 3	1.5 1.5 3	1 2 3	0.78
11	1 3 2	1 3 2	1 2.5 2.5	1 2 3	1 3 2	1 2 3	1 3 2	1 3 2	1 3 2	1 2.5 2.5	1 3 2	.65
12	1 2 3	1 2 3	1 2 3	1 2 3	1 2 3	1 2 3	2 2 2	1 2 3	2 1 3	1.5 1.5 3	1 2 3	.83

To measure the agreement among judges without reference to the "correctness" of what they agree upon, Kendall's coefficient of concordance [15], W, was used.

$$W=\frac{12\sum_{1}^{3}{}_j(\sum_{1}^{10}{}_i Y_{ij}-20)^2}{2400-10\sum_{1}^{10}{}_i(t_i^3-t_i)}, \qquad (14)$$

where

$$t_i=\begin{cases}0 \text{ for no ties}\\ 2 \text{ for two specimens tied}\\ 3 \text{ for three specimens tied.}\end{cases}$$

The results of the computation of W are listed in table 5. These results show a high concordance among the judges for the 12 sets selected.

We may therefore conclude that, where the image brightness range is not great, image distinctness is evaluated by the two-parameter method in accord with subjective evaluation. Thus the two-parameter method may be considered to be a successful technique for evaluating image distinctness when image brightness is relatively constant.

TABLE 5. *Measure of agreement among judges, Kendall's coefficient of concordance,* W

Set	W
1	0.91
2	.89
3	.96
4	1.00
5	0.79
6	1.00
7	0.91
8	1.00
9	1.00
10	0.77
11	.83
12	.80
Average	0.90

8. Summary

A complete description of the gloss characteristics of any specimen requires multiparameter data, obtained on either a multiplane or a monoplane goniophotometer. For reasons of economy simpler techniques are sought that can adequately describe the gloss characteristics of any specimen. The simplest method, using one parameter, does not always provide a sufficient description.

Two-parameter gloss methods provide more adequate description of the gloss of specimens than do one-parameter methods. A two-parameter technique employing specular reflection measurement for two incidence angles reveal specimen incidence-angle dependency. A gloss index may state the difference of specular reflectance for a difference of specular angle, $dG/d\theta$.

A two-parameter technique employing specular reflection measurement with a large and a small receptor aperture will reveal the existence of more than one gloss type. A specification may state the ranges of G_L and G_S, or S and D, thereby indicating the desired surface-appearance type.

The author thanks M. Zelen and Joan R. Rosenblatt for advice and assistance in the analysis of the round-robin data and the subjective evaluations, and W. A. Hall for assistance in this investigation.

9. References

[1] H. J. McNicholas, J. Research NBS **13,** 211 (1934) RP704.
[2] F. Thaler, Ann. Physik [4] **11,** 996 (1903).
[3] L. A. Wetlaufer and W. E. Scott, Ind. Eng. Chem., Anal. Ed. **12,** 647 (1940).
[4] P. Moon and J. Laurence, J. Opt. Soc. Am. **31,** 130 (1941).
[5] H. K. Hammond and I. Nimeroff, J. Research NBS **44,** 585 (1950) RP2105.
[6] W. E. K. Middleton and A. G. Mungall, J. Opt. Soc. Am. **42,** 572 (1952).
[7] W. W. Barkas, Proc. Phys. Soc. (London) **51,** 274 (1939).
[8] ASTM Standards Suppl. **6,** 434 (1954).
[9] C. L. Dows and G. R. Baumgartner, Trans. Illum. Eng. Soc. **30,** 746 (1935).
[10] I. Nimeroff, J. Research NBS **48,** 441 (1952) RP2335.
[11] ASTM Book of Standards **6,** 695 (1952).
[12] W. E. K. Middleton and A. G. Mungall, Can. J. Technol. **31,** 160 (1953).
[13] ASTM Standards Suppl. **4,** 84 (1953).
[14] A. McF. Mood, Introduction to the theory of statistics (McGraw-Hill Book Co., Inc., New York, N. Y., 1950).
[15] M. G. Kendall, Rank correlation methods (Charles Griffin & Co., Ltd., 1948).

WASHINGTON, April 19, 1956.

Journal of Research of the National Bureau of Standards Vol. 58, No. 3, March 1957 Research Paper 2745

Glassy State Transitions of Poly-(Chlorotrifluoroethylene), Poly-(Vinylidene Fluoride), and Their Copolymers[1]

L. Mandelkern, G. M. Martin, and F. A. Quinn, Jr.

The glass transition temperatures, T_g, of poly-(chlorotrifluoroethylene), poly-(vinylidene fluoride), and copolymers prepared from these two comonomers were determined using dilatometric and interferometric methods. The glass temperature of poly-(chlorotrifluoroethylene) was found to be at 45° C, an upper limit for the glass temperature of poly-(vinylidene fluoride) was set at −35° C, and the glass temperatures for the copolymers were between the values for the two homopolymers.

These results are found to substantiate the recent theoretical deductions of Fox and Loshaek relating the glass temperature of a copolymer to its composition, and indicate that the glass temperature of a copolymer is a monotonic function of its composition. The effect of crystallization of a copolymer on the location of its glass temperature is illustrated and the various contradictory results of this effect that have been reported are discussed.

1. Introduction

It is well recognized [1][2] that the glass transformation temperature, T_g, of a polymer is an important constant that characterizes the material. This temperature can serve as a convenient reference point in delineating the physical and mechanical properties of polymeric systems. For completely amorphous polymers rubberlike behavior will be observed above the glass temperature, whereas below this temperature the polymer will become hard and inelastic, and will embrittle very easily. Although many polymers are capable of undergoing crystallization they rarely attain complete crystallinity, and the amorphous or liquid-like regions of such systems can also undergo vitrification. The effect of vitrification on the physical properties of polymers of this type cannot be as clearly described as in the case of the completely amorphous polymers. The glass temperature in polymeric systems can be located by the abrupt changes that occur in its physical and mechanical properties as the temperature is varied, as well as by apparent changes that occur in certain thermodynamic quantities such as the volume-temperature coefficient or specific heat [2].

The elucidation of principles to explain the variation of the glass temperature with the chemical nature of the repeating unit of the polymer is one of the major objectives of physicochemical research in this field. Another objective of importance is the quantitative description of the way in which T_g of a given polymer will vary with molecular weight, with dilution by monomeric liquids, by copolymerization, or by branching. Efforts in attaining the latter objective have been in part successful by use of free volume concepts to describe the liquid state [3, 4, 5]. On the other hand, no well-defined theories exist at present that explain the dependence of T_g on the chemical nature of the repeating unit. Discussions of this problem in terms of the configuration of the polymer chain [6, 7, 8] and the interaction energies between chains [6, 7] have been made. The development of such principles would, of course, be extremely helpful in the search for polymers having specific properties in a given temperature interval. As an aid in achieving this goal it is important to have available the values of T_g for polymers of widely differing chemical natures. Although such information is already available for a large variety of polymers [3, 4, 5, 6, 7, 9], reliable information for T_g of the relatively newer fluorine-containing polymers is either lacking or obscure.

The more common polymers of this type, poly-(tetrafluoroethylene), poly-(chlorotrifluoroethylene), and poly-(vinylidene fluoride), usually occur in the partially crystalline state, a fact that in itself makes the determination of T_g more difficult. An additional complication that occurs in the study of polymers of this type is the fact that rotational disordering may occur in the crystalline state. Such a transition has already been observed for poly-(tetrafluoroethylene) [10, 11] and is also suspected to occur in poly-(chlorotrifluoroethylene) [12]. A transition of this type will make difficult the unambiguous determination of T_g as these transitions also manifest themselves by changes in both the mechanical and thermodynamic properties of the polymer.

The complications that can occur in the determination of T_g are clearly indicated in the case of poly-(chlorotrifluoroethylene). Attempts to determine the glass temperature of this polymer have been made by many investigators [6, 7, 13, 14] using various techniques, and values ranging from −120° to +50° C have been assigned. Recently, Tobolsky and McLaughlin [15], by assuming that T_g for this polymer occurs approximately at room temperature, were able to explain their measurements of stress-relaxation as a function of temperature. The wide divergence in values of T_g that have been reported for this polymer is rather unusual and is undoubtedly due to the effect of crystallinity. It would thus appear highly desirable that an effort be made to

[1] This work was supported in part by the Office of Quartermaster General, Washington, D. C.

[2] Figures in brackets indicate the literature references at the end of this paper.

obtain a reliable value of T_g for this polymer. To accomplish this methods must be devised by which the amount of crystallinity is substantially reduced so that the crystalline portions do not obscure the experimental observations.

In the case of poly-(chlorotrifluoroethylene) the reduction in the degree of crystallinity can be accomplished by at least two methods. As Kaufman [16] has previously indicated, by an appropriate thermal treatment the amount of crystallinity in the homopolymer can be substantially reduced and the homopolymer can thus be studied in this state. Another method that can be used is to study the glass temperatures of suitable copolymers over a wide range of compositions. Copolymerization inevitably reduces the amount of crystallinity, and T_g for the homopolymers can be deduced by appropriate theoretical considerations [17].

The present paper describes dilatometric and interferometric experiments that lead to the determination of T_g of poly-(chlorotrifluoroethylene), poly-(vinylidene fluoride), and copolymers prepared from these two comonomers. By using an appropriate thermal treatment prior to the initiation of observations an unambiguous determination of the glass temperature of poly-(chlorotrifluoroethylene) can be made. The value assigned is substantiated by the studies on the copolymers, and these studies also lead to the assignment of an approximate value of T_g for poly-(vinylidene fluoride). No suitable thermal treatment could be devised to reduce the amount of crystallinity for this latter polymer so that studies of the homopolymer itself are not too conclusive.

2. Experimental Procedure

2.1. Materials

The samples of poly-(chlorotrifluoroethylene) and the copolymers of chlorotrifluoroethylene and vinylidene fluoride were kindly supplied to us by the M. W. Kellogg Co., who also determined the copolymer compositions by chemical analyses. Vinylidene fluoride was polymerized in a sealed tube under the influence of gamma-ray irradiation.[3] The polymers were molded at elevated temperatures into rectangular sheets about 3 mm thick. Exploratory dilatometric measurements indicated the presence of volatile material in all the polymers so that prior to the initiation of the length-temperature of volume-temperature measurements the samples were heated in a vacuum at 110° C for about 24 hours.

2.2. Procedures

The volume-temperature measurements were made with volume dilatometers, using mercury as a confining fluid. The dilatometers that were used and the experimental procedures have already been described [18, 19]. The length-temperature measurements were made using the automatic recording interferometer developed by Work [20]. The absolute densities of the samples were obtained by the method of hydrostatic weighing [21], using water as the flotation liquid.

[3] The authors are indebted to J. D. Michaelsen and D. W. Brown of NBS for the preparation of this polymer.

3. Discussion and Results

3.1. Homopolymers

Volume-temperature and length-temperature measurements were made on the molded specimens of poly-(chlorotrifluoroethylene), using dilatometric and interferometric methods. Prior to the initiation of these studies, the samples to be investigated were wrapped in gold foil, heated for 30 minutes in a nitrogen atmosphere at 275° C, and quickly transferred to an ice-water mixture. The X-ray diffraction patterns of specimens that are treated in this manner indicate that the amount of crystallinity is substantially decreased. However, a small but well-defined peak still persists at a Bragg spacing of 5.5 A, which is the major spacing characteristic of this polymer [16]. Reproducible dilatometric results are obtained when the samples are conditioned in this manner and, if the temperature of observation does not exceed 110° C, no further crystallization occurs.

The dilatometric measurements extended over the temperature interval from −30° to +110° C, and in this range the observations were reproducible and independent of whether they were made on a heating or cooling cycle. Above 110° C the volume-temperature relations were no longer reproducible due to crystallization and decomposition. The dilatometric results for poly-(chlorotrifluoroethylene) in this reproducible temperature range are plotted in figure 1. The data are well represented by two straight lines that intersect at +45° C and indicate a glass temperature at this point. The volume-temperature coefficient below this temperature is 1×10^{-4} cm^3 g^{-1} °C^{-1}, which is a value char-

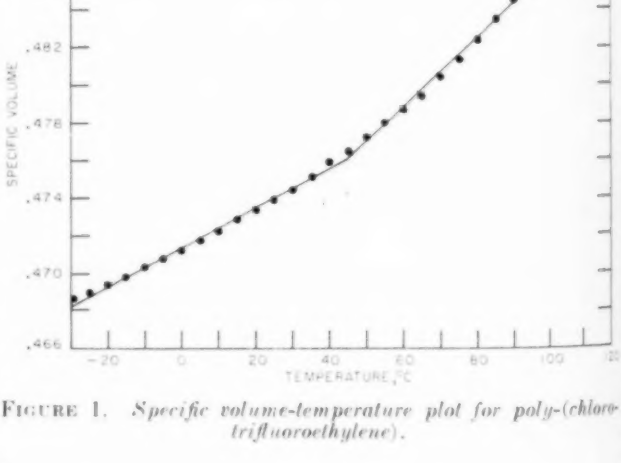

FIGURE 1. *Specific volume-temperature plot for poly-(chlorotrifluoroethylene).*

acteristic of the glassy state, whereas above this temperature this quantity is 2×10^{-4} cm^3 g^{-1} °C^{-1}. This latter coefficient is less than the value of 3.47×10^{-4} that has been recently reported [22] for the liquid polymer above its melting temperature. The differences in the value of the two liquid-like expansion coefficients may be due to the contribution of the crystalline regions to the volume-temperature coefficient above T_g. The possibility also exists that the liquidus is not linear from the melting temperature, about 220° C, to the glass temperature. The location of T_g at 45° C by these dilatometric measurements gives credence to the assumption made by Tobolsky and McLaughlin [15] in their interpretation of the temperature dependence of the mechanical properties of this polymer. This value also agrees with that which has been attributed to Reding [7]. If the amount of crystallinity of this polymer had not been substantially reduced, then the volume-temperature plot would be a gradually curving one in this temperature interval, and T_g would not have been detected by these methods.

Length-temperature measurements, encompassing a temperature range from −180° to +100° C, were also made on this polymer, using interferometric methods. A liquid-to-glass transformation at +45° C is also indicated by this technique of measurement. The length-temperature coefficient is linear from the glass temperature to −60° C, but as the temperature is decreased further, this coefficient also gradually decreases in a manner typical of materials in the glassy state [23]. When the polymer is initially heated in the interferometer its thickness increases by about 1 percent in going from the glassy to the liquid state. This change in thickness is irreversible during subsequent cooling and heating cycles, and no increase in volume is observed at a corresponding temperature by the dilatometric measurements. Because these samples were compression molded, this effect could be caused by the fact that strains induced in the system by the molding process are relieved by the increase in segmental mobility above the glass temperature. Similar results have been reported for the relief of strains in inorganic glasses as they transform to the liquid state [24].

The X-ray diffraction pattern for poly-(vinylidene fluoride) indicates that it is highly crystalline at room temperature. When this polymer is heated in a dilatometer in an effort to determine its melting temperature, excessive decomposition starts to occur at about 160° C, which is well below its melting temperature. This phenomenon precludes the determination or estimation of the melting temperature of this polymer, and as a result, in contrast to the situation for poly-(chlorotrifluoroethylene), no adequate thermal treatment could be devised to reduce substantially the crystallinity content. Thus, by necessity, the length-temperature and volume-temperature measurements had to be made on the highly crystalline polymer, which, as has been previously indicated, is very undesirable for the determination of T_g.

Length-temperature measurements were made in the range −185° to +30° C. Reliable dilatometric data, however, could only be obtained in the temperature interval −30° to +110° C. The results of the interferometric measurements are given in figure 2, where the expansion is plotted as a function of temperature. There is a definite linear portion to this plot that extends from −35° to +30° C and corresponds to a volume-temperature coefficient of 2.1×10^{-4} cm^3 g^{-1} °C^{-1}, a value that is corroborated by the dilatometric data. This value seems to be typical of the volume-temperature coefficient above T_g for this class of semicrystalline polymers. The gradual curvature of the plot in figure 2 below −35° C makes difficult the accurate determination of a glass temperature solely from these data. As measurements of the temperature dependence of the mechanical properties of this polymer have not been reported, we can deduce only that −35° C appears to be an upper limit for its glass temperature. As we shall see in the subsequent discussion, this value of T_g is consistent with the T_g's determined for the copolymers.

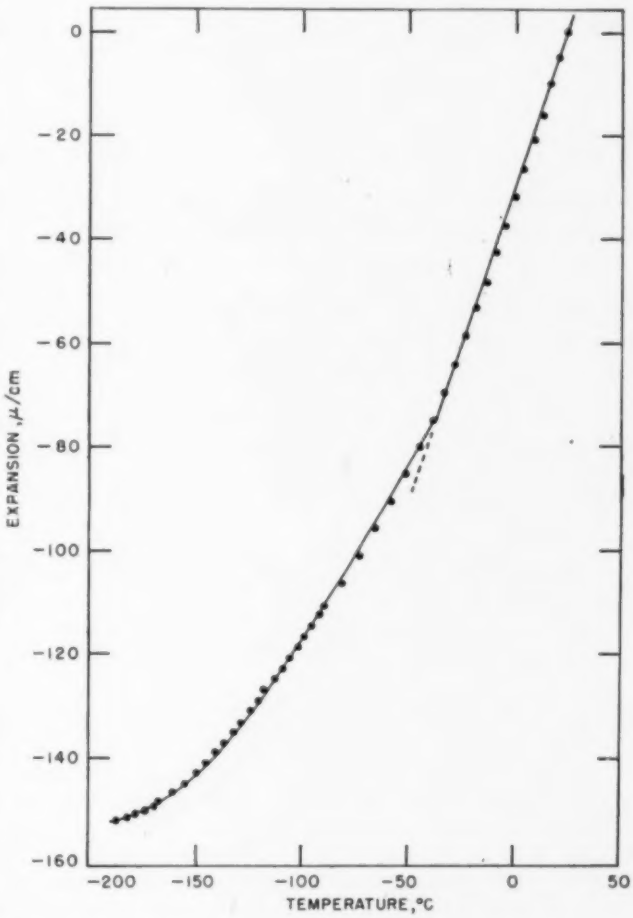

FIGURE 2. *Expansion-temperature plot for poly-(vinylidene fluoride).*

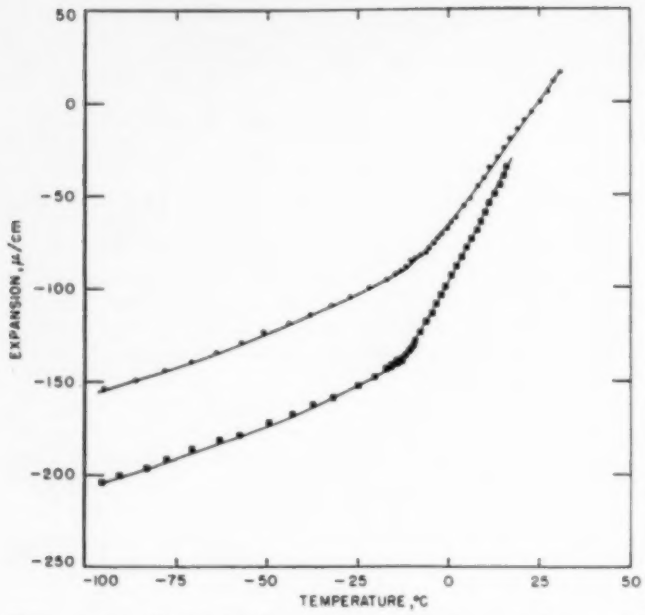

FIGURE 3. *Expansion-temperature plot for copolymers of chlorotrifluoroethylene and vinylidene fluoride.*

Upper curve for copolymer having composition $w_1=0.60$. Lower curve for copolymer having composition $w_1=0.46$.

3.2. Copolymers

The glass temperatures of a series of copolymers prepared from chlorotrifluoroethylene and vinylidene fluoride were determined, again using both dilatometric and interferometric techniques. The composition of the copolymers studied ranged from 0.44 to 0.85 for the weight fraction, w_1, of the chlorotrifluoroethylene component. A typical plot of the expansion as a function of temperature for the copolymers containing 46 and 60 percent of chlorotrifluoroethylene, respectively, is given in figure 3, whereas curve B of figure 6 is a plot of the specific volume as a function of temperature of the copolymers whose composition is given by $w_1=0.85$. The glass temperatures of all the copolymers studied are summarized in table 1.

TABLE 1. *Glass temperatures of copolymers of chlorotrifluoroethylene and vinylidene fluoride of various compositions* [a]

w_1	T_g
	°C
0.85	+20
.64	−2
.60	−8
.46	−15
.43	−20

[a] w_1 = weight fraction of chlorotrifluoroethylene.

The crystallization behavior of the copolymers in the temperature interval of interest depends on composition, so that care must be exercised in the interpretation of the data in table 1 because it might be expected that T_g for a copolymer will depend on the amount of crystallization. The copolymers containing about 60 percent of chlorotrifluoroethylene do not crystallize. Thus T_g for copolymers of this composition could be unambiguously determined, and the value given in table 1 is for the amorphous polymers. Copolymers of this composition have a glass temperature slightly below 0° C and hence have little utility as elastomers below this temperature.

The copolymer having a composition specified by $w_1=0.85$, though crystallizable, could be quenched and maintained amorphous through the glass-transformation range. The value of T_g given in table 1 is that for the amorphous polymer. The effect of crystallization on T_g for this copolymer is discussed in a subsequent section. The values of T_g given for the polymers containing the higher amounts of vinylidene fluoride are for the polymers in the semicrystalline state because they could neither be melted nor adequately quenched. The glass temperatures for the copolymers range from +20° to −20° C and are in qualitative agreement with the value determined for poly-(chlorotrifluoroethylene) and the upper limit that has been estimated for poly-(vinylidene fluoride).

From theoretical considerations, Fox and Loshaek [17] have developed quantitative relations between the glass temperatures of a copolymer of specified composition and the glass temperature of each of the homopolymers derived from the respective comonomers. The free-volume concepts, which have been successful in predicting the dependence of glass temperature on molecular weight [3] and the effect of crosslinking [4], have been extended by these investigators to copolymer systems. A brief outline of their considerations is given in the following paragraphs, and their theoretical results are applied to the experimental data reported here.

At a reference temperature in the liquid state the specific volume of a polymer is considered to be composed of two parts, the occupied volume and the free volume. The occupied volume represents a closely packed liquid structure. For simplicity in the subsequent analyses, it is assumed that the specific volume and occupied volume of a copolymer are additive functions of each of its components. Thus for the specific volume, $\overline{V}$, of the copolymer, we write

$$\overline{V}=w_1\overline{v}_1+w_2\overline{v}_2, \tag{1}$$

where $\overline{v}_1$ and $\overline{v}_2$ are the specific volumes of the two corresponding homopolymers, and w_1 and w_2 are the respective weight fractions of the two components. The dependence of the occupied volume on copolymer composition can be expressed in a manner similar to eq (1), and as a consequence the free volume of the copolymer becomes an additive function of composition.

Various criteria for glass formation can be considered. However, Williams, Landel, and Ferry [25] have concluded from an analysis of the temperature dependence of the viscosity-temperature coefficient of a variety of glass forming liquids that glass formation occurs when the ratio of the free volume to specific volume reaches a critical and constant value

independent of the nature of the liquid. We thus assume that at T_g for each of the homopolymers and of the copolymers the ratio of the free volume to specific volume is a constant designated as k; according to Williams, Landel, and Ferry [25], k is equal to 0.025.

Utilizing these assumptions, the result is obtained that [4]

$$1/T_g=[1/(w_1+Rw_2)][w_1/T_{g_1}+w_2/T_{g_2}], \quad (2)$$

where

$$R=[(\alpha_{L_2}-\alpha_2{}^*-k\alpha_{L_2})/(\alpha_{L_1}-\alpha_1{}^*-k\alpha_{L_1})][T_{g_2}/T_{g_1}]. \quad (3)$$

In eq (2), T_g is the glass temperature of the copolymer of composition w_1, T_{g_1} and T_{g_2} are the glass temperatures of the respective homopolymers, and the α_L's represent their volume-temperature coefficients in the liquid state and the α^*'s the corresponding coefficient for their occupied volumes. Equation (2) is similar in form to an equation previously derived by Gordon and Taylor [26]. Because it is difficult to express α^* in terms of any of the measured volume-temperature coefficients, R is best considered an arbitrary parameter in eq (2). For the special case where $R=1$, eq (2) reduces to the simple relation that

$$1/T_g=w_1/T_{g_1}+w_2/T_{g_2}. \quad (4)$$

Because T_g for poly-(vinylidene fluoride) has only been estimated, the best way of comparing the experimental results of this paper with the conclusions of eq (2) would be to calculate theoretical curves for different values of R and T_g for this polymer. In figure 4 the experimental results are represented by the solid circles and the theoretical curves, which best fit the data, are also given. In this plot curves A and B represent the simplest case where $R=1$ and T_g for poly-(vinylidene fluoride) has the values $-50°$ C and $-60°$ C, respectively. For curve C, $R=1.5$ and $T_g=-40°$ C, whereas curve D represents the situation where $R=1.2$ and $T_g=-50°$ C. No reasonable theoretical curves could be drawn when the glass temperature of poly-(vinylidene fluoride) was assigned a value greater than $-40°$ C. From the representation in figure 4 we can conclude that the results for the chlorotrifluoroethylene-vinylidene fluoride copolymer system are quantitatively consistent with the theoretical considerations of Fox and Loshaek [17]. However, due to the facts that values for T_g are not available for copolymers containing less than 45 percent trifluorochloroethylene and that there is uncertainty in the value of T_g for poly-(vinylidene fluoride), these data alone could not serve as a substantiation of eq (2).

Experimental verification of eq (2) was obtained by Fox and Loshaek [17], who determined T_g of a series of copolymers that were derived from a variety of comonomers and covered a wide composition range. Excellent agreement was found between the experimental observations and eq (2), whereas the value of the parameter R required to fit the data did not vary appreciably from unity for the different series of copolymers studied. These results substantiate eq (2) and indicate that T_g for a copolymer is a monotonic function of its composition, so that maxima or minima in the T_g-composition curve would not be expected. Thus, in an attempt to prepare copolymers having low glass temperature, comonomers should be selected whose homopolymers also have low glass temperatures.

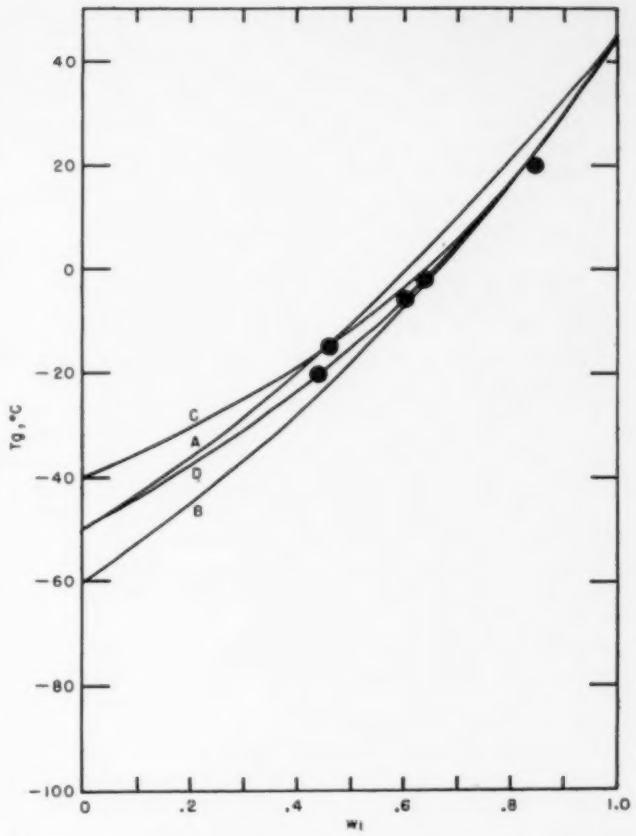

FIGURE 4. *Theoretical curves of glass temperature against composition.*

Solid circles represent experimental results.

3.3. Effect of Crystallization on Glass Transformation Temperature

Polymers in general do not crystallize completely, so that the amorphous or liquid-like regions, which may in some instances constitute more than half the volume of the polymer, are still capable of undergoing glass transformation. The random introduction of noncrystallizing copolymeric units into a homopolymer chain that can crystallize will reduce further the final amount of crystallinity that can be attained. It is of interest to know whether the glass temperature is affected by the amount of crystalli-

[4] The above derivation of eq (2) and the subsequent definition of R differ slightly from that originally given by Fox and Loshaek [17]. However, the differences are minor and imperceptible when applied to experimental data.

zation when the crystallization is induced solely by cooling without the application of any external stress. Contradictory experimental evidence exists as to whether there are any effects of this type in homopolymers and no definitive results appear to have been reported for copolymers.

Because the composition of the amorphous regions of a homopolymer does not change with crystallization one might expect that the glass temperature would also remain invariant. The results obtained by Bekkedahl [9] support this premise because, for natural rubber, T_g remained constant at $-70°$ C irrespective of whether the polymer was partially crystalline or completely amorphous. However, the results obtained by Kolb and Izard [27] and by Woods [28] for poly-(ethylene terephthalate), presumably a homopolymer, are in contradiction to those obtained for natural rubber. These investigators found from volume-temperature measurements that the glass temperature of poly-(ethylene terephthalate) increases by about 20 deg after crystallization ensues. A similar effect of the change in T_g with the amount of crystallinity, using dynamical mechanical methods, was also observed by Woods. Thus the experimental evidence for the effect of crystallization on the glass temperature of a homopolymer is at present contradictory and would appear to be specific for a given polymer.

If we consider a random copolymer composed of A and B units and if only the A units participate in the crystallization, then the amorphous regions of the copolymer will have a greater concentration of B units than the total composition. Because only the amorphous regions participate in the glass transformation we might expect the glass transformation of the copolymer to shift in the direction characteristic of the component that does not crystallize as the crystallization process progresses.

The situation just described can be realized for the copolymers of chlorotrifluoroethylene and vinylidene fluoride having the composition of $w_1=0.85$. If this copolymer is heated above its melting point and quickly quenched to 0° C, only a small amount of crystallinity develops. This is illustrated by the X-ray diffraction pattern for the copolymer treated in this manner given by curve B of figure 5, where an almost completely amorphous pattern is obtained. The volume-temperature curve for this copolymer is given in curve B of figure 6, and, as has already been mentioned, a glass temperature at $+20°$ C is indicated.

When this polymer is heated above 35° C more rapid crystallization ensues and the X-ray diffraction pattern A of figure 5 is obtained. The Bragg spacings in this pattern indicate that only the chlorotrifluoroethylene units are crystallizing, and hence the amorphous regions must contain a greater concentration of vinylidene fluoride units than the nominal composition. The volume-temperature curve corresponding to the more crystalline copolymer is given by curve A of figure 6. The specific volume for this copolymer is, of course, less than that for the amorphous polymer and the glass temperature

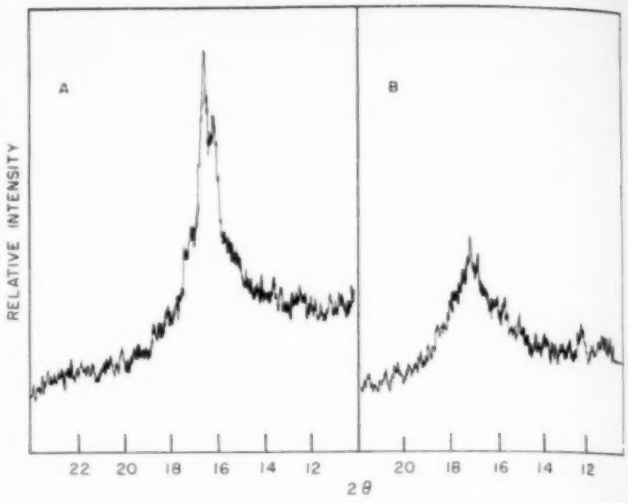

FIGURE 5. *A, X-ray diffraction pattern of crystalline copolymer having composition $w_1=0.85$. B, Same copolymer after thermal treatment to reduce amount of crystallinity.*

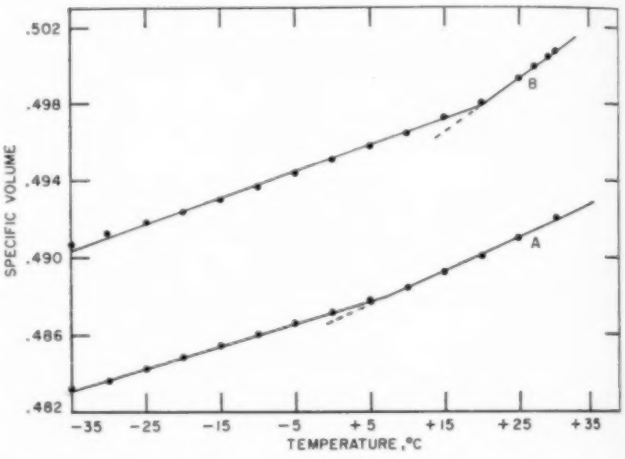

FIGURE 6. *Volume-temperature plots of copolymer having composition corresponding to $w_1=0.85$.*

Curve A, highly crystalline material; curve B, crystallinity substantially reduced.

occurs at $+7°$ C. These results are a clear indication that the crystallization of one type of unit in a random copolymer results in a shift in the glass temperature in the direction of higher compositions of the noncrystallizing component. Coincident with the development of crystallinity the volume-temperature coefficient above the glass temperature decreased from 3.0×10^{-4} cm^3 g^{-1} °C^{-1} for the amorphous polymer to 1.8×10^{-4} cm^3 g^{-1} °C^{-1} for the partially crystalline polymer. In their study of Saran, a copolymer of vinylidene chloride and vinyl chloride, Boyer and Spencer [29] found that as the fraction of the polymer that was crystalline varied from 0.187 to 0.67 the glass temperature remained constant. However, in this study the nature of the crystallizing units was not described and the possibility of cocrystallization exists. It is evident that

with the contradictory evidence now available more systematic studies of the effect of crystallization on T_g must be undertaken both for homopolymers and copolymers, though the results reported here indicate that crystallization will cause a shift in the value of T_g.

4. References

[1] R. F. Boyer and R. Spencer, Advances in Colloid Chemistry **II,** 21 (Interscience Publishers, Inc., New York, N. Y., 1946).
[2] W. Kauzmann, Chem. Revs. **43,** 219 (1948).
[3] T. G. Fox and P. J. Flory, J. Appl. Phys. **21,** 581 (1950); T. G. Fox and P. J. Flory, J. Polymer Sci. **14,** 315 (1954).
[4] T. G. Fox and S. Loshaek, J. Polymer Sci. **15,** 371 (1955).
[5] S. Loshaek, J. Polymer Sci. **15,** 391 (1955).
[6] R. F. Boyer, Changement des phases, Compt. rend. de la 2d reunion de chimie physics, p. 384 (1952).
[7] R. F. Boyer, J. Appl. Phys. **25,** 185 (1954).
[8] J. H. Gibbs, J. Chem. Phys. **25,** 185 (1956).
[9] N. Bekkedahl, J. Research NBS **13,** 411 (1934) RP717.
[10] C. W. Bunn and E. R. Howells, Nature **174,** 549 (1954).
[11] F. A. Quinn, Jr., D. E. Roberts, and R. N. Work, J. Appl. Phys. **22,** 1084 (1951).
[12] J. D. Hoffman, Bul. Am. Phys. Soc. [II] **1,** 110 (March 15, 1956).
[13] F. P. Price, J. Am. Chem. Soc. **74,** 311 (1952).
[14] J. D. Hoffman, J. Am. Chem. Soc. **74,** 1696 (1952).
[15] A. V. Tobolsky and J. R. McLaughlin, J. Phys. Chem **59,** 989 (1955).
[16] H. S. Kaufman, J. Am. Chem. Soc. **75,** 1477 (1953).
[17] T. G. Fox, Bul. Am. Phys. Soc. [II] **1,** 123 (March 15, 1956).
[18] P. J. Flory, L. Mandelkern, and H. K. Hall, J. Am. Chem. Soc. **73,** 2532 (1951).
[19] L. Mandelkern and P. J. Flory, J. Am. Chem. Soc. **73,** 3206 (1951).
[20] R. N. Work, J. Research NBS **47,** 80 (1951) RP2230.
[21] L. A. Wood, N. Bekkedahl, and F. L. Roth, J. Research NBS **29,** 391 (1942) RP1507.
[22] S. Furuya and M. Honda, J. Polymer Sci. **20,** 587 (1956).
[23] G. M. Martin, S. S. Rogers, and L. Mandelkern, J. Polymer Sci. **20,** 579 (1956).
[24] S. M. Cox, J. F. Stirling, and P. L. Kirby, J. Soc. Glass Tech. **35,** 103 (1951).
[25] M. L. Williams, R. F. Landel, and J. D. Ferry, J. Am. Chem. Soc. **77,** 3701 (1955).
[26] M. Gordon and J. S. Taylor, J. Appl. Chem. **2,** 493 (1952).
[27] H. J. Kolb and E. F. Izard, J. Appl. Phys. **20,** 564 (1949).
[28] D. W. Woods, Nature **174,** 753 (1954).
[29] R. F. Boyer and R. S. Spencer, J. Appl. Phys. **15,** 398 (1944).

WASHINGTON, October 12, 1956.

Journal of Research of the National Bureau of Standards Vol. 58, No. 3, March 1957 Research Paper 2746

Measurement of the Corrosion Rate of Iron by Polarization Techniques

W. J. Schwerdtfeger

Corrosion-rate-measuring techniques previously shown to be applicable to low-carbon steel exposed to corrosive soils are also shown to apply to low- and medium-carbon steels in a sodium chloride solution having a concentration of 2,000 parts per million. Unlike the work previously reported, *IR* drops, attributable to polarizing currents, are included in the potential measurements.

It is shown how corrosion-rate measurements can be made automatically by using a synchronously driven voltage divider and a two-pen electronic recorder.

The polarizing characteristics of high-silicon cast iron when exposed to a 2,000-parts-per-million sodium chloride solution were also studied. It is shown that the corrosion rate becomes relatively low as the corrosion reaction changes from cathodic to anodic control.

1. Introduction

Iron and steel are the most commonly used structural materials and under certain conditions of exposure are very susceptible to severe damage by corrosion. In the laboratory, the extent of corrosion is usually expressed in such terms as "weight loss" or "pit depth," whereas, in the case of permanent field structures, visual inspection is probably the chief way of evaluating damage.

When the degree of corrosion is based on weight loss, the test specimens must be exposed sufficiently long to render the cleaning errors negligible in comparison with the actual weight losses. Also, in order to study the effect of exposure time on the rate of corrosion of a given material, removals of similar specimens at several intervals must be resorted to. Under these conditions, the results depend on the uniformity of the electrolyte. If the electrolyte is a soil, the corrosion rates of similar specimens may differ unless the degree of aeration around each is the same.

On permanent field structures, corrosion products must be removed in order to estimate the extent of corrosion damage. After inspection, unless preventive measures are taken, corrosion will be resumed, temporarily at least, at an accelerated rate.

The foregoing encourages the search for any method of measuring corrosion rate in which the disadvantages discussed above might be overcome. Previous work has shown that the corrosion rates on small low-carbon steel specimens exposed to soils in the laboratory can be measured electrically by the analysis of polarization curves [1].[1] During that investigation, weighed steel disks (exposed area—2.4 in.^{2}) were exposed to 6 soils for a period of 2 months. Cathodic and anodic polarization curves were obtained on the specimens at periodic intervals, followed by cleaning and reweighing. On the average, the calculated weight losses based on the electrolytic measurements and Faraday's law were within 4 percent of the measured weight losses. In each of the 6 soils, it was observed that a relatively constant ratio existed between the calculated corrosion current and a value of current, designated I_p, obtained from a break (change-in-slope) in the cathodic-polarization curve. As the corrosion process was cathodically controlled, the use of cathodic polarization, exclusively, in measuring corrosion rate appeared to be justifiable. The simplified approach was suggested by Pearson [2] and by Holler [3]. During that investigation [1] this was tried, using one soil, and found to be satisfactory.

Up to the present time, corrosion-rate measurements, based on cathodic and anodic polarization cruves, have been made with null or current-interruption circuits [1, 2, 3, 4, 5]. Although such circuits are necessary when accurate potential readings are desired, their use is not always necessary for observing breaks in polarization curves. The purpose of this investigation is to show, at least for the conditions of the experiments, that substantially all corrosion can be evaluated by using somewhat more simple electrical measuring techniques than usually employed, in which the *IR* drops are included in the potential measurements. The use of cathodic-polarization measurements, exclusively, is evaluated by measuring the effects of heat treatment and carbon content on the corrosion rate of carbon steel. The adaptability of a duplex electronic recorder for use in studying polarization characteristics and measuring rates of corrosion is also illustrated and discussed.

2. Theoretical Considerations

The hypothetical polarizing characteristics of a galvanic couple exposed to an aqueous medium of negligible resistance are shown graphically in figure 1. Part A shows the polarization of the anode and cathode of the couple and part B represents the effect of external current on the couple.

The symbols used in this paper are identified and defined as follows:

E_a = open-circuit potential of the anode.
E_c = open-circuit potential of the cathode.
E_g = potential of the couple.
i_0 = local action or corrosion current.
I_p = external cathodic current applied to the couple when the anode current (local-action current) becomes zero. This is the minimum current required for cathodic protection.

[1] Figures in brackets indicate the literature references at the end of this paper.

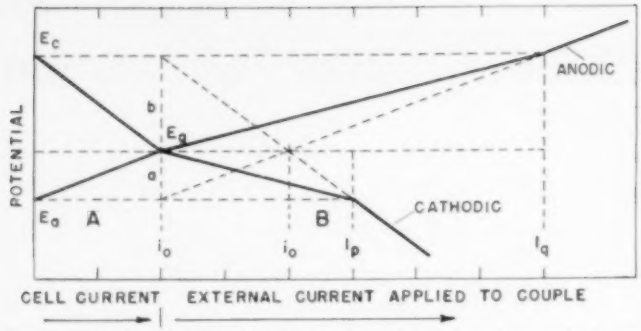

FIGURE 1. *Hypothetical polarization of a galvanic couple in an electrolyte of high conductivity.*

I_q = external anodic current applied to the couple when the cathode current (local-action current) becomes zero.

a = change (ΔE_g) in the potential of the couple from the value at zero applied current to the value at I_p.

b = change (ΔE_g) in the potential of the couple from the value at zero applied current to the value at I_q.

With reference to figure 1, it has been shown previously [1] that

$$\frac{a}{b}=\frac{I_p}{I_q} \tag{1}$$

and

$$i_0=\frac{b}{a+b}I_p=\frac{I_q}{I_p+I_q}I_p. \tag{2}$$

The ratio a/b might be regarded as a measure for expressing the type of polarization control. Complete cathodic control is approached as the current I_q becomes large as compared with the current I_p. Under such conditions, on the basis of eq (2), i_0 is substantially equal to I_p.

It can be seen (fig. 1) that as the ratio a/b becomes smaller the change-in-slope of the curve at I_q becomes increasingly difficult to observe. Fortunately, the change-in-slope at the current I_p is relatively easy to observe in many cathodically controlled reactions, where it is also more significant than I_q. Such happens to be the case with low-alloy ferrous materials exposed to soils and solutions.

It has been shown that, for steel exposed to soils, the cathodic-protection current, I_p, bears a nearly linear relationship to the corrosion current, i_0, and as a consequence the rate of corrosion can be estimated from cathodic-polarization curves [1]. Based on eq (2), it is interesting to note that a variation in the ratio I_p/I_q from 0.1 to 0.25, for a given value of I_p, results in a change in the corrosion current of only about 11 percent. Thus, it is desirable to establish the ratio empirically and to base corrosion-rate calculations on the cathodic-polarization curves, exclusively, whenever possible, as some degree of error is possible even when estimating I_p from the polarization curve. Evans [6] has pointed out that, in the absence of passivity, cathodic polarization bears a greater influence on corrosion rate than does anodic polarization.

In obtaining polarization curves by ordinary potential measurements between a reference electrode and the specimen during passage of the polarizing current, the IR drop in the corroding medium is included in the measurements. However, whether measuring this potential, or the potential, free of IR drop (as in fig. 1), obtainable by special methods of measurement, there will occur a break in the potential-current curve at I_p or I_q as dependent on the type of polarization being employed. Thus, in corrosion-rate studies, potential measurements including IR drops are satisfactory.

Although most corrosion reactions are said to be cathodically controlled, the polarization method of measuring corrosion rate also applies to reactions that are anodically controlled. In reactions under anodic control the current I_q (eq 2) becomes the more significant as it is then smaller than I_p. Also, the slope (a/i_0) of the anodic-polarization curve beyond the current I_q will be steeper than the slope (b/i_0) of the cathodic-polarization curve beyond the current I_p. This follows from eq (1), which could be written,

$$\frac{I_p}{I_q}=\frac{a/i_0}{b/i_0}, \tag{3}$$

and will be shown later to apply to experimental data on high-silicon cast iron.

3. Experimental Procedure

All the electrical measurements to be described later were made on ferrous specimens exposed to a solution containing 0.2 percent (2,000 ppm) of sodium chloride in tap water, which varied in temperature between 20° and 27° C. Based on data in the Corrosion Handbook [7], this solution is almost as corrosive to iron as one containing 3 percent of sodium chloride. Thus, sizable weight losses could be expected in a reasonable length of time, and yet the concentration was low enough to provide IR drops of sufficient magnitude to affect the potential readings and thus permit study of the usefulness of the proposed method. The electrolyte was contained by an open cylindrical wooden vat (fig. 2) having an inside diameter of about 66 in. and was maintained to a depth of about 18 in. The arrangement of supporting bars, shown fastened across the top of the vat, was used for mounting and positioning of the specimens and a half-cell probe. Auxiliary anodes are shown mounted on the inner wall of the vat. The solution was renewed between the individual tests described in the experimental results.

Except for one tubular-steel specimen, all steel specimens were of rod material. Specific dimensions are given in the section on experimental results. The ends of the rods and edges of the tubing were rounded and all burrs removed so as to avoid weight-loss errors and accelerated corrosion at the edges. This was followed by degreasing with carbon tetrachloride. The aluminum- and silicon-killed steel specimens were immersed in a 5-percent sulfuric acid solution for 2 hr, with intermittent scrubbing to remove loosened mill scale, followed by immersion

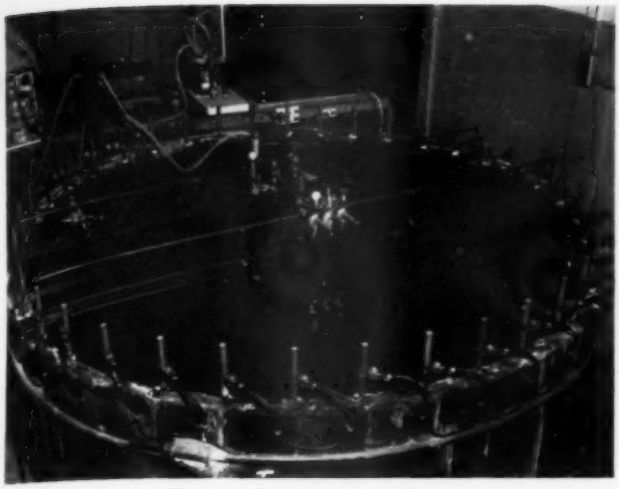

FIGURE 2. *View of the experimental arrangement.*

in a 10-percent calcium hydroxide solution for 15 min and finally washing the specimens in running hot water. All specimens were then steel-wire brushed so as to produce a bright surface and weighed to the nearest 5 mg. The high-silicon cast-iron specimen, although wire brushed, was exposed without weighing, in anticipation of negligible corrosion. Having a rough surface, a cleaning error could easily exceed the actual weight loss due to corrosion.

All specimens were protected against corrosion at the water line by covering a 3-in. intermediate section with plastic electrical tape (half-lapped). The unexposed portion of the specimen (bare surface above the tape) was covered with a film of oil in order to prevent atmospheric corrosion, the portion on the other side of the tape being exposed to the electrolyte. The rod specimens were each fitted with a perforated rubber stopper over which a clamp was fitted for holding the specimen in a vertical position during exposure.

Polarization data were obtained on a given set of specimens at fairly regular intervals during the exposure periods, which ranged from 14 to 45 days. After the exposure of the specimens, the tape was removed and the corrosion products loosened and removed by cathodically cleaning the specimens in the test electrolyte for a period of 2 to 3 hr at a current density of about 1 amp/ft.^{2} Following this, the specimens were lightly brushed under running hot water with a steel wire brush and then, when dry, more vigorously with a brass wire brush. The specimens were then reweighed in order to measure the actual weight losses attributable to corrosion.

All potential measurements were made with reference to a saturated calomel half-cell, which was bridged to the electrolyte by a flexible plastic tube filled with a saturated potassium chloride-agar mixture. When measurements were to be made, the agar bridge was slipped into a sleeve made of insulating material mounted vertically inside of the wooden vat and also symmetrically with respect to the set of specimens under exposure. The end of the flexible tube just protruded from the lower end of the sleeve. The end of the flexible tube was in a horizontal plane through the centers of the exposed lengths of the specimens and off to the side a distance not less than one-quarter of the length of an exposed section. In the beginning, when the recorder was not used, potentials were measured with a high-resistance voltmeter (200,000 ohms/v) and the polarizing current, supplied through graphite anodes, was adjusted manually. The polarization data were obtained by increasing the current in equal increments of 2-min duration. Later, when using the recorder, polarizing current was applied by linearly increasing the applied voltage by means of a synchronously driven voltage divider. Metal anodes were used when measurements were made with the recorder in order to eliminate the polarization difficulties present with the graphite anodes.

4. Experimental Results

4.1. Evaluation of i_0/I_p for Carbon Steel

In order to find the relationship between the polarizing currents I_p and I_q pertaining to carbon steel exposed to the 0.2-percent sodium chloride solution, and consequently the evaluation of i_0/I_p, a $\frac{3}{16}$-in.-diameter cold-rolled specimen was exposed for 29 days.

In addition to the preparatory procedure outlined in section 3, the exposed tip of the specimen was coated by dipping the rod into molten bitumen, leaving 12 in. for exposure to the electrolyte.

The data obtained as a result of cathodically and anodically polarizing the specimen are tabulated in table 1. Typical polarization curves from which the values of I_p and I_q were obtained are shown in figure 3. The weight loss of the rod during the exposure period, not stated in the table, was 345 mg. By Faraday's law, 30 mg was removed electrolytically during the 8 anodic polarization runs, each of which was 45 min in duration at an average current of 5 ma. The total calculated weight loss of 313 mg (283 mg during exposure plus 30 mg during anodic polarization runs) differs by about 9 percent from the measured weight loss of 345 mg. The estimated effect of the cathodic runs on weight-loss reduction is less than 1 percent and is therefore neglected. Aside from the possible errors attributable to the interpretation of the polarization curves (fig. 3), the degree of variation between the calculated and measured weight losses also depends on the margin of error in assuming linear changes in corrosion rate between successive measurements (table 1).

It will be noted (table 1) that the values of I_p/I_q lie within a range that corresponds to only a relatively small variation of i_0/I_p. In fact, in view of the reasoning already presented in section 2, the use of the expression $i_0=0.9\ I_p$ would appear to be justifiable. Accordingly, therefore, a considerably larger specimen was prepared for exposure in order to further test the i_0/I_p ratio. The specimen was a 3.25-in. o. d. cold-drawn steel tube with 9.25 in. of its outer length exposed to the salt solution. The exposed lower end of the tube was fitted with a rubber

TABLE 1. *Relationship between the corrosion current and cathodic protection current for carbon steel exposed to a 0.2-percent sodium chloride solution*

Exposure time	Polarizing current at break in curve		Corrosion current,[a] i_0	Weight loss calculated[b]	Ratio $\frac{I_p}{I_q}$	Ratio $\frac{i_0}{I_p}$
	Cathodic, I_p	Anodic, I_q				
Days	*ma*	*ma*	*ma*	*mg*		
4	0.34	3.0	0.31	31	0.11	0.91
5	.34	3.0	.31	8	.11	.91
6	.50	4.0	.44	9	.12	.88
7	.51	4.0	.45	11	.13	.88
13	.33	3.8	.30	56	.09	.91
18	.29	3.2	.27	36	.09	.93
22	.66	5.0	.58	43	.13	.88
29	.50	4.1	.45	89	.12	.90
				[c] 283	[d] .11	[d] .90

[a] $i_0 = I_p I_q / (I_p + I_q)$, eq (2).
[b] Weight loss (grams) $= Kti_0$, where $K = 2.8938 \times 10^{-4}$ g/coulomb and i_0 is the average current (amp) for the period, t, in seconds, between successive readings during exposure. For the periods before the initial and following the final polarization runs, the values of i_0 for the initial and final runs, respectively, were taken as average.
[c] Total value attributed to normal corrosion.
[d] Average value.

stopper and sealed around the edge with molten asphalt in order to confine the corrosion to the external surface of the tube. This end rested on an inverted glass beaker, centrally positioned in the wooden vat. The tube was held in a vertical position and protected against corrosion at the electrolyte line and above as previously described.

Cathodic- and anodic-polarization curves were obtained on the specimen. The I_p/I_q ratio was found to be approximately the same as that observed with the 3/16-in. rod and therefore the weight-loss calcula-

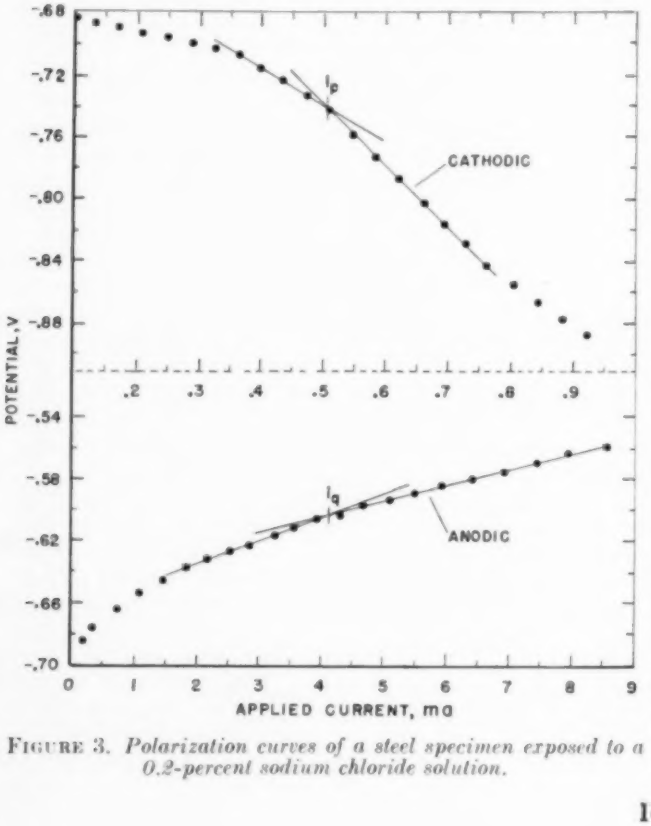

FIGURE 3. *Polarization curves of a steel specimen exposed to a 0.2-percent sodium chloride solution.*

TABLE 2. *Corrosion rate on a 3¼-in.-diameter steel tube, as calculated from cathodic-polarization curves only, when exposed to a 0.2-percent sodium chloride solution*

Exposure time	Polarizing current at break in curve, I_p	Corrosion current,[b] i_0	Weight loss, calculated[c]
Days	*ma*	*ma*	*mg*
[a] 0	2.4	2.2	------
2	3.6	3.2	135
6	3.1	2.8	300
8	4.4	4.0	170
10	3.2	2.9	175
13	2.9	2.6	202
15	2.8	2.5	125
17	3.6	3.2	145
20	2.5	2.2	202
22	2.4	2.2	110
24	2.5	2.2	110
27	3.2	2.9	188
29	2.9	2.6	140
30	------	------	65
			[d] 2,067

[a] After 4 hr of exposure.
[b] $i_0 = 0.9 I_p$ (see footnote d, table 1).
[c] See footnote b of table 1.
[d] Total value attributed to normal corrosion.

tions are based on $i_0 = 0.9\ I_p$ (table 2). During the running of the 13 anodic polarization curves, it was estimated that an additional 98 mg of iron went into solution; the effect of the cathodic runs on weight loss was neglected, it being less than 1 percent. The tube lost 2,245 mg during the 30-day exposure period. Based on this measured total value, the calculated weight loss of 2,165 mg (2,067 mg during exposure plus 98 mg during anodic-polarization runs) differed by 3.6 percent.

4.2. Comparison of Aluminum- and Silicon-Killed Low-Carbon Steels—Normal and Heat-Treated

It has been shown that cathodid-polarization curves are useful alone as a means for measuring the corrosion rate of carbon steels. This section will be devoted to further study of the sensitivity and practicability of this method.

The specimens were prepared as discussed in section 3 and were cut from ½-in. rod with 12 in. of rod length exposed to the corrodent. Four specimens were simultaneously exposed to the 0.2-percent salt solution for a period of 14 days. Two of the specimens were of aluminum-killed steel, one being heated to 1,650° F and water-quenched before exposure. The other two specimens were of silicon-killed steel, one being similarly heat-treated.

The data (table 3) indicate that the corrosion rates of the two steels are approximately alike. However, water-quenching appears to have increased the corrosion rates by about 10 percent, on the basis of both the calculated and the actual weight losses. The agreement between the calculated and actual weight losses is remarkably good. As the polarization curves were obtained on the 4 rods within a period of 3 hr, the average values of I_p (table 3) are probably just as valid as the calculated weight losses for comparing the relative rates of corrosion.

TABLE 3. *Comparative corrosion rates of aluminum- and silicon-killed steels—effects of water-quenching*

Exposure time	Polarizing current at break in curve, I_p	Weight loss	
		Calculated [d]	As weighed
Aluminum-killed, no heat treatment [a]			
Days	*ma*	*mg*	*mg*
4	1.60	144	-------
7	1.16	93	-------
10	0.66	61	-------
12	.68	30	-------
14	-------	30	-------
	[c] 1.02	[c] 358	365
Aluminum-killed, water-quenched [a]			
4	1.60	144	-------
7	1.28	97	-------
10	1.00	77	-------
12	0.86	42	-------
14	-------	39	-------
	[c] 1.18	[c] 399	400
Silicon-killed, no heat treatment [b]			
4	1.70	153	-------
7	0.92	88	-------
10	.68	54	-------
12	.78	33	-------
14	-------	35	-------
	[c] 1.02	[c] 363	360
Silicon-killed, water-quenched [b]			
4	1.82	164	-------
7	0.94	93	-------
10	.97	64	-------
12	.78	39	-------
14	-------	35	-------
	[c] 1.12	[c] 395	390

[a] Composition of steel in percent: 0.20 C, 0.53 Mn, 0.016 P, 0.027 S, 0.03 Si.
[b] Composition of steel in percent: 0.19 C, 0.42 Mn, 0.015 P, 0.025 S, 0.14 Si.
[c] Average value.
[d] $\frac{I_p}{2}=0.9I_p$ (see footnotes b and d, table 1).
[e] Total value.

4.3. Corrosion-Rate Measurements, Using Automatic Equipment

These data were obtained by using a two-pen "continuous balance" electronic recorder. One of the pens recorded the potential of the corroding specimen as measured with a high-impedance circuit, and the other pen recorded the polarizing current to the specimen produced by a linearly increasing applied voltage. The applied voltage was taken from a 10-turn potentiometer (voltage divider) geared down to a speed of 0.2 rpm by a synchronous motor equipped with a gear train. Thus, the potential and the current were recorded simultaneously.

In addition to minimizing human error, the recorder offers other advantages over indicating instruments. For example, upon interruption of the applied voltage, the magnitude of IR drop included in the polarized potential can be estimated from the polarization decay curve following the removal of applied current.

a. Preliminary Measurements

The data were taken on the aluminum-killed non-heat-treated specimen previously discussed in section 4.2. A composite photograph (fig. 4) of a series of strip-chart records shows the effect on the corrosion rate of the specimen, as reflected by the cathodic-polarization curves, when air was forced into the electrolyte. Charts A and B were run on the fourth

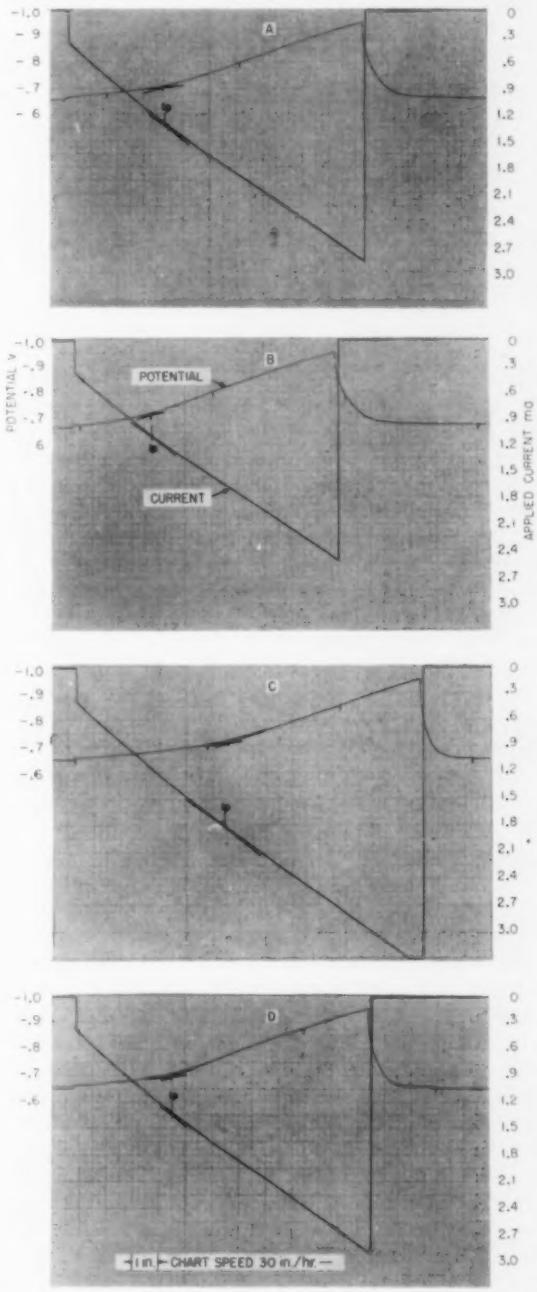

FIGURE 4. *Cathodic polarization of a steel specimen exposed to the 0.2-percent sodium chloride solution as recorded by the electronic recorder.*

A, 4 days after initial exposure, solution is still; B, 5 days after initial exposure solution is still; C, 7 days after initial exposure, air forced into the solution since B; D, 8 days after initial exposure, solution is still, air off since C.

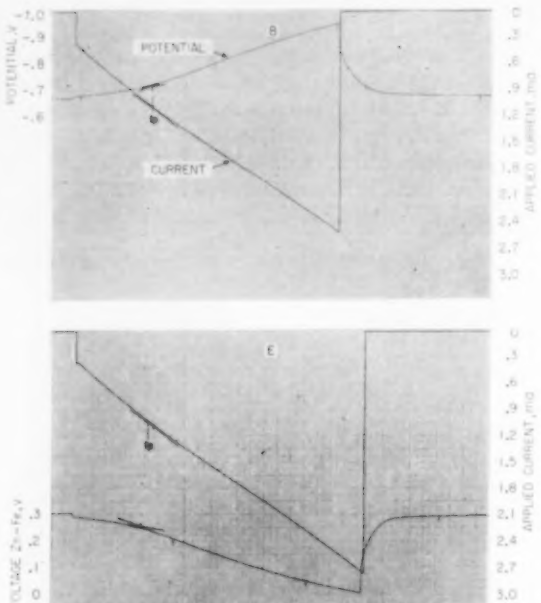

FIGURE 5. *Use of auxiliary anode* (Zn) *as a reference electrode* (*chart E*).

and fifth days, respectively, of exposure. After recording chart B, air was introduced into the salt solution at an arbitrary rate, continuously for 2 days when the curves (chart C) were obtained. The aeration was then discontinued and the following day chart D was recorded.

It will be noted (fig. 4) that the breaks, I_p, are reflected by both the current and the potential curves. The aeration of the electrolyte caused the corrosion rate of the steel to be increased (chart C) by about 50 percent. This is shown by a reduction in the rate of corrosion (chart D) with the air off.

On charts A and D, the breaks I_p indicate approximately equal rates of corrosion and the respective changes in both the current and the potential-versus-time curves are almost identical.

The coincidence of the break in the current curve with that in the potential curve is due to the fact that the zinc, used as the auxiliary anode, did not polarize appreciably throughout the range of polarizing current. Such being the case, an anode might also be made to serve as a reference electrode. Figure 5 is composed of two curves obtained on this steel specimen; the first B, reproduced from figure 4, being obtained with the saturated calomel reference electrode, and the second, E, was obtained 6 days later, using the zinc anode as the reference. It will be observed that the break due to the polarization of the specimen is clearly shown by the voltage (Zn-Fe) curve and agrees fairly well with the break in the current curve.

b. Comparison of Low- and Medium-Carbon Steel and Effects of Heat-Treating the Medium-Carbon Steel

Four specimens were exposed to a 0.2-percent sodium chloride solution for 45 days. One specimen was of low-carbon steel (0.15 C) and the others were of medium-carbon steel (0.45 C). One of the medium-carbon specimens was in the hot-rolled condition (as received), one, water-quenched from 1,650° F., and the other, water-quenched from 1,650° F and tempered at 1,400° F. All were cut from $\frac{5}{8}$-in.-diameter stock and 12 in. of length was exposed to the salt solution. The specimens were symmetrically positioned around the reference electrode, which was mounted in the center of the wooden tank.

TABLE 4. *Corrosion rates of low- and medium-carbon steels based on strip-chart records—effect of heat-treating the medium carbon steel*

Exposure: 45 days in 0.2-percent sodium chloride solution.

Exposure time	Polarizing current, I_p (strip chart)			
	Low-carbon steel [c]	Medium-carbon steel [d]		
		No heat treatment	Heat-treated	
			Quenched [e]	Quenched and tempered [f]
Days	*ma*	*ma*	*ma*	*ma*
0	1.50	1.60	1.40	1.50
2	1.30	1.35	1.20	1.35
6	1.50	1.46	1.25	1.22
7	1.27	1.10	1.20	0.95
9	1.30	1.10	1.20	0.96
12	1.20	1.03	1.20	1.00
15	1.15	1.10	1.25	0.95
16	1.50	1.30	1.60	1.10
19	1.45	1.05	1.43	1.05
20	1.05	0.97	1.14	0.97
21	1.15	1.05	1.23	1.05
22	1.05	1.05	1.30	1.07
23	1.08	1.08	1.30	1.05
26	1.20	1.20	1.38	1.10
27	1.23	1.23	1.35	1.15
28	1.10	1.10	1.27	1.10
29	1.28	1.35	1.43	1.20
30	1.48	1.45	1.45	1.44
33	1.20	1.20	1.35	1.15
34	1.45	1.45	1.55	1.10
36	1.18	1.20	1.28	1.10
37	1.16	1.20	1.30	1.10
40	1.30	1.30	1.44	1.25
41	1.26	1.25	1.35	1.25
42	1.35	1.35	1.45	1.35
Avg I_p	1.27	1.22	1.33	1.15
Calculated weight loss [a] ..... mg..	1,286	1,235	1,347	1,164
Actual weight loss ..... mg..	1,300	1,285	1,285	1,225
Difference between actual and calculated weight loss [b] ..... %	−1.1	−3.9	4.8	−5.0

[a] $i_0 = 0.9\ I_p$ (see footnotes b and d, table 1).
[b] Based on the actual weight loss.
[c] Not over 0.15 C.
[d] 0.45 C.
[e] 1,650° F, then water-quenched.
[f] 1,650° F, then water-quenched, then tempered from 1,400° F.

Data obtained from the cathodic polarization curves and weight losses are shown in table 4. In order to check the i_0/I_p ratio, previously evaluated, anodic polarization curves, in addition to cathodic, were obtained on the 7th, 19th, 30th, and 42d days of exposure for each of the four specimens. The average i_0/I_p ratio, resulting from the 16 sets of

data, was again approximately 0.9, ranging from 0.88 to 0.92. The calculated weight losses (table 4) are based on the average values of I_p, as measurements were made frequently. The net effect of both cathodic and anodic polarization on the weight losses was estimated to be less than 1 percent and therefore is neglected.

The differences in the corrosion rates of the specimens, both actual and calculated, must be considered negligible with possibly the exception of the tempered specimen. These and previous measurements seem to indicate that variations in values of I_p as low as 10 percent can be considered as revealing significant differences in rates of corrosion when the control of the corrosion reaction is within the limits previously described.

c. Measurements on High-Silicon Cast Iron

High-silicon cast iron is known for its good corrosion resistance in many aqueous environments. The material is not machinable and comes fabricated only in the form of castings. Because of these characteristics, accurate corrosion weight-loss measurements cannot be made when high-silicon cast iron is exposed for relatively short periods of time, but the polarization technique of corrosion-rate measurement would appear to be particularly adaptable.

A specimen of high-silicon cast iron (Duriron), in the form of an anode ordinarily sold for use in cathodic protection, was exposed to a 0.2-percent sodium chloride solution for a period of 28 days, during which time the polarizing characteristics of the material were studied. The specimen had a diameter of 1 in., and 12 in. of its length was exposed to the electrolyte. Contrary to the behavior of carbon steel, the potential of the high-silicon cast iron started to change toward more cathodic values after having been exposed for 1 hr.

Cathodic and anodic polarization curves recorded during the first 14 days of exposure are shown in figure 6. The cathodic curve A was obtained after the specimen had been exposed for 3½ hr. Then, after a lapse of another 2 hr, allowed for the decay of the cathodic polarization, the anodic curve A was recorded. The break in the cathodic-potential curve, A, occurred at a current I_p of 1.8 ma, whereas no break appeared in the corresponding anodic-potential curve for the range of applied currents shown. This initial set of curves is typical of those for carbon steel in that the cathodic polarization is greater than the anodic polarization, and the magnitude of I_p is about what would be expected for the exposed area involved. There was visible evidence of a fairly high corrosion rate during the first 24 hr in the form of rust, which commenced to appear around the high-silicon cast iron a few hours after exposure. The action is considered normal for this material during the early stages of exposure. The change in potential toward more cathodic values continued and in 24 hr amounted to approximately 0.3 v, at which time the second pair of curves, B, was obtained. It will be observed that anodic polarization now occurs at a greater rate than on the previous day and that the corrosion reaction is now anodically controlled (table 5). Thus, the corrosion rate is now determined chiefly by the break in the anodic-potential curve as evaluated by the current I_q. The slope of the anodic-potential curve now becomes steeper at currents greater than I_q, whereas when the reaction was cathodically controlled (curves A) the slope of the cathodic potential curve became steeper at currents greater than I_p.

TABLE 5. *Polarization-curve data on high-silicon cast iron exposed to a 0.2-percent sodium chloride solution*

Exposure time	Curve (fig. 6)	Corrosion potential	Polarizing current		Slope [a]	
			cathodic, I_p	anodic, I_q	cathodic, b/i_0	anodic, a/i_0
Days		*v*	*ma*	*ma*	*mv/ma*	*mv/ma*
0.2	A	−0.530	1.80	>1.80	100	14
1	B	−.235	>0.40	0.40	80	480
5	C	−.075	.30	.05	117	700
14	D	−.060	.40	.05	115	960

[a] See the text.

The next set of polarization curves, C, were obtained after 5 days of exposure. It will be noted that the corrosion potential had changed still farther in the noble direction and that the corrosion rate as indicated by the current I_q is even smaller than previously. The final set of curves, D, shown in figure 6, were run on the 14th day of exposure. The corrosion potential is about the same as it was on the 5th day of exposure, as is the corrosion rate. Curves, not shown, were again obtained on the 28th day of exposure when breaks in the potential curves appeared at substantially the same values of current as revealed by curves D. The specimen was then removed from the salt solution. The little evidence of rust was readily removed with a wire brush.

That eq (3) is fairly well substantiated by the results obtained from the polarization curves is shown by the data (table 5). This is particularly so for the data from curves C and D where values are given for both I_p and I_q. Excessive IR drop, if included in the polarized potentials, would disturb the relation, but in the experiment under discussion it can be seen that the IR component, as can be estimated from the decay curves (fig. 6) following the removal of polarizing current, was only a small part of the potential change.

As previously mentioned, the values of I_p and I_q from curves D (table 5) represent a condition that is substantially stabilized for longer periods of exposure. Therefore, by substituting these values of I_p and I_q into eq (2) and using the resultant value of i_0 in Faraday's equation, the weight-loss equivalent figures out to be about 0.055 (oz/ft²)/yr. That this is a realistic value can be judged by comparing it with weight-loss measurements on high-silicon cast iron made by Logan [8] after approximately 12 years of underground exposure. The average weight loss was 0.031 (oz/ft²)/yr on specimens buried in 35 soils ranging in resistivity from 60 to 45,000 ohm-cm.

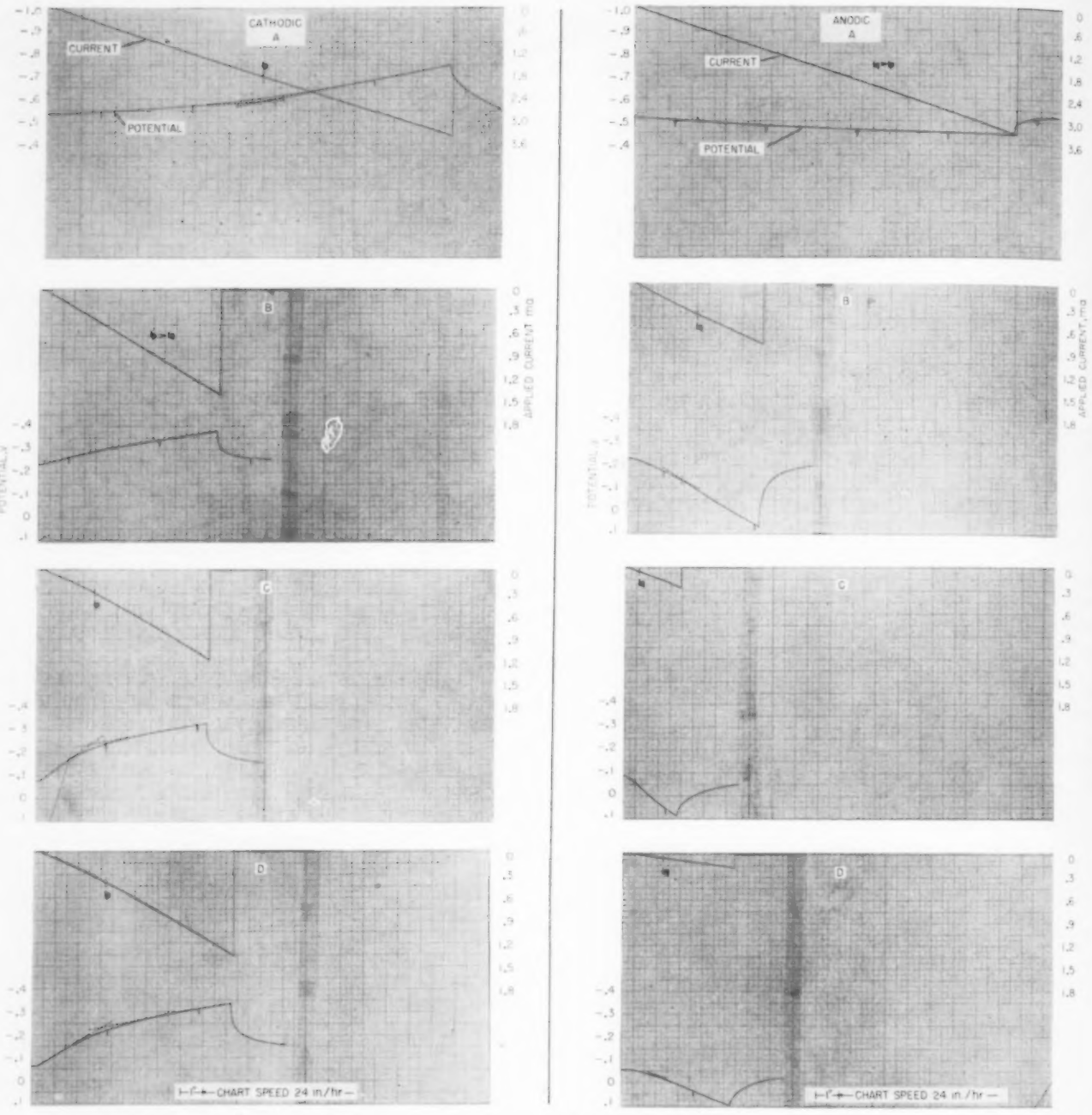

FIGURE 6. *Polarization of high-silicon cast iron exposed to a stagnant 0.2-percent sodium chloride solution.*

A, 3 to 5 hr after initial exposure; B, after 24 hr of exposure; C, after 5 days of exposure; D, after 14 days of exposure.

5. Summary

The corrosion of carbon steel in a 0.2-percent sodium chloride solution was found to be cathodically controlled to the extent that the ratio between corrosion and cathodic protection currents was relatively constant, being about 0.9. This value corresponds to an average ratio, 0.83, previously found applicable for carbon steel exposed to a variety of corrosive soils [1].

The sensitivity of the cathodic-polarization technique, as a means for measuring relative rates of corrosion, was studied by simultaneously exposing aluminum- and silicon-killed carbon steels, having approximately the same composition, to the 0.2-percent sodium chloride solution for 14 days. Also included were additional specimens of the same steels after water-quenching from 1,650° F. Neither the polarization nor the weight-loss measurements revealed any differences in the corrosion rates of

aluminum-killed or silicon-killed steel specimens, but both methods of measurement showed that quenching presumably caused the rates of corrosion to be slightly increased.

The use of polarization curves for measuring rates of corrosion is also shown by strip chart records made with a two-pen electronic recorder. Preliminary measurements illustrated the effect of increasing the rate of corrosion of carbon steel exposed to a 0.2-percent salt solution when air was bubbled into the electrolyte. Zinc used as the auxiliary anode was also found to be satisfactory as a reference electrode for the range of polarizing current involved.

The sensitivity of polarization curves in measuring rates of corrosion was further explored by using automatic equipment for recording the cathodic polarization on simultaneously exposed low and medium carbon steels. Some of the medium carbon specimens were heat-treated before exposure. The corrosion rates calculated from the polarization curves were within ± 5 percent of the corrosion rates shown by the actual weight losses.

Upon exposing a specimen of high-silicon cast iron to the 0.2-percent sodium chloride solution, the control of the corrosion reaction was observed to shift from cathodic to anodic within a period of 24 hr; automatic recording equipment was used. After 14 days of exposure, the corrosion rate appeared to be quite stable; and, based on breaks in the polarization curves, chiefly the anodic curves, the corrosion rate was estimated as being about 0.055 $(oz/ft^2)/yr$. This value is shown to be comparable to the corrosion rate of the same material based on 12 years of underground exposure, thus showing the value of polarization curves in quickly estimating rates of corrosion that could not be measured accurately by weight loss for short periods of exposure.

It is not suggested that the measurement of polarization curves be used as a substitute for long-time-exposure tests, as one is unable to extrapolate with a high degree of certainty the corrosion rates over long periods of time. However, it is believed that the polarization technique of corrosion-rate measurement is a good way of screening materials for underground- or marine-exposure studies.

The author expresses his thanks to William T. Bryan of the Duriron Co. and to Samuel Epstein of the Research Department of the Bethlehem Steel Co. for supplying some of the materials for specimens, and to Carl R. Johnson of the Thermal Metallurgy Section, National Bureau of Standards, for heat-treating specimens used in this investigation.

6. References

[1] W. J. Schwerdtfeger and O. N. McDorman, Measurement of the corrosion rate of a metal from its polarizing characteristics, J. Electrochem. Soc. **99,** 407 (1952).
[2] J. M. Pearson, "Null" methods applied to corrosion measurements, Trans. Electrochem. Soc. **81,** 485 (1942).
[3] H. D. Holler, Studies on galvanic couples. I & II. Some potential-current relations in galvanic corrosion, J. Electrochem. Soc. **97,** 271 (1950); also Corrosion **7,** 52 (1951).
[4] P. A. Johnson and A. L. Babb, Thermodynamics of irreversible processes applied to corrosion, Ind. Eng. Chem. **46,** 518 (Mar. 31, 1954).
[5] W. J. Schwerdtfeger, Electrical measurements in the selection of bolt materials for service underground, J. Research NBS **52,** 265 (1954) RP2499.
[6] U. R. Evans, Metallic corrosion, passivity, and protection (Longmans, Green, & Co., New York, N. Y., 1946).
[7] Corrosion Handbook, Electrochemical Society, p. 131 (John Wiley & Sons, Inc., New York, N. Y., 1948).
[8] K. H. Logan, Soil-corrosion studies, 1934. Rates of loss of weight and pitting of ferrous specimens, J. Research NBS **16,** (May 1936) RP883

WASHINGTON, October 19, 1956.

Journal of Research of the National Bureau of Standards Vol. 58, No. 3, March 1957 Research Paper 2747

Numerical Computation of the Transfinite Diameter of Two Collinear Line Segments

Philip Davis

Orthonormal polynomials are employed to compute the transfinite diameter of a set consisting of two collinear line segments. With polynomials of degree 10, two-place accuracy has been achieved.

The concept of the transfinite diameter $\tau(E)$ of a closed bounded point set E was introduced by M. Fekete [5],[1] and the relation between this domain functional and conformal mapping and potential theory has been stressed by both Fekete and Szegö [7]. According to Fekete's original definition,

$$\tau(E)=\lim_{n\to\infty}\sqrt[\binom{n}{2}]{V_n}, \tag{1}$$

where

$$V_n=\max_{z_i\in E}|V(z_1,z_2,\ldots,z_n)|, \tag{2}$$

and where V is the Vandermonde determinant.

The transfinite diameter is known explicitly for a number of elementary geometrical configurations, but in general, its numerical evaluation is attended by considerable difficulty. In a previous paper [4], Davis and Rabinowitz showed that complex orthogonal polynomials may be employed profitably for its numerical determination in the case of certain simply connected domains, a square and nonconvex "bean-shaped" domain having been tested. Recently, Professor Fekete called the attention of the author to the possibility of using an analogous relationship in the case where E consists of a finite number of rectifiable Jordan arcs. Making use of very general theorems recently established by Fekete and Walsh [6, p. 61], we may assert:

Let $p_n(z)=a_nz^n+\ldots$, $a_n>0$ $(n=0,\ldots)$ be complex polynomials that are orthonormal over E in the sense that

$$\int_E p_m(z)\overline{p_n(z)}ds=\delta_{mn}. \tag{3}$$

Then we have

$$\lim_{n\to\infty}(1/a_n)^{1/n}=\tau(E). \tag{4}$$

For two collinear line segments of equal length placed symmetrically with respect to 0, say, E: $-1\le x\le -a, a\le x\le 1$, $0<a<1$, the value of $\tau(E)$ is known theoretically and is simply

$$\tau(E)=\tfrac{1}{2}\sqrt{1-a^2}. \tag{5}$$

For two collinear line segments of unequal length, its value has been obtained by N. Achiezer (1) and can be expressed as the ratio of certain elliptic functions. For more than two line segments a closed-form value of $\tau(E)$ is not known to the author.

The relationship (4) was tested numerically on SEAC to see what could be achieved by way of accuracy, using single precision codes. In these computations, the value $a=1/2$ was selected, leading in (5) to

$$\tau=\tfrac{1}{4}\sqrt{3}\approx 0.4330127. \tag{6}$$

The computation was carried out by making use of a single precision (8 significant decimals) floating point orthonormalizing routine developed by J. Bram. This multiple-purpose code has already been described in [3]. The inner products (3) were computed by means of a 10-point Gaussian quadrature rule on each of the two segments $(-1,-\frac{1}{2})$ and $(\frac{1}{2},1)$. The machine was programmed to print out the coefficients of the orthonormal polynomials, as well as the values of these polynomials at the Gaussian abscissas employed. In this way, it was possible to monitor the obvious global properties of the orthonormal polynomials, as well as to see where the accumulated round-off began to vitiate the computations. One way in which this was done was as follows: The polynomials $p_n(x)$, orthonormal over the set E:$(-1,-\frac{1}{2})$, $(1\frac{1}{2},1)$, are alternately even and odd. As n increases, the theoretical zero values for the alternate coefficients of p_n become contaminated by round-off, and these "zeros" begin to assume the proportions of the nonzero coefficients and of the values of the orthonormal polynomials themselves (see table 1). It was found that all significance was lost when attempt was made to go beyond $n=10$. The last value of $(1/a_n)^{1/n}$ gave the value of $\tau(E)$ correct to within 0.009. Additional accuracy is obtainable from (4) only by employing double-precision coding and going beyond $n=10$.

Although closed-form expressions for the orthonormal polynomials over E:$(-1,-\frac{1}{2}),(\frac{1}{2},1)$ are not available, such expressions are available for the Tschebyscheff polynomials for E [2, p. 287]. Here the even and odd polynomials have a totally different structure. Using the latter polynomials as a guide (in the theory of domain polynomials these two sets frequently behave alike), we can confirm the slightly higher values for $(1/a_n)^{1/n}$ registered in table 2 for

[1] Figures in brackets indicate the literature references at the end of this paper.

TABLE 1. *Orthonormal polynomials on* $(-1, -\frac{1}{3}), (\frac{1}{3}, 1)$ *exhibiting effect of roundoff*

Coefficient of—	1	x	x^2	x^3	x^4	x^5	x^6	x^7	x^8	x^9	x^{10}
p_0	1.0000000										
p_1	0.000000001	1.3093073									
p_2	−2.6843775	−0.000000003	4.6017900								
p_3	−0.000000002	−4.1140778	0.000000002	6.1932355							
p_4	7.6721535	−0.000000004	−26.177018	0.000000004	23.822212						
p_5	0.000000007	11.694461	−0.000000003	−40.918493	0.000000003	31.868611					
p_6	−22.558405	−0.000005	131.20021	0.000017	−216.99467	−0.000014	125.35317				
p_7	−0.000083	−34.093102	0.000018	189.08749	−0.000085	−319.27433	0.000046	167.38838			
p_8	66.959357	0.000078	−324.56943	−0.00043	1435.1255	0.00071	−1637.5651	−0.00037	663.46546		
p_9	0.00065	100.83287	−0.005	−763.6782	0.013	2022.6110	−0.015	−2241.6237	0.0059	885.36970	
p_{10}	−199.48823	−0.0021	1963.8362	0.015	−7312.7657	−0.059	12922.714	0.041	−10891.666	−0.0157	3521.1597

TABLE 2. *Computation of transfinite diameter from leading coefficients of orthonormal polynomials*

n	a_n	$1/\sqrt[n]{a_n}$	$\sqrt{a_n/a_{n+2}}$
1	1.3093073	0.76376	0.45979
2	4.6017900	.46616	.43951
3	6.1932355	.54454	.44084
4	23.822212	.45264	.43594
5	31.868611	.50041	.43633
6	125.35317	.44700	.43467
7	167.38858	.48120	.43481
8	663.46546	.44389	.43408
9	885.36970	.47048	----------
10	3521.1597	.44191	----------
		Theoretical value: 0.4330127	

odd n. We can also conclude from the form of the Tschebyscheff polynomials that the ratio $(a_n/a_{n+2})^{1/2}$ would be a good estimator for $\tau(E)$. Table 2 also presents these values, and it will be seen that the last entry, $(a_8/a_{10})^{1/2}$, yields $\tau(E)$ correctly to within 0.001.

The author thanks Morris Newman and Patricia Ferrant for their assistance with the numerical portions of this paper.

---

[1] N. Achiezer, Über einige Funktionen welche in zwei gegebenen Intervallen am wenigstein von Null abweichen, Bul. Ac. Sci. Leningrad, 1163–1202, 309–344, 449–536 (1932–33).
[2] N. Achiezer, Vorlesungen über Approximationstheorie (Akademie Verlag, Berlin, 1953).
[3] P. Davis and P. Rabinowitz, A multiple purpose orthonormalizing code and its uses, J. Assoc. Computing Machinery **1,** 183–191 (1954).
[4] P. Davis and P. Rabinowitz, Numerical experiments in potential theory using orthonormal functions, J. Wash. Acad. Sci. **46,** 12–17 (1956).
[5] M. Fekete, Über die verteilung der Wurzeln bei gewissen algebraischen Gleichung mit Ganzzahligen Koeffizienten, Math. Z. **17,** 228–249 (1923).
[6] M. Fekete and J. L. Walsh, On the asymptotic behavior of polynomials with extremal properties and of their uses, J. Analyse Math. **4,** 49–87 (1955).
[7] G. Szegö, Bermerkung zu einer Arbeit von Herrn M. Fekete, Math. Z. **21,** 203–208 (1924).

WASHINGTON, October 18, 1956.

Journal of Research of the National Bureau of Standards Vol. 58, No. 3, March 1957 Research Paper 2748

Influence of Crystallographic Orientation on the Corrosion Rate of Aluminum in Acids and Alkalies

Theodore H. Orem

The corrosion of single crystals of high-purity aluminum in strong acid and alkali media is disclosed as an orderly process, the rate of attack being dependent on the orientation of the corroding surface. For a 15-percent NaOH solution, corrosion apparently progressed by revealing facet surfaces of the [335] type, resulting in gross corrosion of spheres into cubes; in contrast, substantiating other investigations, corrosion in aqua regia-hydrofluoric acid mixture revealed etch pits with surfaces of the [100] type, resulting in gross corrosion of spheres into equilateral octahedra. Observations of the corrosion by acid and alkali solutions of disks with central holes, and rectangular prisms, both of monocrystalline aluminum, result in interesting conclusions and comparisons with respect to the corrosion process.

1. Introduction

Corrosion is such an extremely complex destructive process, influenced by so many factors, that a study of metals and alloys in their commercially usable state affords little information concerning the basic nature of the process. The fundamental corrosion characteristics of metals can best be determined by a study of the least complex form of the metal that has the basic characteristics of the whole, i. e., of single crystals. By such a study many of the corrosion-influencing characteristics of polycrystalline materials, aside from the environmental factors, are eliminated or at least minimized, and the basic behavior of the metal can be observed.

Those concerned with the study of metals have observed, particularly under the microscope, overetched specimens whose individual grain surfaces appear to be at different elevations, as though the individual grains had been attacked at different rates, such as may be seen in figure 1. In this specimen the grains were at several different levels, with the central grain at the highest level of all. Further, it can be observed that there has been a preferential attack within an individual grain as revealed by variations in rates of etching in an orderly pattern. Those familiar with the preparation of surfaces for metallographic examination are also aware of the variation in behavior of different etchants (corrodents) on the surface. It thus becomes apparent that not only is a metal preferentially attacked when subjected to a corrosive medium, but also that different corrosive media attack the metal in different ways.

The above suggests that the corrosion of aluminum is an ordered attack on the structure in accordance with a definite pattern, the pattern varying with the nature of the corrodent.

Extensive work by Gwathmey and his associates [1,2,3,4] [1] has shown that the atomic arrangement on affected surfaces has great influence on the oxidation and electrochemical characteristics of copper, and significantly affects the catalytic behavior of metals.

[1] Figures in brackets indicate the literature references at the end of this paper.

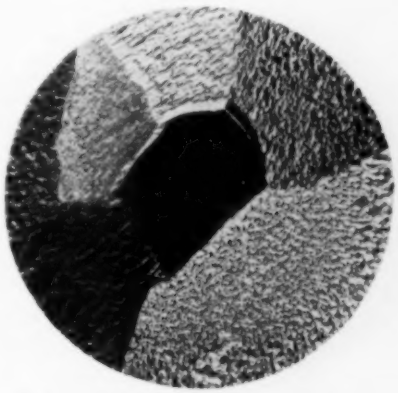

FIGURE 1. *High-purity, polycrystalline aluminum deep-etched in an aqua regia-HF solution.* ×3.

Glauner and Glocker [5] investigated single-crystal spheres of copper and found that the rate of attack by various etchants varied with crystallographic face. Kostron, Hoffler, and Sautter [6] demonstrated that crystallographic orientation had significant influence on the corrosion of single-crystal spheres of aluminum. Politycki and Fischer [7] also did excellent work on the behavior of various acids on monocrystalline aluminum. Straumanis [8] investigated monocrystalline zinc and measured the electrochemical potential of various crystal faces as corrosion progressed.

It is the purpose of this paper to report on the results of an investigation undertaken to determine the basic differences between the corrosion of aluminum in acids and in alkalies.

2. Orientation Relationships in Test Specimens

In investigating the relation between corrosion rates for various surfaces of a single-crystal corresponding to different crystallographic planes, it was believed that a qualitative study alone might yield much useful information; quantitative studies related to surfaces of single crystals had been attempted

by the author and found to be very difficult to undertake and interpret.

Judging from experience obtained with metallographic etching, it could be presumed that the corrosion of aluminum single crystals would occur in a very orderly fashion, being dependent upon the orientation of atoms in the surfaces of the test specimen being attacked. The change in shape effected by corrosion on a single crystal of simple geometrical shape would permit a qualitative evaluation of the relative rates of corrosion in various crystallographic directions.

In this investigation the relative rates of corrosion of variously oriented surfaces were determined by corroding spheres, disks, cubes, and rectangular prisms of monocrystalline aluminum.

The sphere is an ideally shaped specimen for such work because every crystallographic plane of the system is tangent to the sphere at some point on its surface.

As it developed, the circular monocrystalline disk proved to be the most satisfactory of the geometrical forms utilized in this investigation because it best illustrated the differences in corrosion rates among the various planes.

Figure 2 is a sketch of a sphere showing the relationship of the cubic planes to the sphere, the position of two of the cubic planes being shown by the shaded areas passing through the pertinent great circles; the third cubic plane is in the plane of the paper. The cubic planes will thus be tangent to the spherical surface at the six points where the intercepts of the three mutually perpendicular meridional planes intersect the surface.

Figures 3, 4, and 5 are plan views of the sphere shown in figure 2, positioned with the cubic, dodecahedral, and octahedral planes, respectively, parallel to the plane of the paper, the azimuthal orientations being as indicated.

There are also shown in each of the diagrams, lying within the plane of the diagram, the poles of various principal crystallographic planes. Inasmuch as the correspondingly numbered planes are perpendicular to the plane of the diagram, they are said to be lying within its zone. Thus in figure 3 can be observed the poles of certain cubic (100) and dodecahedral (110) planes, which planes are in the zone of the cubic plane of the diagram.

These diagrams will become useful in the study of spherical single crystals of aluminum corroded by acids or alkalies.

Figures 6, 7, and 8 show a monocrystalline aluminum sphere, corroded in an aqua regia-hydrofluoric acid mixture, positioned to conform to the orientations indicated in figures 3, 4, and 5. They are shown here for comparison with the sketches and will be discussed later.

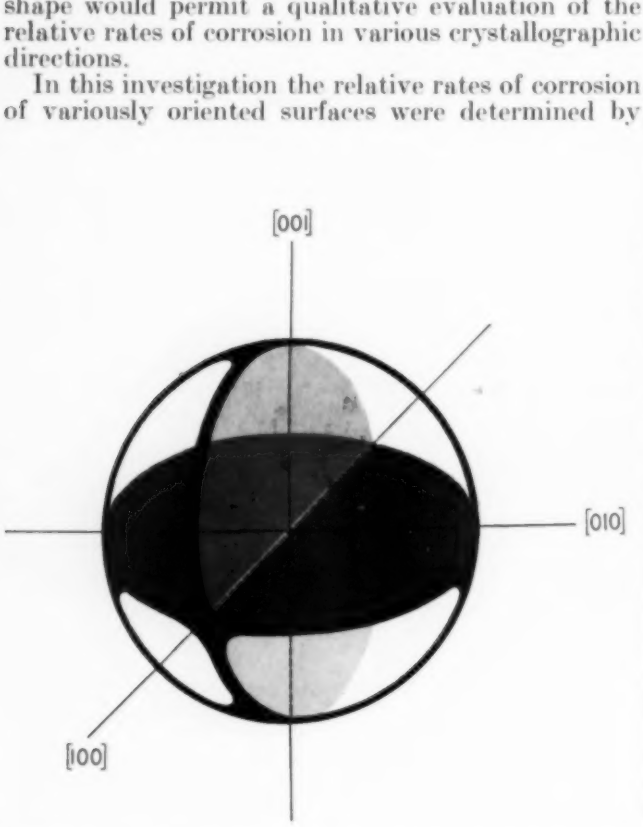

FIGURE 2. *Sketch of sphere showing the location of the cubic planes.*

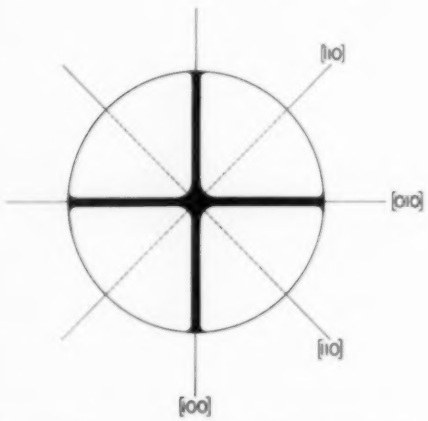

FIGURE 3. *Sketch of sphere shown in figure 6, oriented with cubic plane parallel to paper and showing loci of the cubic and dodecahedral directions.*

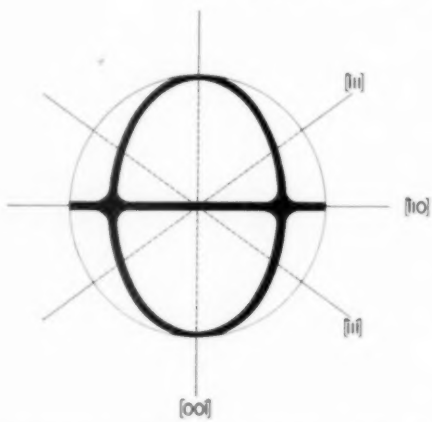

FIGURE 4. *Sketch of sphere shown in figure 7, oriented with the dodecahedral plane parallel to the paper and showing loci of cubic, dodecahedral, and octahedral directions.*

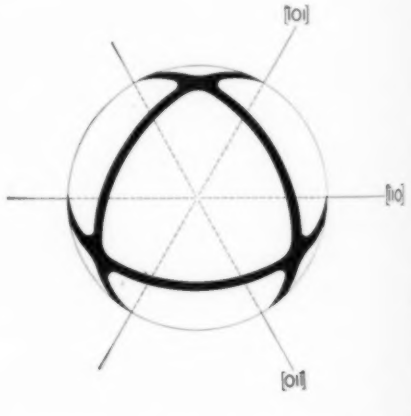

FIGURE 5. *Sketch of sphere shown in figure 8, oriented with the octahedral plane parallel to the paper and showing loci of the dodecahedral directions.*

The relationship between corrosion characteristics of all the low-index planes can be shown by corroding a series of disks, the flat surfaces of which are parallel to the cubic, dodecahedral, or octahedral planes.

Figure 9, a, represents the plan and edge views of a monocrystalline aluminum disk whose flat surfaces are parallel to a cubic plane. The various figures grouped about the plan view represent principal planes within the crystal, which are parallel to the cylindrical surface of the disk at the eight indicated positions. These are the cubic (A) and dodecahedral (B) planes; they lie within the zone of the cubic plane of the disk surface. All other crystallographic planes (not shown), which lie parallel to the cylindrical surface of the disk at other parts on its periphery, also lie in this cubic zone.

Figures 9, b, and 9, c, represent the corresponding relationships for monocrystalline aluminum disks whose flat surfaces are parallel to the dodecahedral and octahedral planes, respectively. Thus, cubic (A), dodecahedral (B), and octahedral (C) planes lie in the zone of the surface dodecahedral plane of figure 9, b, whereas dodecahedral planes (B) lie in the zone of the surface octahedral plane of figure 9, c. The unit cell shown at D in the front view of the disk of figure 9, c, is as the cell would appear when viewing it in a direction normal to the one plane of {112} which is tangent to the cylindrical surface of the disk at that position. There are 6 locations (D) where planes of {112} are tangent to the cylindrical surface of the disk, 1 each being equidistant between the 6 locations where the dodecahedral planes are tangent to the cylindrical surface of the disk. The comparative corrosion rates between {110} and {112}, and such other lesser planes, as {123}, {134}, and {235}, which lie in the octahedral zone and are therefore tangent to the cylindrical surface of such a disk, will be shown by corroding such a disk.

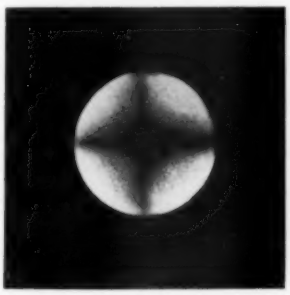

FIGURE 6. *Monocrystalline aluminum sphere after corrosion in aqua regia-HF solution.*

Cubic plane parallel to paper. ×¾.

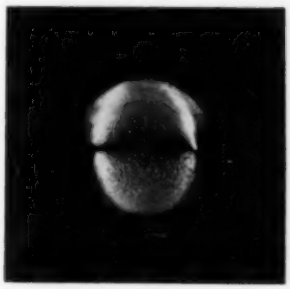

FIGURE 7. *Monocrystalline aluminum sphere after corrosion in aqua regia-HF solution.*

Dodecahedral plane parallel to paper. ×¾.

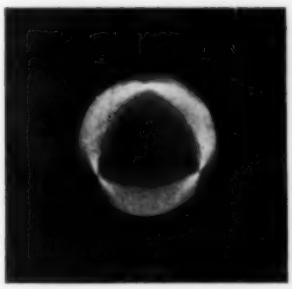

FIGURE 8. *Monocrystalline aluminum sphere after corrosion in aqua regia-HF solution.*

Octahedral plane parallel to paper. ×¾.

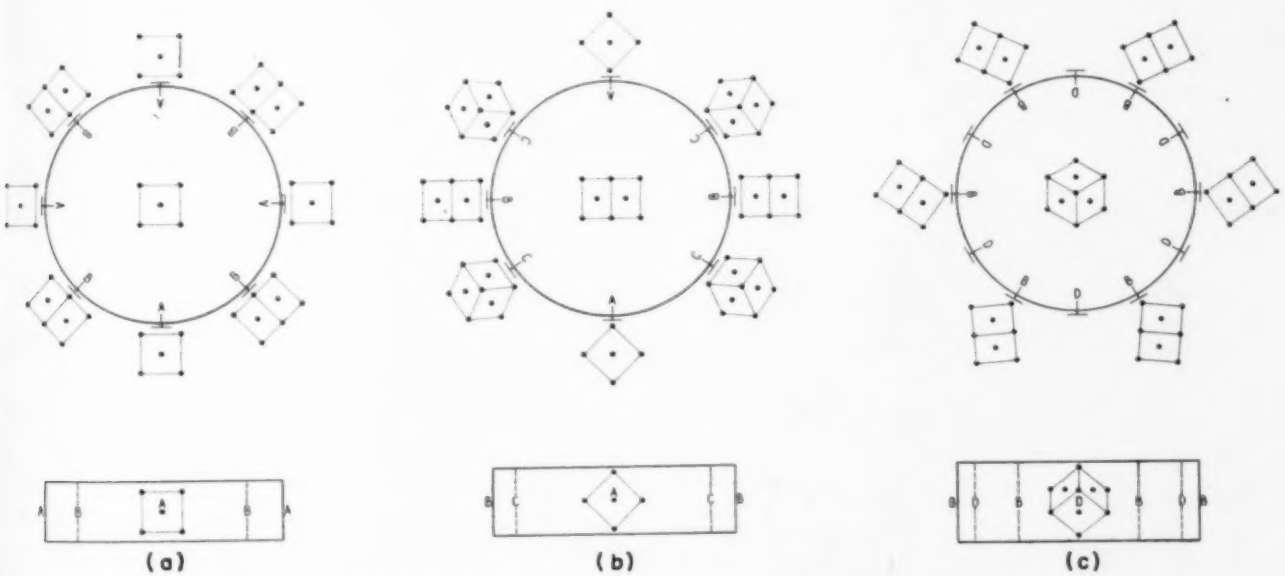

FIGURE 9. *Orthographic projection of disks having various surface orientations and showing the unit-cell arrangement when viewed in directions normal to the flat and cylindrical surfaces of the disks.*

(a) Surface parallel to a cubic plane; (b) surface parallel to the dodecahedral plane; (c) surface parallel to the octahedral plane.

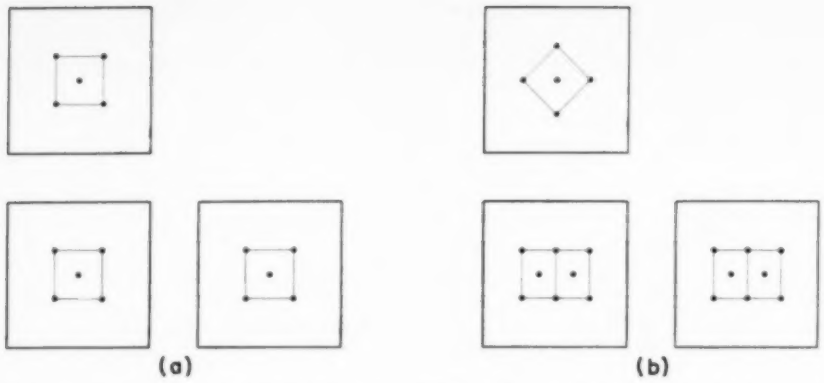

FIGURE 10. *Orthographic projections of cubes having faces parallel to cubic and dodecahedral planes and showing the unit-cell arrangement when viewed in directions normal to these planes.*

(a) All faces parallel to cubic planes; (b) two faces parallel to cubic planes and four faces parallel to dodecahedral planes.

The use of cubes or rectangular prisms was of value only for determining the relative corrodibilities of surfaces parallel only to planes that are mutually normal. Figures 10, a, and 10, b, are orthographic projections of two such cubes, 10, a, being of a cube that has all 6 faces parallel to the cubic plane, and 10, b, that of a cube that has 2 faces parallel to a cubic plane and 4 faces parallel to the dodecahedral planes. The views of the unit cell indicate the crystal orientation on the faces of the cubes in these two sketches.

3. Preparation of Test Specimens

For this investigation monocrystalline spheres of high-purity aluminum 1 in. in diameter were grown by what is known as the Bridgman method [9] of slow cooling from the melt. The aluminum used was furnished by the Aluminum Company of America and was of 99.99+ percent purity. The disks, cubes, and rectangular parallelopipeds were machined from cylindrically shaped ingots, 1¼ in. in diameter, grown by the same method. Any desired orientation of a single crystal specimen was obtained by seeding the melt.

4. Corrosion of Single-Crystal Specimens

4.1. Acid Media

A sphere of monocrystalline aluminum subjected to the corrosive action of aqua regia (65 ml HCl, sp gr 1.18, plus 35 ml HNO_3, sp gr 1.41), to which HF had been added in the ratio of 5 ml of 48-percent HF to 100 ml of aqua regia, corroded in such a manner as to produce the surfaces shown in figures 6, 7, and 8. In these photographs the corroded sphere has been positioned to conform to the orientations of figures 3, 4, and 5, respectively. It will be observed, particularly in figures 7 and 8, that those areas coinciding with the loci of the cubic poles in the sketches stand out in relief to other surfaces of the sphere. This indicates that the attack has been slowest in in these areas, or in a direction normal to the cubic planes.

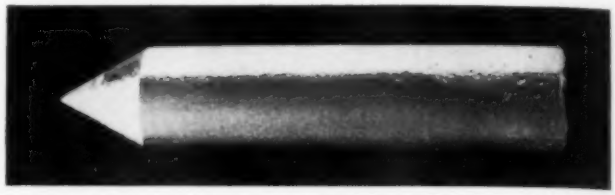

FIGURE 11. *Aluminum monocrystal used for machining of specimens.* ×½.

It could be observed in figures 7 and 8, and, less noticeably, in figure 6, that the areas other than those in the immediate vicinity of the cubic poles (compare with figs. 3 to 5) are uniformly pitted, there being some semblance of pattern to the attack. In the areas around the cubic poles there was no evidence of the pitting type of attack.

This lack of pitting around the cubic-pole areas is because only surfaces parallel to the cubic planes are exposed when aluminum is attacked by acids [10,6,7]. This exposure of cubic planes is demonstrated by the etching characteristics of plane surfaces parallel to the cubic, dodecahedral, and octahedral planes.

A monocrystalline cylindrical ingot (see fig. 11) was sectioned to produce disks whose surfaces were approximately parallel to the cubic, dodecahedral, and octahedral planes. The specimens were electropolished to remove cold work induced by the cutting and grinding operations, and back-reflection Laue diffraction patterns, using unfiltered radiation from a copper target, were obtained from specimens whose flat surfaces were normal to the X-ray beam. The actual orientations of the flat surfaces of the disks were obtained by using the Greninger [11] method, and the specimens were subsequently reground, repolished, and again X-rayed, as became necessary, until the surfaces were within ½° of being parallel to the desired crystallographic planes.

The above specimens were then subjected to the corrosive action of the aqua regia-HF mixture, and then examined with an optical goniometer [12]. This operation revealed that only the cubic planes were exposed as the result of the attack; the same planes

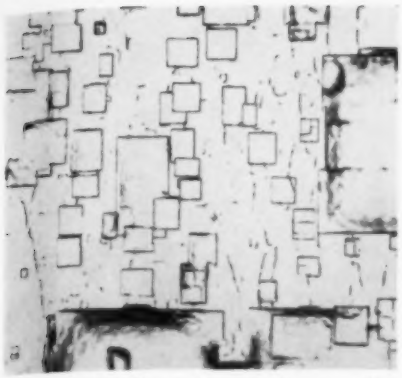

FIGURE 12. *Photomicrograph of etched surface of monocrystalline aluminum approximately parallel to (100).*

Etchant—a solution of aqua regia, HF, and $FeCl_3$. ×200.

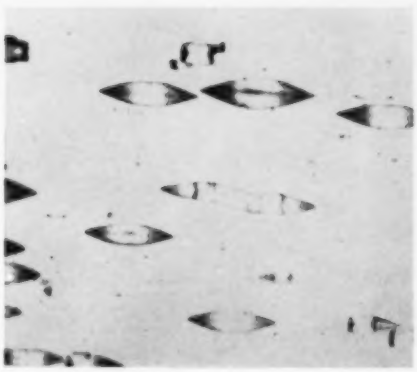

FIGURE 13. *Photomicrograph of etched surface of monocrystalline aluminum approximately parallel to (110).*

Etchant—a solution of aqua regia, HF, and $FeCl_3$. ×200.

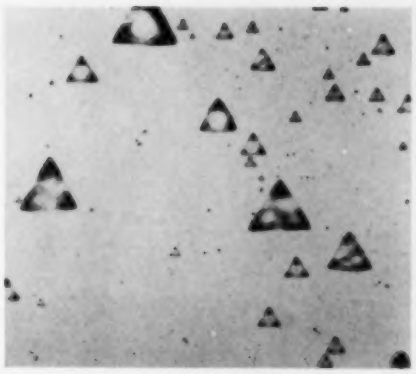

FIGURE 14. *Photomicrograph of etched surface of monocrystalline aluminum approximately parallel to (111).*

Etchant—a solution of aqua regia, HF, and $FeCl_3$. ×200.

were exposed when similar specimens were subjected to concentrated HCl in preliminary experiments. All of the planes exposed were mutually perpendicular; this type of attack was described by Mahl [13] and by Mahl and Pawlek [14] and observed by Roald and Streicher [15] in their work on the corrosion of aluminum in HCl.

Since the attack by the aqua regia-HF mixture was much more rapid than that by the concentrated HCl and the pattern of attack so much more clearly discernible, the acid mixture was employed in this investigation for all experiments relating to the acidic type of attack on aluminum.

Photomicrographs of the above specimens, etched with the aqua regia-HF mixture, to which a small amount of $FeCl_3$ had been added to improve the detail of the microstructure, are shown in figures 12, 13, and 14. The etch pits in the figures possess fourfold, twofold, and threefold symmetry details, respectively, similar to those observed in figures 3, 4, and 5.

The sketch of a cube sectioned so as to reveal the cubic, dodecahedral, and octahedral faces, figure 15, shows the configuration of etch pits on these faces. Comparing these pits with those on the corresponding specimens, it can be observed that the confines of each pit are composed of cubic faces only. The single etch pit on the dodecahedral face of the sketch is a schematic conception of the ellipse-like character of the pits shown in figure 13, the illusion of roundness or ellipticity being the result of a multiplicity of minute facets, all parallel to cubic planes, and diminishing in size toward the ends of the pit.

Because only cubic planes are exposed as a result of corrosion in the aqua regia-HF mixture, and because corrosion consequently progresses at the slowest rate in a direction normal to these planes, it should be evident that the corrosion rates in directions normal to all other planes will exceed that in directions normal to cubic planes.

Prolonged exposure of the sphere to the corrosive action of the aqua regia-HF mixture caused it to evolve into the form shown in figure 16. It is

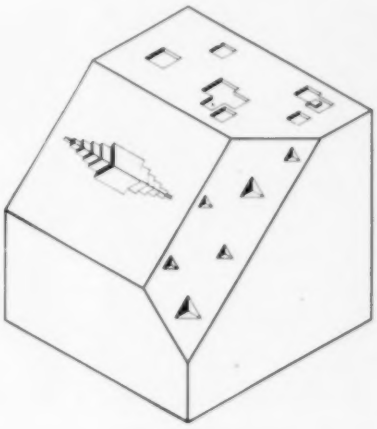

FIGURE 15. *Sketch of cube showing etch pits bounded by cubic planes on cubic, dodecahedral, and octahedral faces.*

FIGURE 16. *Monocrystalline aluminum sphere deeply corroded in an aqua regia-HF mixture.* ×2.

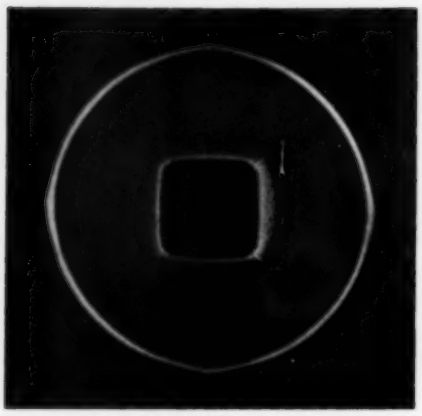

FIGURE 17. *Disk with surface parallel to cubic plane after corrosion in aqua regia-*HF *solution.*

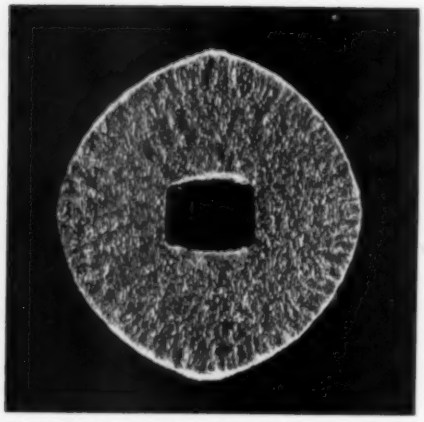

FIGURE 18. *Disk with surface parallel to dodecahedral plane after corrosion in aqua regia-*HF *solution.*

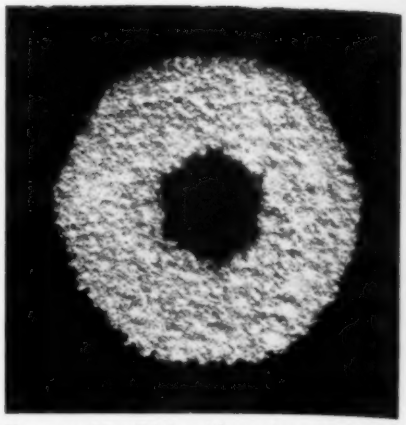

FIGURE 19. *Disk with surface parallel to octahedral plane after corrosion in aqua regia-*HF *solution.*

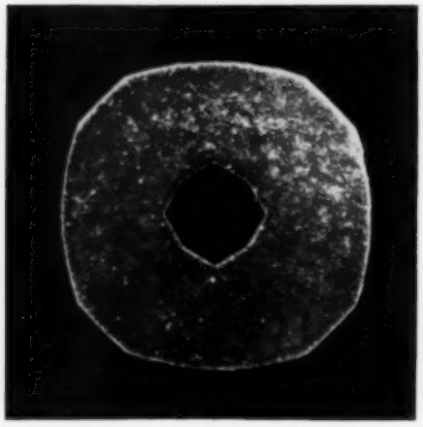

FIGURE 20. *Disk with surface parallel to cubic plane after corrosion in 15-percent* NaOH *solution.*

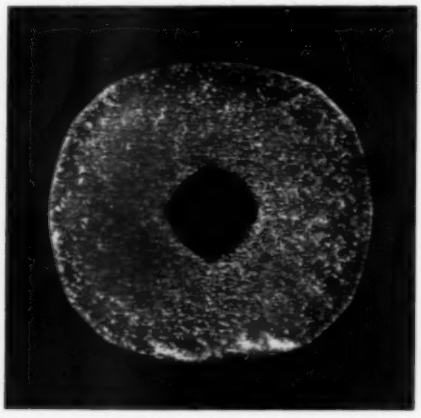

FIGURE 21. *Disk with surface parallel to dodecahedral plane after corrosion in 15-percent* NaOH *solution.*

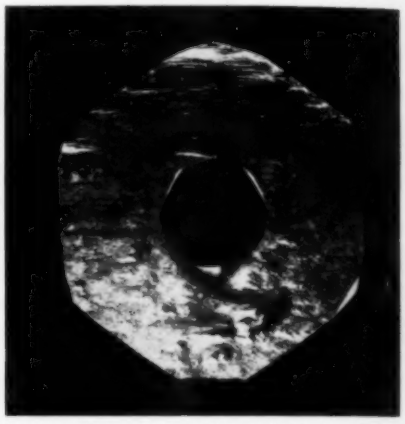

FIGURE 22. *Disk with surface parallel to octahedral plane after corrosion in 15-percent* NaOH *solution.*

FIGURE 23. *Rectangular parallelopiped with six faces parallel to cubic planes after exposure to an aqua regia-*HF *mixture.* ×3.

FIGURE 24. *Rectangular parallelopiped with two faces parallel to cubic planes and four faces parallel to dodecahedral planes after exposure to an aqua regia-*HF *mixture.* ×3.

apparent that an octahedron is evolving from the sphere, indicating that corrosion is progressing at the fastest rate in a direction normal to the surfaces that are parallel to the octahedral planes. This observation is in full accordance with the findings of Kostron, et al. [6] and others, that when aluminum is subjected to a corrosive medium which exposes the cubic planes only, the rate of corrosion is fastest in a direction normal to the octahedral planes, slowest in a direction normal to the cubic planes, and at some intermediate rate in a direction normal to the dodecahedral planes.

To further substantiate these findings, disks of monocrystalline aluminum 1⅛ in. in diameter by ¼ in. thick were machined from ingots that were grown in such a manner that the axes of the ingots were parallel to the cubic, dodecahedral, and octahedral axes. A very small diameter hole was drilled through the center of the face of each disk. Disks having these orientations were discussed earlier. Their orientations are shown schematically in figures 9, a, b, and c, respectively.

When disks of such surface orientations are corroded in an aqua regia-HF mixture, the behavior of the cylindrical surfaces of the disks should be comparable to that which was observed when a monocrystalline sphere was corroded in the same medium. That is, the corrosion rates will vary, depending upon the orientation of the planes tangent to the cylindrical surfaces, and on examination after immersion in the corroding medium the cylindrical disks will no longer have circular right sections. Thus, in a disk having its flat surfaces parallel to a cubic plane, figure 9, a, corrosion in a direction normal to the dodecahedral planes will be faster than that in a direction normal to the cubic planes and, after prolonged exposure in the aqua regia-HF mixture, the disk will corrode to the shape shown in figure 17. Note that the originally small, round hole in the center of the disk has corroded so that its plan is now roughly a square. The diagonals of this square coincide with the dodecahedral directions, the directions in which the corrosion is progressing at the fastest rate for a disk of this particular surface orientation. The cylindrical surface of the disk, while not as radically corroded as the hole in the center, nevertheless shows that corrosion progressed at a slower rate in a direction normal to the cubic planes than it did in a direction normal to the dodecahedral planes.

A photograph of a disk having its surface parallel to the dodecahedral plane and oriented as is the sketch in figure 9, b, after prolonged exposure to an aqua regia-HF mixture, is shown in figure 18. This particular disk, as explained above, is the most favorable for illustrating the relationship between rates of corrosion in directions normal to low-index planes of the face-centered cubic system.

By referring to figure 9, b, the shape of such a corroded disk reveals that corrosion has progressed at the slowest rate in a direction normal to the cubic planes (A), and at the fastest rate in a direction normal to the octahedral planes (C), as observed by the remaining radial width of the disk at these positions. It may be similarly deduced that corrosion in a direction normal to the dodecahedral planes (B) has progressed at an intermediate rate.

A third disk, one having its surface parallel to an octahedral plane and oriented as in figure 9, c, is shown in figure 19 as it appeared after prolonged exposure in an aqua regia-HF mixture. It is evident that corrosion in a direction normal to the dodecahedral planes (B) was at a slower rate than that in a direction normal to {112}, (D).

Figures 20, 21, and 22 show similarly oriented disks corroded in an alkaline medium and are placed in the same diagram as figures 17, 18, and 19 for purposes of comparison; they are discussed later.

In order to determine the relative corrodibility of surfaces that are mutually normal, rectangular prisms oriented as in figures 10, a, and 10, b, were exposed to the acid mixture. In figure 23 is the specimen having all faces parallel to cubic planes (see fig. 10, a). Corrosion at cube edges and corners is evidently greater than on cube faces. Figure 24 shows the specimen having four sides parallel to dodecahedral planes. After prolonged exposure, the edges where these sides join are still sharp, thus indicating a greater rate of corrosion normal to dodecahedral planes than to any other plane in the cubic zone. The edges where the top joins the sides are beveled, inasmuch as corrosion in directions normal to dodecahedral planes is less than for directions normal to other planes in the dodecahedral zone such as the octahedral plane. As would be expected, corrosion in such directions is also somewhat greater than in those normal to the cubic planes.

4.2. Alkaline Media

It is well known that the grain-boundary structure of aluminum is generally developed readily in acid media. The grain boundary is distinguishable because each adjoining grain reflects light in different directions. Because the acid attacks the metal with the exposure of cubic planes only, the light from any one grain is thus reflected from a maximum of only three reflecting surfaces. In alkaline media, however, it is difficult to distinguish grain boundaries on etch-polished surfaces of aluminum. This is due to the inability to distinguish between adjoining grains, all of which have a satiny or frosted appearance. This would indicate that light is being reflected from many more facets than in the case of an acid etchant.

To illustrate the radical difference between the modes of attack of acids and alkalies, spheres and various oriented disks of monocrystalline aluminum were corroded in a 15-percent NaOH solution. Figures 25, 26, and 27 are different views of a sphere after prolonged exposure to such a solution. Figure 25 shows the sphere oriented with its cubic pole normal to the paper and its azimuthal orientation as in figure 3. It has the same orientation as the acid-corroded sphere shown in figure 6. Figure 26 has the dodecahedral pole of the crystal normal to the paper,

its azimuthal orientation is as in figure 4, and it is oriented the same as that of the acid-corroded sphere in figure 7. The octahedral pole of the sphere in figure 27 is normal to the paper, its azimuthal orientation is as in figure 5, and it is oriented the same as the acid-corroded sphere shown in figure 8. Figures 28, 29, and 30, representing deeply corroded spheres in the acid mixture, are placed on the same diagram as figures 25, 26, and 27, for comparison with the alkali-corroded spheres; reference will be made to these photographs later in the paper.

A study of the different views of the sphere discloses little difference between the corrosion rates normal to the cubic and dodecahedral planes. The rates in both of these directions appear to be about the same, but both are definitely faster than that in a direction normal to the octahedral plane. However, examination of appropriately oriented disks comparably exposed to attack does indicate that there is a difference between the rate of corrosion in a direction normal to the cubic plane and that in a direction normal to the dodecahedral plane.

Figure 20, which shows a disk with its surface parallel to a cubic plane, as in figure 9, a, clearly indicates that corrosion in a direction normal to the cubic planes has been at a greater rate than that in a direction normal to the dodecahedral planes. The configuration of the hole in the center of the disk especially demonstrates this difference in corrosion rates. Figure 31, which is a sketch of the corroded hole, the shaded area indicating the portion of the disk that has corroded away, shows that corrosion has progressed at a faster rate in a direction normal to the cubic planes than it has in a direction normal to the dodecahedral planes, because the A dimensions are greater than the B dimensions. The sketch is oriented as in figures 9, a, and 20.

A disk whose surface is parallel to a dodecahedral plane, figure 21, shows clearly that a difference exists in the rates of corrosion in directions normal to the cubic, dodecahedral, and octahedral planes. Figure 32, a sketch of this hole, oriented as in figure 9, b, clearly shows that corrosion has progressed further in a direction normal to the cubic planes than it has in a

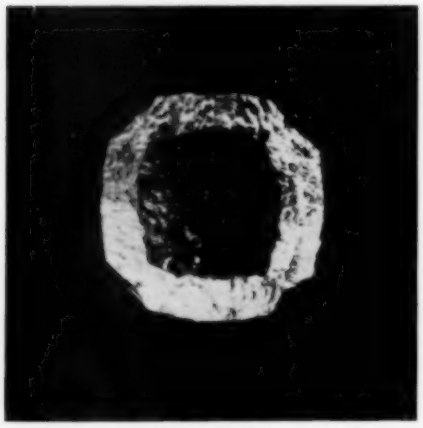

FIGURE 25. *Monocrystalline aluminum sphere corroded in 15-percent* NaOH.
Cubic plane parallel to paper. ×2.

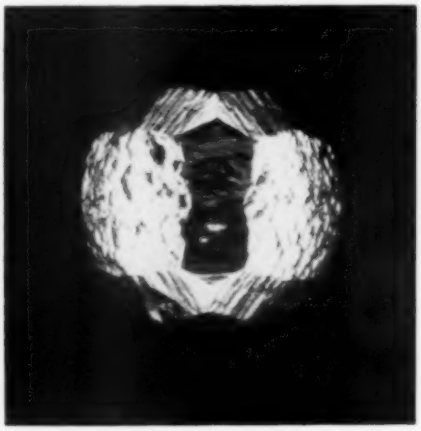

FIGURE 26. *Monocrystalline aluminum sphere corroded in 15-percent* NaOH.
Dodecahedral plane parallel to paper. ×2.

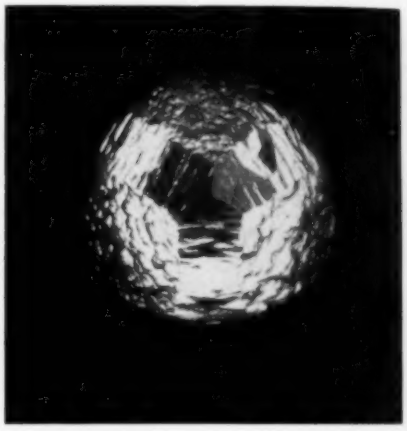

FIGURE 27. *Monocrystalline aluminum sphere corroded in 15-percent* NaOH.
Octahedral plane parallel to paper. ×2.

FIGURE 28. *Deeply corroded version of sphere shown in figure 6.*
Cubic plane parallel to paper. ×3.

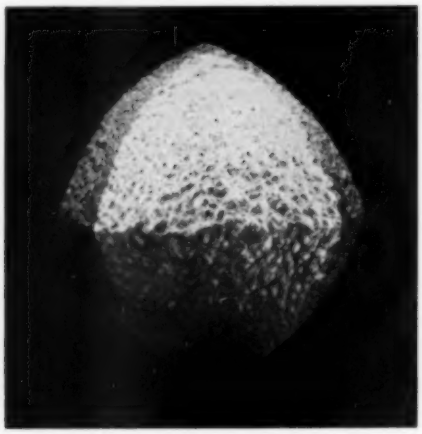

FIGURE 29. *Deeply corroded version of sphere shown in figure 7.*
Dodecahedral plane parallel to paper. ×3.

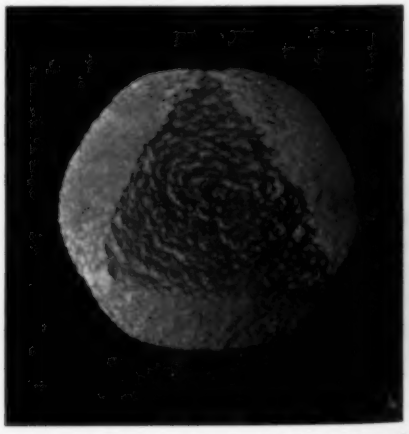

FIGURE 30. *Deeply corroded version of sphere shown in figure 8.*
Octahedral plane parallel to paper. ×3.

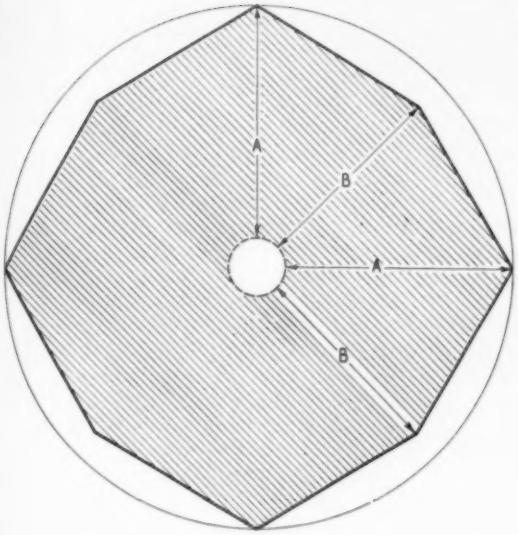

FIGURE 31. *Sketch of hole in disk whose surface is parallel to cubic plane after corrosion in 15-percent* NaOH.

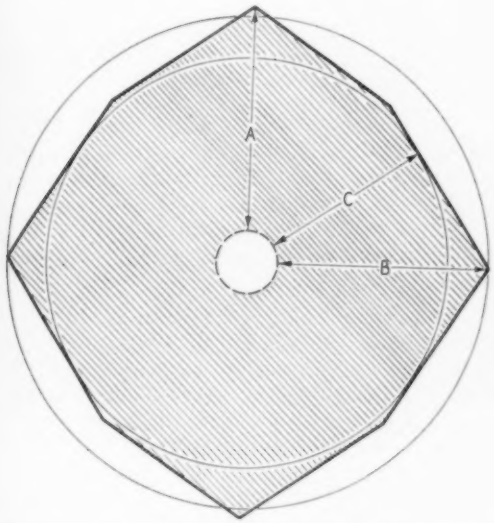

FIGURE 32. *Sketch of hole in disk whose surface is parallel to dodecahedral plane after corrosion in 15-percent* NaOH.

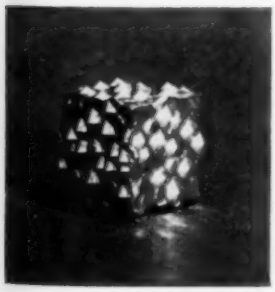

FIGURE 33. *Cube with six faces parallel to* {100} *after exposure to a 15-percent* NaOH *solution.* ×1½.

FIGURE 34. *Cube with two faces parallel to* {100} *and four faces parallel to* {110} *after exposure to 15-percent* NaOH *solution.* ×1½.

direction normal to the dodecahedral planes because dimension A is greater than dimension B. Both rates of corrosion are at a faster rate than in a direction normal to the octahedral planes since dimension C, which lies approximately in the octahedral direction, is somewhat less than both dimensions A and B.

The specimen in figure 22 oriented as in figure 9, c, shows the relationship between the rates of corrosion in directions normal to planes in the octahedral zone.

It is quite evident, both from the peripheral appearance and from the corroded hole, that corrosion in a direction normal to the dodecahedral planes (B) has been at a faster rate than that in a direction normal to {112}, (D). Thus, for such a disk, it is apparent that corrosion progresses at the fastest rate in a direction normal to the dodecahedral planes, and at the slowest rate in a direction normal to {112}.

The determination of the relative corrodibility of mutually normal surfaces was obtained by exposing cubes oriented as in figures 10, a, and 10, b, to 15-percent NaOH for a prolonged period. The specimen having all sides parallel to cubic planes is shown in figure 33, corrosion apparently having occurred at an equal rate in all three cubic directions with the three dimensions remaining essentially equal. The specimen having its four sides parallel to dodecahedral planes is shown in figure 34, its height having become considerably less than its lateral dimensions, indicating a more rapid corrosion rate normal to the cubic planes than to the dodecahedral planes.

Another feature of the exposure of these cubes, which is also evident in the exposure of spheres and disks in an alkaline medium, is the appearance of protruding facets on the surfaces of these specimens. The lack of beveling, as might be expected on the vertical edges of the cube specimen in figure 34, is apparently due to the predominant effect of the occurrence of such facets in these regions.

5. Discussion of Results

In the investigation of the corrosion of aluminum in the aqua regia-HF mixture, the originally round holes in the centers of the disk corroded to various geometrical shapes after prolonged immersion in the corrodent, the shape of the hole bearing a direct relationship to the orientation of the surface of the disk. These variously shaped holes, caused by corrosion with the exposure of cubic planes only, conformed to the projected shape of the outermost boundaries of a cube, the crystallographic orientation of the cube determining the shape of the hole.

Shadow photographs of a cube oriented so that either cubic, dodecahedral, or octahedral planes lie in the plane of the projection are shown in figures 35, a, b, and c, respectively; these are similar in shape to the projections of the unit cubes shown in the centers of the plan views of figures 9, a, b, and c. It will be observed that these also conform approximately to the shapes of the center holes of specimens corroded in acid media in figures 17, 18, and 19.

Applying the above logic to the disks corroded in 15-percent NaOH, in an effort to determine the

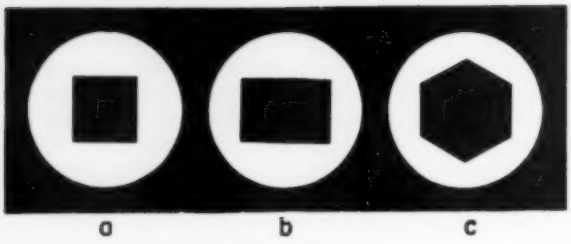

FIGURE 35. *Shadow photographs of cube.*
(a) Cubic plane; (b) dodecahedral plane; (c) octahedral plane parallel to paper

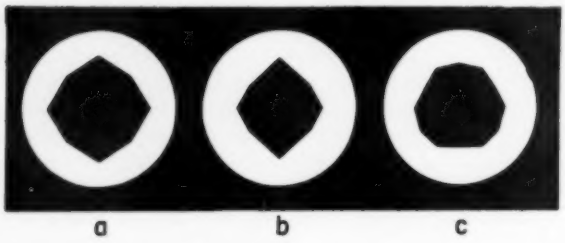

FIGURE 36. *Shadow photographs of tetragonal trisoctahedron having sides parallel to* {335}.
(a) Cubic plane; (b) dodecahedral plane; (c) octahedral plane parallel to paper.

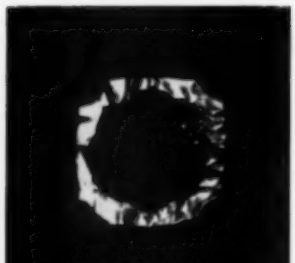

FIGURE 37. *Corroded sphere shown in figure 25 after longer exposure to 15-percent* NaOH. ×3.

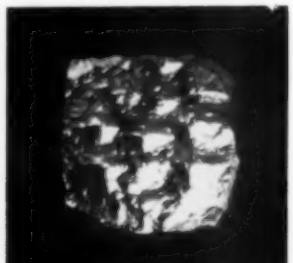

FIGURE 38. *Corroded sphere shown in figure 37 after still longer exposure to 15-percent* NaOH. ×5.

crystallographic planes exposed during corrosion in this medium, a study was made of the corroded holes in the specimens of figures 20, 21, and 22, comparing them with the appropriately projected shapes of polyhedra with faces corresponding to various crystallographic indices.

The most suitable polyhedron appears to be one whose faces are parallel to {335}. In figure 36 is shown a shadow photograph of such a polyhedron, oriented so that either cubic (a), dodecahedral (b), or octahedral (c) planes lie in the plane of projection. Figures 36 a and c correspond closely with the holes in the disks of figures 20 and 22. However, some discrepancy occurs between figure 36, b, and the hole in the disk of figure 21, in that the relative lengths of the sides and the angles between sides are not similar for the two figures. No simple mode of corrosion process can be hypothesized to explain

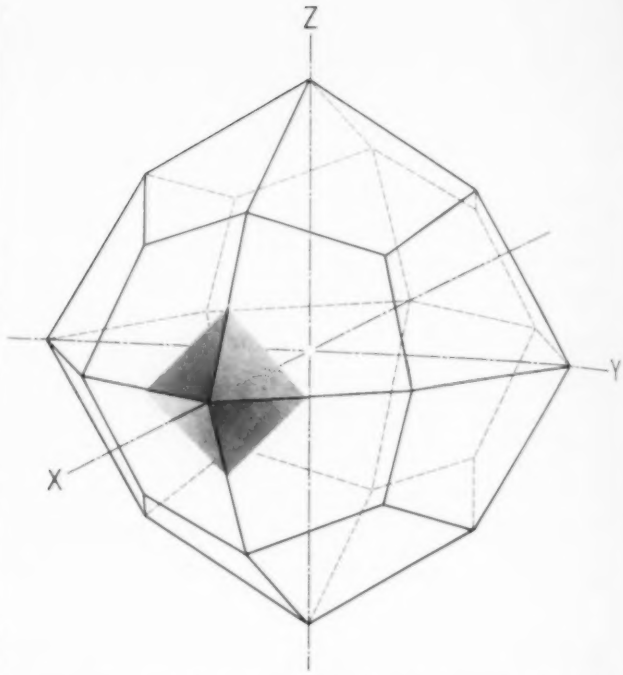

FIGURE 39. *Sketch of tetragonal trisoctahedron showing hillock as viewed in a direction normal to the cubic plane.*

how such a polyhedron might be formed wherein the hole produced would conform to the assumed model on only two of the three planes of projection.

It will be recalled that, whereas acid corrosion of monocrystalline aluminum resulted in producing etch pits exposing only cubic planes, its gross features consisted of the most rapid rate of corrosion in a direction normal to octahedral planes. Figures 28, 29, and 30 show the specimen of figure 16, when oriented in the positions corresponding to figures 3, 4, and 5, respectively. This clearly shows that an octahedron-like shape is evolving from the original sphere.

Conversely, specimens subjected to alkaline corrosion revealed protuberances having facets which are presumed to parallel {335} planes, whereas in its gross features, corrosion apparently progressed most rapidly in the cubic direction. Figure 37 shows a view parallel to the cubic plane of the specimen of figure 25 after a somewhat longer exposure. It apparently has become more cube-like inasmuch as the areas lying on other than cubic planes have become smaller owing to the further development of such cube faces. After the specimen becomes essentially cubic in form, as shown in figure 38, further corrosion would only decrease the dimensions of the cube. The least rapid corrosion apparently occurs in directions normal to the octahedral plane, whereas an intermediate corrosion rate occurs normal to the dodecahedral plane.

The protrusions on all faces of specimens in figures 33 and 34 are considered to be the facets exposed during the attack by the alkali. As stated above, they are identified as being probably parallel to

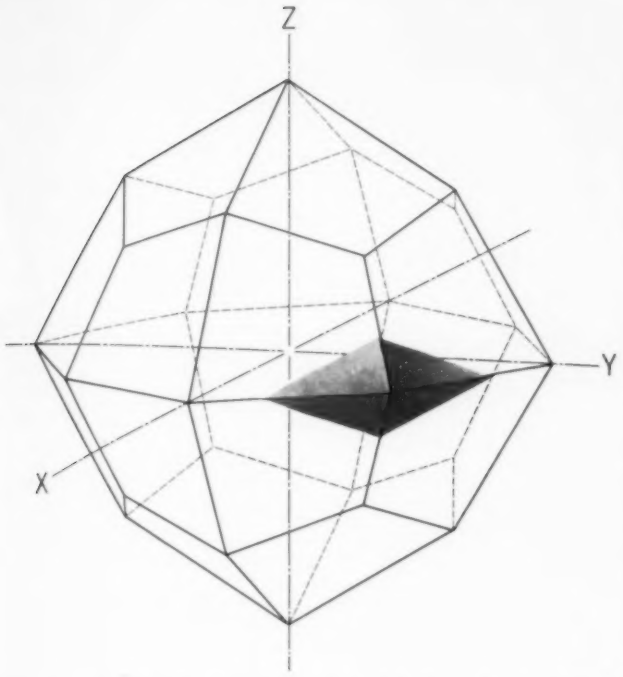

FIGURE 40. *Sketch of tetragonal trisoctahedron showing hillock as viewed in a direction normal to the dodecahedral plane.*

{335}. The difference between the appearance of the protrusions on the vertical sides of the specimen in figure 34 and all the other protrusions on both specimens, will be clarified by viewing figures 39 and 40. This shows two views of the polyhedron formed by such planes. The shaded areas in figure 39 cover four intersecting planes of the tetragonal trisoctahedron whose faces are parallel to {335} when cut by a cubic plane. Its appearance is similar to the shape of all the protrusions on the specimen in figure 33 and the protrusions on the top face of the specimen in figure 34. They are the facets exposed when the corrosion progressed in a direction normal to the cubic planes. The shaded area of the polyhedron in figure 40 covers four intersecting planes when cut by a dodecahedral plane. Its configuration is similar to the protrusions on the sides of the specimen in figure 34.

6. Conclusions

An investigation of the influence of corrosion by a 15-percent NaOH solution and by an aqua regia-hydrofluoric acid mixture on high purity monocrystalline aluminum in various geometrical shapes results in the following conclusions:

1. The process of corrosion is an orderly one, the rate of attack being dependent on the arrangement of the atoms relative to the surface upon which the attack is taking place.

2. For the alkali mixture, the attack is such as to reveal facets whose surfaces probably are parallel to {335} planes, with the most rapid corrosion taking place in directions normal to cubic planes. Thus, when thin single-crystal disks having various surface orientations and containing small central holes were exposed to the NaOH mixture, these holes corroded so as to form shapes roughly similar to the trace of a polyhedron bounded by {335} planes when intersected by a plane oriented to correspond to the surface of the disk.

3. For the acid mixture, a pitting type of attack occurs which exposes only the cubic planes. However, corrosion is observed to progress at a very slow rate in directions normal to such planes, the most rapid corrosion occurring in directions normal to octahedral planes. This is similar to the attack observed by earlier investigators when using various acids.

Thus, when thin single-crystal disks having various surface orientations and containing small central holes were exposed to the acid mixture, these holes corroded so as to form shapes similar to those of the trace of a cube when intersected by a plane oriented to correspond to the surface of the disk.

4. The gross effect of corrosion by these media on spherical single crystals is such as to cause them to acquire the general shape of equilateral octahedra, when attacked by the acid mixture and of cubes when attacked by the NaOH solution.

The author is grateful to W. F. Gerhold for assisting in construction of apparatus and growing of monocrystals, to H. C. Vacher for assistance in interpretation of X-ray diffraction patterns, and to R. W. Mebs for enlightening discussions during the course of the investigation and for critical review of the manuscript.

7. References

[1] A. T. Gwathmey and F. W. Young, Rev. mét. **48,** 434 (1951).
[2] A. T. Gwathmey and A. F. Benton, Trans. Electrochem. Soc. **77,** 210 (1940).
[3] H. Leidheiser and A. T. Gwathmey, Trans. Electrochem. Soc. **91,** 97 (1947).
[4] R. E. Cunningham and A. T. Gwathmey, J. Am. Chem. Soc. **76,** 391 (1954).
[5] R. Glauner and R. Glocker, Z. Krist. **80,** 377 (1931).
[6] H. Kostron, E. Hoffler, and W. Sautter, Z. Metallkunde **44,** 17 (1953).
[7] A. Politycki and H. Fischer, Z. Elektrochem. **57,** 393 (1953); **56,** 326 (1952).
[8] M. Straumanis, Z. Physik. Chem. **147,** 161 (1930).
[9] P. W. Bridgman, Proc. Am. Acad. Arts Sci. **60,** 305 (1935).
[10] C. J. Walton, Trans. Electrochem. Soc. **85,** 239 (1944).
[11] A. B. Greninger, Trans. Am. Inst. Mining Met. Eng. **117,** 61 (1935).
[12] C. S. Barrett, Structure of metals, 2d ed. (McGraw-Hill Book Co., Inc., New York, N. Y., 1952).
[13] H. Mahl, Metallwirtschaft **29,** 1082 (1940).
[14] H. Mahl and F. Pawlek, Z. Metallkunde **34,** 232 (1942).
[15] B. Roald and M. A. Streicher, J. Electrochem. Soc. **97,** 283 (1950).

WASHINGTON, October 16, 1956.

U. S. GOVERNMENT PRINTING OFFICE: 1957

Recent Publications of the National Bureau of Standards

Journal of Research of the National Bureau of Standards, Volume 58, No. 1, January 1957 (RP2727 to RP2734, incl.), 60 cents. Annual subscription $4.00.

Technical News Bulletin, Volume 41, No. 1, January 1957. 10 cents. Annual subscription $1.00.

Basic Radio Propagation Predictions for April 1957. Three months in advance. CRPL–D 149. Issued January 1957. 10 cents. Annual subscription $1.00.

Research Papers

(Journal of Research, volume 58, No. 1, January 1957)

RP2727. Influence of a ridge on the low-frequency ground wave. James R. Wait and Anabeth Murphy.

RP2728. Phase-diagram study of alloys in the iron-chromium-molybdenum-nickel system. C. J. Bechtoldt and H. C. Vacher.

RP2729. Construction of a Kösters double-image prism. J. B. Saunders.

RP2730. The Kösters interferometer. J. B. Saunders.

RP2731. Spectral absorbance of some aqueous solutions in the range 10° to 40° C. Elizabeth E. Sager and Fleur C. Byers.

RP2732. Radiant-heat transfer between nongray parallel plates. Stanley Goodman.

RP2733. Wavelengths from iron-halide lamps. Robert W. Stanley and William F. Meggers.

RP2734. Resistance of flow in Teflon and brass tubes. Marion R. Brockman.

Circulars

C510. Supplement 1. Tables of chemical kinetics: Homogeneous reactions. $3.25.

Publications in Other Journals

Clues to ionospheric conditions in the southern auroral zone. A. H. Shapley. Antarctica in the Intern. Geophys. Year. (American Geophys. Union, 1515 Massachusetts Ave., N. W., Washington 5, D. C.) Geophys. Monograph No. 1 (1956).

Electron interference experiments. J. Arol Simpson. Rev. Mod. Phys. (American Inst. of Physics, 57 E. 55th St., New York 22, N. Y.) **28**, No. 3, 254 (July 1956).

Electron affinity of atomic sulfur and empirical affinities of the light elements. Lewis M. Branscomb and Stephen J. Smith. J. Chem. Phys. (American Inst. of Physics, 57 E. 55th St., New York 22, N. Y.) **25**, No. 3, 598 (Sept. 1956).

Plastics. Gordon M. Kline. J. Eng. Mech. Div. Am. Soc. Civil Engrs. (American Society of Civil Engineers, 33 W. 39th St., New York 18, N. Y.) **82**, No. EM4 (Oct. 1956).

Sources of error in various methods of airplane camera calibration. Francis E. Washer. Photogrammetric Eng. (1515 Massachusetts Ave., N. W., Washington 5, D. C.) **22**, No. 4, 727 (Sept. 1956).

Spin-spin absorption in chromic methylammonium alum and manganous chloride tetrahydrate at very low temperatures. E. Ambler and R. P. Hudson. Physica (Treas. Physica Foundation, Bijlhouwerstr. 6, Utrecht, Netherlands) **22**, 866 (1956).

The nature, cause and effect of porosity in electrodeposits. II. Radiographic detection of porosity in electrodeposits. F. Ogburn and M. Hilkers. Annual Tech. Proc. Am. Electroplaters' Soc. (Am. Electroplaters' Soc., 445 Broad St., Newark 2, N. J.), p. 256 (1956).

Specifications, standards and codes. R. S. Dill. Symposium Am. Soc. Heating and Air-Conditioning Engrs. (52 Worth St., New York 13, N. Y.), p. 138 (August 1956).

The infrared spectrum and rotational constants of carbon disulfide. Harry C. Allen, Jr., Earle K. Plyler, and L. R. Blaine. J. Am. Chem. Soc. (American Chemical Society, 1155 16th St., N. W., Washington 6, D. C.) **78**, 4843 (1956).

Contributions to the theory of rank order statistics—the two-sample case. I. Richard Savage. Ann. Math. Stat. (Waverly Press, Inc., Baltimore, Md.) **27**, No. 3 (Sept. 1956).

Publications for which a price is indicated are available only from the Superintendent of Documents, U. S. Government Printing Office, Washington 25, D. C. (foreign postage, one-fourth additional). Reprints from outside journals and the NBS Journal of Research may often be obtained directly from the authors.

UNIVERSITY OF MICHIGAN
GENERAL LIBRARY
DOCUMENTS DIVISION
1276 ANN ARBOR MICH

UNI
GOVERNMEN
DIVISION OF PUBLIC DOCUMENTS
WASHINGTON 25, D. C.

OFFICIAL BUSINESS

PENALTY FOR PRIVATE USE TO AVOID PAYMENT OF POSTAGE, $300 (GPO)

Journal of Research of the National Bureau of Standards Vol. 58, No. 3 March 1957

Contents

		Page
Relative dimensional stabilities of a selected series of stainless-steel decimeter bars. Benjamin L. Page.	RP2742	119
Thermal quenching in alpha- and gamma-excited fluorescent solutions. H. H. Seliger and C. A. Ziegler.	RP2743	125
Two-parameter gloss methods. I. Nimeroff.	RP2744	127
Glassy state transitions of poly-(chlorotrifluoroethylene), poly-(vinylidene fluoride), and their copolymers. L. Mandelkern, G. M. Martin, and F. A. Quinn, Jr.	RP2745	137
Measurement of the corrosion rate of iron by polarization techniques. W. J. Schwerdtfeger.	RP2746	145
Numerical computation of the transfinite diameter of two collinear line segments. Philip Davis.	RP2747	155
Influence of crystallographic orientation on the corrosion rate of aluminum in acids and alkalies. Theodore H. Orem.	RP2748	157

[A list of recent NBS publications is given on page 3 of the cover.]

For sale by the Superintendent of Documents, U. S. Government Printing Office, Washington 25, D. C. Price 60 cents (single copy). Subscription price: $4.00 a year; $1.25 additional for foreign mailing.

UNITED STATES GOVERNMENT PRINTING OFFICE, WASHINGTON : 1957